University of Nebraska Medical Center
BREAKTHROUGHS FOR LIFE

University of Nebraska Medical Center
DigitalCommons@UNMC

Theses & Dissertations

Graduate Studies

Spring 5-9-2020

Smart Delivery of Genes and Drugs for Treatment of Cancer

Feng Lin
University of Nebraska Medical Center

Tell us how you used this information in this short survey.

Follow this and additional works at: https://digitalcommons.unmc.edu/etd

 Part of the Other Pharmacy and Pharmaceutical Sciences Commons

Recommended Citation

Lin, Feng, "Smart Delivery of Genes and Drugs for Treatment of Cancer" (2020). *Theses & Dissertations*. 425.
https://digitalcommons.unmc.edu/etd/425

This Dissertation is brought to you for free and open access by the Graduate Studies at DigitalCommons@UNMC. It has been accepted for inclusion in Theses & Dissertations by an authorized administrator of DigitalCommons@UNMC. For more information, please contact digitalcommons@unmc.edu.

Smart Delivery of Genes and Drugs for Treatment of Cancer

By

Feng Lin

A Dissertation

Presented to the Faculty of

the Graduate School in the University of Nebraska Medical Center

in Partial Fulfillment of the Requirements

for the Degree of Doctor of Philosophy

Department of Pharmaceutical Sciences

Under the Supervision of Professor Ram I. Mahato

University of Nebraska Medical Center

Omaha, Nebraska

January, 2020

Supervisory Committee:

Ram I. Mahato. Ph.D. Jered C. Garrison, Ph.D.

David Oupicky, Ph.D. Rongshi Li, Ph.D.

Smart Delivery of Genes and Drugs for Treatment of Cancer

Feng Lin, Ph.D.

University of Nebraska Medical Center, 2020

Supervisor: Ram I. Mahato. Ph.D.

The ineffective delivery of genes and drugs have become a big obstacle for the treatment of cancer, due to either poor stability or low aqueous solubility. In the first part, A ROS responsive polymer named poly(ethylene glycol)–poly[aspartamidoethyl(p-boronobenzyl)diethylammonium bromide] (PEG-B-PAEBEA) was developed for codelivery miR-34a mimic and small molecule PLK1 inhibitor volasertib (BI6727) for the treatment of pancreatic ductal adenocarcinoma (PDAC), since tumor suppressor microRNA-34a (miR-34a), which targets many oncogenes related to proliferation, apoptosis, and invasion is significant downregulated while Polo-like kinase 1 (PLK1) closely associated with short survival rates of pancreatic cancer patients is remarkably upregulated . In part 2, due to increased number of cancer stem cells (CSCs), a pH and glutathione (GSH) sensitive delivery system, fabricated by DTX and a pH responsive diisopropylamino ethanol and GSH responsive RUB prodrug conjugated polycarbonate DTX loaded P-RUBs (DTX/P-RUBs), was developed to overcome the chemoresistance by targeting both of tumor bulk cells and CSCs. Rubone (RUB) is a miR-34a activator which is downregulated in CSCs. Fast release of DTX and RUB in the cytoplasm after endocytosis could upregulate the intracellular miR-34a, which then affected the expression of proteins involved in chemoresistance, thus sensitizing the tumor cells towards DTX and further leading to significant inhibition of TXR tumor progression. Thus, DTX/P-RUBs has the potential to treat TXR prostate cancer. By taking advantage of this dual responsive strategy, the successful delivery of many other hydrophobic drugs can be achieved for cancer treatment.

Acknowledgements

First and foremost, I would like to show my sincere gratitude to my advisor Dr. Ram I. Mahato. With his guidance and inspiration, I gradually entered the scientific world and developed a big interest in drug delivery. Though problems always came out in my research and life, he is always available to help me out with his wisdom and constantly supported me. From him, I learned to be an independent researcher with enthusiasm, persistency, the integrity and creative and critical thinking.

I would also like to sincerely thank my graduate supervisory committee members Drs. Jered C. Garrison, David Oupicky and Rongshi Li for their valuable suggestions and inputs on my research work throughout my Ph.D. training. I would also like to acknowledge Dr. Xiaofang Wang and Dr. Yuxiang Dong for providing me with valuable suggestions. I would also like to thank Dr. Wenzhu Zhang for her suggestions on my histological study.

I was fortunate to join Dr. Mahato's lab and worked with wonderful colleagues. I would like to thank Drs. Di Wen and Yang Peng teaching me animal related techniques and mouse model establishment; I would like to thank Dr. Xiaofei Xin for her hard work on the biological evaluation on our own project. Besides that, I would as well like to thank Dr. Virender Kumar, Dr. Vinod Kumar, Dr. Qiyue Wang, Dr. Amit K. Chaudhary, Dr. Jitender Bariwal and Saud Almawash, Rajan sharma Bharttarai, Bharti Sethi and Jingyi Ma for their help during all these years.

I would like to thank all administrative stuff at International Health & Medical Education, UNMC Graduate Studies and Department of Pharmaceutical Sciences for their help in my life.

I would like to thank all the UNMC core facility staff and members in the UNMC animal facility for their extreme cooperation.

Last but not the least, I would like to thank my family and friends. I would also like to thank, Dr. Yajuan Su, Dr. Zhiyi Lin, Dr. Shixuan Chen, Xiyuan Xi, Catherin Orzechowski, Zhen Ye,

Junying Wang, Chunkai Wang, Derek A. Leas, Dr. Hang Su, and Yunfan Kong. I appreciate all the people who have helped and encouraged me in past several years.

Feng Lin

University of Nebraska Medical Center

January, 2020

Table of Contents

List of Figures

List of Tables

List of abbeviation

EPR enhanced permeability and retention effect

HIF1 Hypoxia-inducible factor 1

ECM extracellular matrix

CSCs Cancer stem cells

VEGF vascular endothelial growth factor

FAP fibroblast-activation proteins

α-SMA α-smooth-muscle actin

MMPs matrix metalloproteinases

ROS reactive oxygen species

FN fibronectin

TGF-β Transforming growth factor-β

EMT epidermal to mesenchymal transition

FGF fibroblast growth factor

TAMs tumor-associated macrophages

FDA Food and Drug administration

anti-PD-1 anti-programed death

anti-CTLA-4 anti-cytotoxic T lymphocyte antigen

NDDS Nano-sized drug delivery systems

MPS mononuclear phagocyte system

RES reticulo-endothelial system

p(HMEMA) 2-(hexamethyleneimino)ethanol to poly(methacrylic acid)

GSH glutathione

ER endoplasmic reticulum

CPT Camptothecin

DOX Doxorubicin

DTX docetaxel

QD quantum dot

LCST lower critical solution temperature

PNIPAAm poly(N-isopropylacrylamide)

SWNT single wall nanotubes

ELPs Elastin-like polypeptides

PDAC pancreatic ductal adenocarcinoma

miR-34a microRNA-34a

PLK1 Polo-like kinase 1

BI6727 volasertib

PEG-B-PAEBEA poly (ethylene glycol)-poly[aspartamidoethyl (p-boronobenzyl) diethyl ammonium bromide]

mPEG-b-PCC-g-DC-g-TEPA poly(ethylene glycol)-*block*-poly(2-methyl-2-carboxyl-propylene carbonate-*graft*-dodecanol-*graft*-tetraethylene pentamine)

DEEDA N, N-diethylethylenediamine

DTT dithiothreitol

IHC immunohistochemistry

ROP ring-opening polymerization

PBA phenyl boronic acid

TLRs toll-like receptors

DMEM Dulbecco's Modified Eagle Medium

FBS fetal bovine serum

THF tetrahydrofuran

DMF *N*,*N*-dimethylformamide

TEA Triethylamine

PEG-PAsp(DIE) poly(ethylene glycol)-poly(beta-diisoethylamino-ethyl-aspartamide)

HPDE human pancreatic duct epithelial cells

BPE bovine pituitary extract

DLS dynamic light scattering

TEM transmission electron microscopy

EE% encapsulation efficiency%

DL% drug loading%

EB ethidium bromide

CMC Critical micelle concentration

FRET fluorescence resonance energy transfer

DCFDA 2',7'-dichlorofluorescin diacetate

DCFH dichlorofluorescein

DRI dose reduced index

CI combination index

Cp crossing point

PVDF polyvinylidene difluoride

RIPA radioimmunoprecipitation assay

NIH National Institutes of Health

IACUC the Institutional Animal Care and Use Committee

H&E haematoxylin and eosin

WB Western blot

SD standard deviation

ANOVA One-way analysis of variance

RUB rubone

TXR taxane resistant

DTX/P-RUB DTX loaded P-RUB micelles

PDPA poly(diisopropylaminoethanol)

PEG-PCD poly (ethylene glycol)-block-poly (2-methyl-2-carboxyl-propylene carbonate-graft-dodecanol

P-RUB RUB/diisopropylaminoethanol conjugated polycarbonate

NaOH sodium hydroxide

KOH potassium hydroxide

EDCI *N*-(3-dimethylaminopropyl)-*N′*-ethylcarbodiimide hydrochloride *N*-(3-dimethylamino-propyl)-*N′*-ethylcarbodiimide hydrochloride

HOAt 1-hydroxy-7-azabenzotriazole

DCM dichloromethane

TES-Cl chlorotriethylsilane

DBU 1,8-diazabicyclo [5.4.0]undec-7-ene

MBC 2-Methyl-2-benzyloxycarbonyl-propylene carbonate

TBAF tetrapropylammonium fluoride

IPA isopropanol

PEG-PCC poly (ethylene glycol)-*block*-poly (2-methyl-2-carboxyl-propylene carbonate)

DAPI 4',6-diamidino-2-phenylindole

CLSM confocal laser scanning microscopy

MRM multiple reaction monitoring

BSO buthionine sulphoxime

MDR multidrug resistance

P-gp P-glycoprotein

Chapter I

Introduction

1.1 Cancer and its microenvironment

Cancer has become the leading cause of death worldwide, accounting for around 9.6 million deaths in 2018 [1]. Patients who have cancer often show a lump, abnormal bleeding, prolonged cough, unexplained weight loss etc. Cancer is a collection of diseases (over 100 types) that are known for uncontrolled cell division, immortality and abnormal microenvironment, including prostate cancer, pancreatic cancer, liver cancer, medulloblastoma, etc [1]. Cancer cells proliferate and grow into tumor (an abnormal cell mass) and hematologic cancer, in which the cancer cells spread among the blood, lymph systems and bone marrow [2]. Malignant tumor can spread into or invade nearby tissues, with some cancer cells breaking off from the original disease site and traveling to distant parts by taking advantages of blood stream or the lymph system, forming new tumors [3].

Cancers start when genetic changes affect the natural orderly process. They are mainly caused by genetic mutation of oncogenes that induce cell proliferation and differentiation, and cancer suppressor genes that inhibit cell growth or stimulate apoptosis by the alteration of intracellular signaling pathway from environmental and lifestyle factors (tobacco, radiation, pollution, obesity infections, etc.) [4-7]. It is often hard to postulate what factors may lead to the onset of cancer because the oncogenic causes do not have specific fingerprints. The genetic change in cancer cells is clonally bias to aberrant cell division, lack of excessive growth inhibition, immune system avoidance, cell death transmission blockade and genetic materials error accumulation [8, 9]. Heterogeneity is another feature of tumors that even tumors cells within the same tumor site may have different genetic mutations. This great genetic diversification that different cancer cells may have different genetic changes consists of one of the fundamental difficulties for the cancer treatment [10-12]. In the following sections, we will mainly focus on solid tumors, rather than other categories of cancers (leukemia, lymphoma, sarcoma and melanoma).

The tumor and its microenvironment are closely associated and interacted. By influencing the normal cells, immune cells and blood vessels with released extracellular signals and promoted angiogenesis, cancer cells can generate a tumor microenvironment that favor the growth of tumors by providing nutrients and oxygen, removing wastes and evading the immune system [9, 13].

Most of cancers are not well vascularized due to uncontrolled cell proliferation. As a result, the blood vessels formed in the tumors differ from the one in other normal tissues. The permeable vasculature is thought to have insufficient pericytes and a malformed basement membrane [14, 15]. The leaky vasculature opens a door for large molecules and particles with a size, ranging from 10 to 500 nm to accumulate in the tumor, ensuring high demand of nutrient and oxygen supply for rapid tumor growth [16, 17]. This phenomenon is well defined as the enhanced permeability and retention (EPR) effect. Nonetheless, EPR effect also provides us with an increasing promising paradigm for tumor targeting and anticancer drug developments through its unique facilitated accumulation of macromolecules given that normal tissues have intact vasculature.

The rapid growth of tumor can contribute to the overall **hypoxia** in tumors because the interior of the tumors become distant from the blood vessels and more cancer cells from high cell proliferation demand more oxygen and nutrients than before, which cannot be compensated by angiogenesis [18, 19]. Being underfed, the cancer cells are more genetically instable. Hypoxia-inducible factor 1 (HIF-1), a key regulatory transcription factor, is also upregulated on account of hypoxia. HIF-1 is responsible for adaptive cellular changes. For example, it is found to influence glycolytic genes that take effect in reduction of oxygen consumption and availability. HIF-1can also contribute to increased cell migration and extracellular matrix (ECM) remodeling [18, 20].

Hypoxia can lead to the change of metabolism in cancer cells to aerobic glycolysis, where this process produces lactate from glycose. This switch generally resulted from the tumor cells fast metabolism and proliferation as discussed above to meet the high energy supply. To remain the neutral intracellular pH value (7.2-7.4), cancer cells will continuously excrete the generated lactate, leaving the extracellular tumor microenvironment acidic (pH 6.5-6.9). In addition, the CO_2

produced from respiration of a surging population of cancer cells exacerbate the acidic tumor microenvironment [21, 22]. It was reported that the acidic microenvironment will induce the degradation of ECM to facilitate the migration of cancer cells.

About 20 years ago, tumors were first described as wounds that do not heal by H.F Dworak [23]. Different types of cells and some other non-cellular components, including ECM and soluble factors coexist in tumors. Cancer stem cells (CSCs) are a type of cancer cells that possess the ability of self-renewal and differentiation into any cells in the overall tumor population. They are generally quiescent, making it more resistant to chemotherapy. Thus, treatment of cancer that fails to eradicate the CSCs inevitably gives rise to the tumor relapse after a chemotherapy-induced remission [24, 25]. By targeting both tumor bulks cells and CSCs, we can expect a more effective cancer therapy that reduce the risk of relapse and metastasis.

Cancer-associated fibroblasts are another type of predominant cells in tumors, which originate from normal cells that closely interact with tumor cells [26, 27]. They are responsible for the synthesis of a variety of components in ECM, including fibronectin, collagen and some proteases for ECM remodeling [28, 29]. In order to construct friendly microenvironment for the rapid tumor growth, cancer-associated fibroblasts synthesized and secrete various factors, including vascular endothelial growth factor (VEGF), fibroblast-activation proteins (FAP) and α-smooth-muscle actin (α-SMA), etc., which are found to be critical for tumor angiogenesis and metastasis [28, 30, 31]. Therefore, the therapeutic intervention for targeting both cancer-associated fibroblasts and cancer cells are promising in antitumor therapy.

Infiltrating inflammatory cells that exhibit pro-tumorigenic phenotype also exist in the tumor microenvironment, including macrophages, lymphocytes, leukocytes, neutrophils and dendritic cells [9, 32]. They are shown to favor angiogenesis, lymphocytes function inhibition, the tumor growth, and metastasis by producing multiple cytokines, chemokines and enzymes (matrix metalloproteinases (MMPs), cysteine cathepsin proteases) [33]. These cells can not only survive in

hypoxic tumor microenvironment, but also take part in the formation of the hypoxic tumor microenvironment by overproduction of reactive oxygen species (ROS) that acts through NF-kB signaling pathway [34]. With its contribution to the establishment of an inflammatory milieu, tumors are well nourished and rapidly expanded.

Endothelial cells and pericytes play an important role in supporting high amount of oxygen and nutrients for tumor growth as they mainly compose the blood vessels [35]. Tumor growth necessitates angiogenesis and prolongation of the pre-existing capillaries, which is mediated by the proliferation and migration of endothelial cells. Pericytes that surround the outer side of blood vessels are structural support for endothelial cells [36, 37]. Due to the high demand of blood supply in tumors, blood vessels are formed at a relatively high speed. As a result, the balance between pericytes and endothelial cells may be impaired, giving rise to malformed vasculature with gaps for EPR effect [38, 39].

Besides the cells, non-cellular components in the tumor microenvironment also contribute to the controlled outgrowth of tumors. ECM is a well-organized network constituted by a large variety of matrix macromolecules, such as collagens, elastin, fibronectin (FN), laminins, glycoproteins, proteoglycans [40-42]. Interstitial ECM and pericellular ECM are the 2 main types of ECMs. The basement membrane is one of pericellular ECM that hold the parenchyma and connective tissue together, preventing them from ripping apart [43]. In addition to providing support, ECM also segregates tissue from one another and regulates intercellular communication (cell crosstalk). The porous, relaxed and relative “soft” ECM creates a favorable environment for tumor cells and stromal cells [41].

MMPs are a group of zinc-dependent endopeptidases that participate in a variety of physiological processes [44, 45] . They are shown to mediate the ECM degradation, thus breaking down the histological barrier of the basement membrane and resulting in the cancer cell invasion and metastasis. Recent insights gained by MMPs regulated processes demonstrate that MMPs affect growth signals, regulate apoptosis and involve in tumor angiogenesis [46].

Integrins are the cell membrane receptors that are highly expressed on multiple cells in tumors [47]. They act to anchor cells by mediating adhesion of cells through its two subunits (αv and βv) by linking cytoskeleton with ECMs. Integrins can bidirectionally signal the information either from ECM to cell interior (outside-in) or from cell interior to the outside of tumor cell (inside-out). Until today, several integrins are identified with tumor initiating and promoting ability [48, 49].

Meanwhile, chemokines, cytokines and other soluble factors overexpressed by tumors cell and other types of cells act on a series of signaling pathways by binding to their relating receptors [50-52]. Transforming growth factor-β (TGF-β) induces the epidermal to mesenchymal transition (EMT), promoting tumor metastasis [53]. As discussed above, the overproduction of VEGF and fibroblast growth factor (FGF) also stimulates tumor angiogenesis [54]. The secretion of IL-10 by the tumor-associated macrophages (TAMs) can inhibit lymphocyte functions for immune escape [9].

To this end, and the non-cellular components constitute a supporting scaffold for the tumor growth as well as expansion.

1.2 Current Managements of Cancer

Current therapeutic strategies of solid tumors include surgery, chemotherapy, radiation, immunotherapy, laser therapy, etc. Surgery and radiation are valuable tools, but only applicable to the local non-metastatic cancer. As desirable treatments for cancer need to spread over to every corner of human bodies, drugs including small molecules and macromolecules (DNAs, RNAs, peptides and proteins) and immune-mediated therapy become fascinating to scientists. Chemotherapy is old but still a dominant approach to intervene the tumor progression. It was first applied for tumor treatment about 70 years ago when scientists observed tumor regression after the administration of the nitrogen mustard [55, 56]. Though effective, chemotherapy still has some notorious side effects such as nausea, diarrhea and alopecia due to indiscriminate cell destruction.

Nonetheless, chemotherapy evolved to effective treatments for both of hematological cancers and solid tumors, with the successive approval of a series of chemotherapeutic agents by Food and Drug administration (FDA) such as antifolate drugs, methotrexate, paclitaxel and cisplatin because it was once for many years only approach for metastatic cancer [57-59]. Thus, many efforts were devoted to discovering more potent drug candidates, among which a few drugs were approved since many of them failing to meet the Lipinski's rule of five, within which the moderate solubility requirement inhibits the further application of many of potent drug candidates. Immunotherapy has long been pursued and is recently emerging as a very promising method to treat tumors. It stimulates and improves the host own immune system to fight tumors with the stunning positive results for the antibody application of anti-programed death (anti-PD1) and anti-cytotoxic T lymphocyte antigen 4 (anti-CTLA-4) in humans [60-64]. Despite the encouraging advances achieved in immunotherapy today, the chemotherapeutic drugs are still the mainstay of most cancer treatments by dominating the pharmaceutical market due to low cost, wide range of application, relatively mild side effects, etc. Gene therapy is another potential and fascinating strategy to treat tumors by counteracting or replacing malfunctioning genes within the cell because its fundamental goal is to modulate the mutated gene expression of specific cells which are the root for the progression of tumors [65, 66]. However, hurdles to realize this concept that sounds simple are dauting when are put into practice. Genes must travel across multiple complex tissue, blood vessel and cellular barriers to deliver the new genetic information to target cells, which accordingly overexpress specific molecules to correct the abnormal conditions without disrupting essential cellular activities. In order to sustain the benefits of gene therapy, the cells, being able to transmit the gene correction to their daughter cells that possess same ability as parent cells, must proliferate to a certain large number, escape capture by immune system and survive in a long term [66]. In this case, drawbacks that are known for gene therapy need to be overcome. For example, given the low transfection efficiency due to large size and negative charge of these macromolecules, the introduction of them to the interior of cells for implementing their function needs mediating by viruses [67]. The immunogenicity can be

overcome by complexing with non-viral large molecules [67]. Chemical modification can be used to improve the stability and enhance the selectivity of genes. [68, 69]. In spite of the challenges, a small interfering RNA-based drug named Patisiran was approved by FDA in 2018 for the treatment of polyneuropathy in people with hereditary transthyretin-mediated amyloidosis, which seems to bring a flourish spring in the development of gene therapy by non-viral delivery system that is less problematic than viruses [70].

Though effective and promising, chemotherapy, immunotherapy and gene therapy are either toxic and mortal or non-specific. Therefore, highly selective and effective therapeutic strategies to improve cancer treatments are highly desirable.

1.3 Nano-Sized Drug Delivery Systems

Nano-sized drug delivery systems (NDDS) provide an alternative approach to resolve the problems facing by the aforementioned therapies. NDDS are generally thermodynamically stable nanoscale delivery systems, with a size less than 200 nm for better penetration as well as avoidance the recognition of mononuclear phagocyte system (MPS) and reticulo-endothelial system (RES) when traveling in bloodstream [71, 72], and are capable of loading chemotherapeutic agents (small molecule drugs) or macromolecules (genes, peptides and proteins) into their core [73]. From this perspective, NDDS not only solve drug related problems by solubilizing the hydrophobic but potent drug candidates and complexing with genes to avoid the use of virus that can cause potential carcinomas and immunogenicity, but also improve the pharmacokinetic profiles of the drugs via protecting drugs from fast degradation, reducing the renal clearance and thus prolonging the blood half-life of the drugs [74, 75]. The heterogeneity of tumors undoubtfully does not allow a “one -fits -all” approach that one nanomedicine can be applied in various cancers. NDDS are nevertheless a wonderful and versatile delivery platform that can be customized to successfully overcome complex physiological barriers to tumors and further effectively transport into the cells [76]. Given the “leaky” property of vasculature and lack of lymphatic drainage in tumors, NDDS can

preferentially accumulate in the diseased sites via EPR effect, resulting in regionally much higher concentration of biologically active drugs than in normal tissues, thus as an indirect approach reducing system toxicity of the free drugs [39, 77]. Active targeting can also be achieved by attaching either natural or synthetic ligands of specific receptors overexpressed on the tumor cells onto the surface of the nano-sized particles, such as small molecules, antibodies, or their fragments, peptides and growth factors [78].

In addition to the application of therapeutic delivery, NDDS can also be developed for diagnostic purpose, where the NDDS allow the detection in molecular scale for the identification of abnormalities including disease markers, precancerous cells and fragments of viruses. In the following section, we will mainly focus on the therapeutic application of NDDS.

NDDS are mainly composed of either polymer-therapeutic molecules conjugates (small molecule drug, gene, peptides and proteins) with chemical bond linkage between the polymers and therapeutic molecules, or particulate drug carriers with the therapeutic agents physically loaded within the assemblies of different structures made from polymers (micelles, dendrimers and nanoparticles), lipids (liposomes), metals (gold, Fe_2O_3, and MnO_2), silica and organometallic compounds (carbon nanotubes) [79, 80]. Several of them have been approved for clinical use, such as Doxil, Abraxane, Marqibo, MM-398.

1.4 Smart Delivery of Drugs and Genes

Given the improvement of pharmacokinetic profile and aqueous solubility of therapeutic agents brought by NDDS， NDDS are promising in taking conventional therapies to a new era and it should be, nonetheless, noted that current NDDS are still far from optimal with respect to unwanted release profile being slow or fast and low cellular uptake as a result of pegylation for long blood circulation, etc.

Being pioneered in the 1970s, there has always been a growing interest in developing smart NDDS with the ability to either spatially (at the target site) and/or temporally (at the right time) release drugs and genes or interaction with biological objects in response to the biological stimuli (pH, redox potential, reactive oxygen, glucose and specific enzyme) or external triggers (magnetic field, temperature, light and ultrasound), as cancers exhibit evident variations in these physiological parameters, rendering them fascinating targets for the design of smart NDDS.

The development of smart NDDS can be a construction process that different functional motifs with biological sensitivities are built together into formulations using appropriate methodologies. We next describe the up-to-date strategies of tailoring these stimuli-responsive biomaterials to meet the current need for nanomedicine advance and clinic translation and their application in controlled release for the treatment of cancer.

1.4.1 pH

Enlightened by the slightly acidic environment in tumor microenvironment (pH 6.5-7.0), acidic intracellular compartments with a pH of 5-6.5 in endosomes and a pH of 4.5-5 in lysosomes, a variety of pH sensitive NDDS have been developed for the controlled release of loaded contents, with physical or chemical changes of swelling, shrinking, dissociation and degradation. Protonation of ionizable groups or the degradation of acid labile bonds compose 2 main categories of pH sensitivity.

One example is the incorporation of tertiary amines in polymethacrylate to precisely target the acidic endocytic compartments (endosomes and lysosomes). With different pendent tertiary amine as ionizable groups to impart pH sensitivity, the polymer formed micelles fast and ultra-sensitively responded to different pH values ranging from 5 to 8 [81]. In light of this, several isopropylaminoethanol containing drug delivery systems with a pKa of 6.5 were developed for cancer treatment via phototherapy in combination with chemotherapy [82, 83]. By involvement of another cationic polymer, pH sensitive NDDS can be achieved for gene therapy [84-86]. Besides,

the acidic tumor microenvironment was also been exploited for drug delivery development. By the introduction of 2-(hexamethyleneimino)ethanol to poly(methacrylic acid) (p(HMEMA), the micelles made from this polymer has a pKa of 6.8~6.9, making them water soluble when accumulating in tumors, thus exposing the cargo or another component of the micelles. By using this strategy, endocytosis of siRNA was significantly improved via exposure the siRNA-TCPA complexes for targeting the overexpressed integrins on HeLa cells [87]. Another two studies showed that the size change of nanoparticles of 80-90 nm due to fast response of p(HMEMA) to tumor microenvironment mediated deep tumor penetration of the resulting smaller nanoparticles (10 nm) for targeting cancer cells and selective release of BLZ-945 in the tumor microenvironment for depletion of TAM [88, 89].

In addition to ionizable p(HMEMA), the cleavage of amide bonds inside the acidic tumor microenvironment was also used to site-specifically release the small size prodrug from dendrimer conjugated platinum prodrug nanoparticles to kill cancer cells in both periphery and center of tumor [90]. The resulting amine group after hydrolysis in tumor microenvironment can also help increase the endocytosis of micelles due to its positive charge under philological conditions.

1.4.2 Redox potentials

High redox potential at tumor tissue and cellular level have been widely exploited for development of NDDS, with the concentration of glutathione (GSH) in the cytosol and nuclei of cancer cells (0.5-10 mM) are 100-1000 times higher than in body fluid including blood and extracellular milieu (2-20 μM). It was also reported that the highly hypoxic region within tumors contains a minimum amount of GSH that is 4-fold higher than normal tissues [91].

The disulfide bonds are cleaved in the presence of GSH, especially at high level. The resulting thiols can reversely form the disulfide bonds under oxidative conditions. There are a wide variety of studies that take advantage of this phenomenon to design smart NDDS for intracellular drug

release. The redox responsive materials that NDDS use are often built in with disulfide bond containing linkers either between therapeutic agents and polymers or between blocks within polymer backbone. For example, the insert of a disulfide containing linker between PEG and polycation segment increased the gene transfection effect because the detachment of PEG reduced the steric repulsion favoring the entry of cellular polyanions [92]. Some other PEG sheddable drug delivery systems for cancer treatment were also developed [93, 94]. For drug conjugation, the incorporation of disulfide containing linker between therapeutic agents and polymer not only solves the undesirable burst release mostly faced by NDDS in which cargo is physically encapsulated, but also achieves site specifically drug/gene release, rendering it an appealing strategy for the design of NDDS [95-100]. Disulfide containing linkers can be used as a cross-linker stabilize nanoparticles [101-104]. The introduction of the disulfide bonds can be either direct incorporation of small molecules with disulfide bonds, reduction of cyclic disulfide bonds or thorough oxidation of thiols by oxidizing agents (O_2). In addition to induced collapse of NDDS or controlled drug release by cleavage of disulfide bond, the consumption of GSH by disulfide bond rich dendrimer can lead to significant increase of ROS level for fighting cancer [105]. Recently, researchers found cell penetration poly(disulfides) could assist the intercellular delivery of NDDS with rapid cellular uptake, minimal cytotoxicity and efficient degradation by GSH [106].

In addition, Au-S bond constitutes another category of chemical bonds that respond to GSH. It is stable under physiological conditions, but bond forming thiol atom can be replaced by free thiols, In a study, drugs with thiol group were conjugated to PAMAM encapsulated gold nanoparticles via Au-S bond and released by the treatment of GSH [107].

The overproduction of ROS is another typical disease hallmark in tumor tissue and tumor cells [108-110]. ROS, including superoxide, hydroxyl radical, hypochlorite ion, hydrogen peroxide, singlet oxygen, etc., are often produced in mitochondria, endoplasmic reticulum (ER) and plasma membrane by NADPH oxidase. The generated ROS participates in multiple biological processes, such as the regulation of proteins and cell signaling, hormone synthesis, cell proliferation and

inflammation mediation. However, the overproduction of ROS can cause the oxidation of proteins and mutation of DNA, thus often accompanying the development of tumor. As a result, the abundant ROS can be treated as a target of tumor or a marker that is distinct from its surrounding normal tissues. This abnormality in tumors inspired researchers to design the site selective NDDS based on this unbalanced ROS levels.

Similar to the development of redox responsive NDDS by incorporation of disulfide bonds and Au-S bond, etc., the sensitivity of NDDS to ROS can be conferred by the introduction of arylboronic acids, thioketal, thioether, proline esters and some other chemical bonds [111, 112]. For example, a polyprodrug was successfully synthesized through thioketal linkage. Upon oxidation by oxidants, polyprodrug in NDDS was degraded and released the relevant parent drug, causing tumor regression [113]. A polymer consisting of polypeptide with pendant arylboronic acids exhibited high drug loading capability for alkyl amine containing drugs and rapidly released the encapsulated DOX at oxidative environment [114]. Furthermore, a variety of ROS responsive gene and/or drug NDDS with arylboronic aids and quaternary amines were developed to treat cancer [115, 116].

Diselenide linkage is another attractive and special motif to be used in the development of smart NDDS, in which diselenide bonds not only react to reductants but also exhibit high sensitivity to oxidants. Compared to disulfide bond, diselenide bond is more sensitive to redox cleavage due to its lower bond energy (172 kJ/mol vs 268 kJ/mol). Thus, similar approaches used in the design of redox responsive NDDS with disulfide bonds can also be applied in gene therapy and chemotherapy [117]. In a recent study, camptothecin (CPT) and doxorubicin (DOX) were released from the nanoparticle in a controlled manner with the reduction of diselenide bond in cross-linker in tumor's redox microenvironment [118]. NDDS with sheddable PEGs linked by diselenide linkage was also constructed to controlled docetaxel (DTX) release [119].

In addition, the diselenide bonds insides NDDS exhibit high sensitivity to oxidants. By treating cross-linked micelles with diselenide bonds containing linkers to tumor mice, the micelles dissembled and released the encapsulated DOX upon the cleavage of diselenide bonds in ROS abundant tumor regions, resulting in suppression of tumor growth [120].

1.4.3 Enzymes

Given the important role of enzymes in various biological process, targeting the enzyme dysregulation has attracted considerable attention in the development of NDDS. For example, ester bonds are often constructed into delivery systems because they subject to enzymatic digestion while are relatively stable under philological conditions. By targeting abundant esterase in tumor cells, charge reversal gene delivery systems were developed, resulting from generation of the pendent negatively charged carboxylic acids after the cleavage of ester bonds [121, 122]. In addition, azobenzene linkers are also exploited by researcher for controlled drug release by oxidoreductase enzymes in the hypoxic tumor environment [123].

MMPs are the enzymes that are overexpressed within tumors and responsible for various tumor processes and hydrolysis of specific amide bonds. A number of NDDS that respond to MMPs were developed, generally with built-in MMP cleavable structures in materials capable of loading and releasing cargos to perform their function. Sizes of NDDS affect the tumor penetration [124, 125]. Being degraded by MMPs after accumulation of multistage quantum dot (QD)-covered gelatin nanoparticles in tumor, quantum dots (QD) (10 nm) was released from gelatin matrix, leading to enhancement of tumor penetration. Although a bunch of natural MMP degradable compounds are available such as collagen, gelatin and fibrinogen, their application in drug delivery are limited due to the big size. Synthetic short-sequence peptides emerge as potential candidates as a result of their small size [126]. As discussed above, prolonging blood circulation time of NDDS by pegylation brings a cost of reduced cellular uptake due to poor interaction between tumor cells and NDDS. A design for polymeric NDDS that utilized the MMP-sensitive linker inserted between PEG and

hydrophobic blocks served the purpose to increase the cellular uptake of related NDDS. Upon accumulation in tumors, de-pegylation occurred on account of the cleavage of MMP-sensitive linkers by the ubiquitous MMPs, contributing to a subsequent improved cellular uptake [127, 128].

Cathepsins are another class of overexpressed lysosomal cysteine proteases in tumors [129]. To target the tumors, drugs are generally conjugated to polymers (including HPMA, PEGylated dendrimer) with a short peptide linker (GFLG) to avoid burst release and selectively release upon uptake by cathepsin-ample cancer cells [130, 131].

1.4.4 Temperature

Amphiphilic polymers that exhibit temperature sensitivity with a lower critical solution temperature (LCST) constitute one of the categories for the development of smart NDDS. These polymers are solubilized in aqueous solution when the environmental temperature is below their LCST but undergo abrupt phase transition that hydrophobically collapse and aggregates at temperature higher than their LCST, or vice versa. By sophistically tuning the LCST of polymers to be greater than the body temperature and lower than the temperature of heated tumors ($T \approx 42\ ^{o}C$), thermal targeting of tumors can be achieved [132].

One of the most used temperature sensitive polymers is poly(N-isopropylacrylamide) (PNIPAAm), with an adjustable LCST ranging from 32 ^{o}C to even higher than 45 ^{o}C by incorporation of hydrophobic motifs. Its application in drug delivery was first proposed in the 1980s [133, 134]. The thermo-sensitivity of PNIPAAm was utilized as a gate for controlled release by inorganic nanotubes, with drug release at temperature > LCST due to sol-to-gel phase transition of PNIPAAm [135]. The usage of single wall nanotubes (SWNT and PNIPAAm to treat gastric cancer reported by another study worked the same way that drug was released after PNIPAAm transformed to coil structure at 37^{o}C due to the surface exposure of SWNT which was immersed in PNIPAAm solution at $T < 37^{o}C$ [136].

Elastin-like polypeptides (ELPs) are another widely used polymer system that comprise a pentapeptide sequence $(VPGXG)_n$ [132]. In contrast to full synthetic PNIPAAm, these biodegradable polymers are genetically encodable, allowing more precise control over the sequence, chain length and the number of repeated monomers in contrast to PNIPAAm. Thermal targeting was achieved by taking advantage of thermally sensitive ELPs, with more accumulation of ELP-drug conjugates in tumor compared to ELPs that do not go through phase transition [137]. Besides, an ELP depot of radiotherapeutics were formed within tumor via coacervation at temperature above its LCST, successfully delayed the tumor growth [138, 139].

1.4.5 Hypoxia

Hypoxia is closely associating with tumor progression and therapy resistance and fascinates researchers to engineer biomaterials for the development of hypoxia responsive NDDS. Enlightened by rapid conversion of nitroaromatic derivatives to hydrophilic 2-aminoimidazoles under hypoxia condition, this motif is exploited to construct hypoxia responsive NDDS for treatment of cancer: original hypoxia of tumor induced NDDS disassembly and fast release of hypoxia activated drug and initiated phototherapy caused by change of solubility in polymer due to the aforementioned conversion; the hypoxia of tumors was exacerbated by phototherapy, further accelerating the first step; cancer cells were killed by chemodrugs and produced ^1O [140]. The introduction of azobenzene between PEG and PEI also increased efficiency of siRNA delivery, resulting from the cleavage of azobenzene under hypoxia conditions [141].

1.5 Significance of Current Study

Current study will focus on the treatment of pancreatic cancer and chemo-resistant cancer. Gene delivery systems often cause severe systemic toxicity and fast clearance by RES due to high positive charge of delivery materials [142]. Hydrophobic interaction for drug loading is not always applying to every drug. For example, rubone that we used in the second project is a highly

hydrophobic drug which had a relatively low drug loading in lipid polymer that generally incorporate drugs through hydrophobic interactions. Benefiting from rapid advances in the material science [67, 143], we successfully synthesized two polymers that is either responsive to abundant ROS within tumors or acidic microenvironment and high levels of intracellular GSH for controlled drug release.

In the first work for treatment of pancreatic cancer, arylboronic acid was incorporated into the cationic polymer with quaternary amines. This polymeric delivery system exhibited high drug loading capacity for amine containing drugs through donor receptor interaction and showed good complexation with miR-34a. The simultaneously solve the co-delivery for small molecule drugs and genes without causing unwanted severe systemic toxicity that generally faced by lots of other gene delivery systems, such as PEIs.

In the second work, we aimed to treat taxane-resistant prostate cancer resulted from populated CSCs. To suppress the tumor growth, rubone was used to kill chemo-resistant CSCs and DTX was used to kill the bulk tumor cells. Given the difficulty in loading rubone, we used conjugation strategy to addresses low loading of rubone. By incorporation of a disulfide containing linker between rubone and the polymer, GSH responsive drug release was achieved. The pendent ionizable isopropylaminoethyl groups confer the polycarbonate with pH sensitivity. When endocytosed into acidic endocytic compartments by cancer cells, the micelles were capable of rapidly releasing the encapsulated DTX and conjugated rubone, maximizing the potential of tumor treatment by overcoming the notorious chemoresistance and minimizing the possibility of induced chemo-resistance due to slow drug release.

By taking advantage of chemotherapy as well as gene therapy, current study successfully inhibited the tumor growth by using stimuli responsive NDDS.

1.6 References

[1] F. Bray, J. Ferlay, I. Soerjomataram, R.L. Siegel, L.A. Torre, A. Jemal, Global cancer statistics 2018: GLOBOCAN estimates of incidence and mortality worldwide for 36 cancers in 185 countries, CA Cancer J Clin, 68 (2018) 394-424.

[2] G.S. Stein, A.B. Pardee, Cell cycle and growth control: biomolecular regulation and cancer, John Wiley & Sons2004.

[3] C.J. Van Noorden, L.C. Meade-Tollin, F.T. Bosman, Metastasis: the spread of cancer cells to distant sites implies a complex series of cellular abnormalities caused, in part, by genetic aberrations, American scientist, 86 (1998) 130-141.

[4] P.M. Pollock, P.S. Meltzer, Lucky draw in the gene raffle, Nature, 417 (2002) 906-907.

[5] D. Hanahan, R.A. Weinberg, Hallmarks of cancer: the next generation, Cell, 144 (2011) 646-674.

[6] C.M. Croce, Oncogenes and cancer, N Engl J Med, 358 (2008) 502-511.

[7] U. Krug, A. Ganser, H.P. Koeffler, Tumor suppressor genes in normal and malignant hematopoiesis, Oncogene, 21 (2002) 3475-3495.

[8] C. Lengauer, K.W. Kinzler, B. Vogelstein, Genetic instabilities in human cancers, Nature, 396 (1998) 643-649.

[9] T. Whiteside, The tumor microenvironment and its role in promoting tumor growth, Oncogene, 27 (2008) 5904.

[10] A. Marusyk, K. Polyak, Tumor heterogeneity: causes and consequences, Biochim Biophys Acta, 1805 (2010) 105-117.

[11] R.A. Burrell, N. McGranahan, J. Bartek, C. Swanton, The causes and consequences of genetic heterogeneity in cancer evolution, Nature, 501 (2013) 338-345.

[12] N.C. Turner, J.S. Reis-Filho, Genetic heterogeneity and cancer drug resistance, The lancet oncology, 13 (2012) e178-e185.

[13] V. Catalano, A. Turdo, S. Di Franco, F. Dieli, M. Todaro, G. Stassi, Tumor and its microenvironment: a synergistic interplay, Seminars in cancer biology, Elsevier, 2013, pp. 522-532.

[14] A. Eberhard, S. Kahlert, V. Goede, B. Hemmerlein, K.H. Plate, H.G. Augustin, Heterogeneity of angiogenesis and blood vessel maturation in human tumors: implications for antiangiogenic tumor therapies, Cancer Res, 60 (2000) 1388-1393.

[15] D. Neri, R. Bicknell, Tumour vascular targeting, Nat Rev Cancer, 5 (2005) 436-446.

[16] S.K. Hobbs, W.L. Monsky, F. Yuan, W.G. Roberts, L. Griffith, V.P. Torchilin, R.K. Jain, Regulation of transport pathways in tumor vessels: role of tumor type and microenvironment, Proceedings of the National Academy of Sciences, 95 (1998) 4607-4612.

[17] R.K. Jain, Transport of molecules, particles, and cells in solid tumors, Annual review of biomedical engineering, 1 (1999) 241-263.

[18] R.G. Bristow, R.P. Hill, Hypoxia, DNA repair and genetic instability, Nat Rev Cancer, 8 (2008) 180-192.

[19] J.M. Brown, W.R. Wilson, Exploiting tumour hypoxia in cancer treatment, Nature Reviews Cancer, 4 (2004) 437.

[20] Q. Ke, M. Costa, Hypoxia-inducible factor-1 (HIF-1), Molecular pharmacology, 70 (2006) 1469-1480.

[21] Y. Kato, S. Ozawa, C. Miyamoto, Y. Maehata, A. Suzuki, T. Maeda, Y. Baba, Acidic extracellular microenvironment and cancer, Cancer cell international, 13 (2013) 89.

[22] A. Karuri, E. Dobrowsky, I. Tannock, Selective cellular acidification and toxicity of weak organic acids in an acidic microenvironment, British journal of cancer, 68 (1993) 1080.

[23] H.F. Dvorak, Tumors: wounds that do not heal, New England Journal of Medicine, 315 (1986) 1650-1659.

[24] C.T. Jordan, M.L. Guzman, M. Noble, Cancer stem cells, New England Journal of Medicine, 355 (2006) 1253-1261.

[25] M.F. Clarke, M. Fuller, Stem cells and cancer: two faces of eve, Cell, 124 (2006) 1111-1115.

[26] N. Erez, M. Truitt, P. Olson, D. Hanahan, Cancer-associated fibroblasts are activated in incipient neoplasia to orchestrate tumor-promoting inflammation in an NF-κB-dependent manner, Cancer cell, 17 (2010) 135-147.

[27] M. Augsten, Cancer-associated fibroblasts as another polarized cell type of the tumor microenvironment, Frontiers in oncology, 4 (2014) 62.

[28] O.E. Franco, A.K. Shaw, D.W. Strand, S.W. Hayward, Cancer associated fibroblasts in cancer pathogenesis, Seminars in cell & developmental biology, Elsevier, 2010, pp. 33-39.

[29] A. Östman, M. Augsten, Cancer-associated fibroblasts and tumor growth–bystanders turning into key players, Current opinion in genetics & development, 19 (2009) 67-73.

[30] P. Cirri, P. Chiarugi, Cancer-associated-fibroblasts and tumour cells: a diabolic liaison driving cancer progression, Cancer and Metastasis Reviews, 31 (2012) 195-208.

[31] S. Madar, I. Goldstein, V. Rotter, 'Cancer associated fibroblasts'–more than meets the eye, Trends in molecular medicine, 19 (2013) 447-453.

[32] M. Johansson, D.G. DeNardo, L.M. Coussens, Polarized immune responses differentially regulate cancer development, Immunological reviews, 222 (2008) 145-154.

[33] B.-Z. Qian, J.W. Pollard, Macrophage diversity enhances tumor progression and metastasis, Cell, 141 (2010) 39-51.

[34] J.M. Lluis, F. Buricchi, P. Chiarugi, A. Morales, J.C. Fernandez-Checa, Dual role of mitochondrial reactive oxygen species in hypoxia signaling: activation of nuclear factor-κB via c-SRC–and oxidant-dependent cell death, Cancer research, 67 (2007) 7368-7377.

[35] D. Hanahan, J. Folkman, Patterns and emerging mechanisms of the angiogenic switch during tumorigenesis, cell, 86 (1996) 353-364.

[36] A. Raza, M.J. Franklin, A.Z. Dudek, Pericytes and vessel maturation during tumor angiogenesis and metastasis, American journal of hematology, 85 (2010) 593-598.

[37] R.S. Kerbel, Tumor angiogenesis, New England Journal of Medicine, 358 (2008) 2039-2049.

[38] J. Fang, H. Nakamura, H. Maeda, The EPR effect: unique features of tumor blood vessels for drug delivery, factors involved, and limitations and augmentation of the effect, Advanced drug delivery reviews, 63 (2011) 136-151.

[39] V. Torchilin, Tumor delivery of macromolecular drugs based on the EPR effect, Advanced drug delivery reviews, 63 (2011) 131-135.

[40] K.Y. Tsang, M.C. Cheung, D. Chan, K.S. Cheah, The developmental roles of the extracellular matrix: beyond structure to regulation, Cell and tissue research, 339 (2010) 93.

[41] P. Lu, V.M. Weaver, Z. Werb, The extracellular matrix: a dynamic niche in cancer progression, J Cell Biol, 196 (2012) 395-406.

[42] M.W. Pickup, J.K. Mouw, V.M. Weaver, The extracellular matrix modulates the hallmarks of cancer, EMBO reports, 15 (2014) 1243-1253.

[43] A.D. Theocharis, S.S. Skandalis, C. Gialeli, N.K. Karamanos, Extracellular matrix structure, Advanced drug delivery reviews, 97 (2016) 4-27.

[44] J. Cathcart, A. Pulkoski-Gross, J. Cao, Targeting matrix metalloproteinases in cancer: bringing new life to old ideas, Genes & diseases, 2 (2015) 26-34.

[45] A. Page-McCaw, A.J. Ewald, Z. Werb, Matrix metalloproteinases and the regulation of tissue remodelling, Nature reviews Molecular cell biology, 8 (2007) 221.

[46] K. Kessenbrock, V. Plaks, Z. Werb, Matrix metalloproteinases: regulators of the tumor microenvironment, Cell, 141 (2010) 52-67.

[47] S.L. Goodman, M. Picard, Integrins as therapeutic targets, Trends in pharmacological sciences, 33 (2012) 405-412.

[48] J.S. Desgrosellier, D.A. Cheresh, Integrins in cancer: biological implications and therapeutic opportunities, Nature Reviews Cancer, 10 (2010) 9.

[49] R. Rathinam, S.K. Alahari, Important role of integrins in the cancer biology, Cancer and Metastasis Reviews, 29 (2010) 223-237.

[50] B.-C. Sheu, W.-C. Chang, C.-Y. Cheng, H.-H. Lin, D.-Y. Chang, S.-C. Huang, Cytokine regulation networks in the cancer microenvironment, Front Biosci, 13 (2008) 6255-6268.

[51] T. Tanaka, Z. Bai, Y. Srinoulprasert, B. Yang, H. Hayasaka, M. Miyasaka, Chemokines in tumor progression and metastasis, Cancer science, 96 (2005) 317-322.

[52] A. Zlotnik, Chemokines and cancer, International journal of cancer, 119 (2006) 2026-2029.

[53] M.K. Wendt, J.A. Smith, W.P. Schiemann, Transforming growth factor-β-induced epithelial–mesenchymal transition facilitates epidermal growth factor-dependent breast cancer progression, Oncogene, 29 (2010) 6485.

[54] B. Elenbaas, R.A. Weinberg, Heterotypic signaling between epithelial tumor cells and fibroblasts in carcinoma formation, Experimental cell research, 264 (2001) 169-184.

[55] R.J. Papac, Origins of cancer therapy, Yale J Biol Med, 74 (2001) 391-398.

[56] A. Gilman, The initial clinical trial of nitrogen mustard, Am J Surg, 105 (1963) 574-578.

[57] B.A. Chabner, T.G. Roberts Jr, Chemotherapy and the war on cancer, Nature Reviews Cancer, 5 (2005) 65.

[58] M.C. Li, R. Hertz, D.M. Bergenstal, Therapy of choriocarcinoma and related trophoblastic tumors with folic acid and purine antagonists, N Engl J Med, 259 (1958) 66-74.

[59] J. Goodman, V. Walsh, The story of taxol: nature and politics in the pursuit of an anti-cancer drug, Cambridge University Press2001.

[60] I. Mellman, G. Coukos, G. Dranoff, Cancer immunotherapy comes of age, Nature, 480 (2011) 480-489.

[61] A. Ribas, J.D. Wolchok, Cancer immunotherapy using checkpoint blockade, Science, 359 (2018) 1350-1355.

[62] S.A. Rosenberg, Decade in review—cancer immunotherapy: entering the mainstream of cancer treatment, Nature reviews Clinical oncology, 11 (2014) 630.

[63] P. Sharma, S. Hu-Lieskovan, J.A. Wargo, A. Ribas, Primary, Adaptive, and Acquired Resistance to Cancer Immunotherapy, Cell, 168 (2017) 707-723.

[64] M. Dougan, G. Dranoff, S.K. Dougan, Cancer immunotherapy: beyond checkpoint blockade, Annual Review of Cancer Biology, 3 (2019) 55-75.

[65] D.J. Glover, H.J. Lipps, D.A. Jans, Towards safe, non-viral therapeutic gene expression in humans, Nat Rev Genet, 6 (2005) 299-310.

[66] L. Naldini, Gene therapy returns to centre stage, Nature, 526 (2015) 351-360.

[67] H. Yin, R.L. Kanasty, A.A. Eltoukhy, A.J. Vegas, J.R. Dorkin, D.G. Anderson, Non-viral vectors for gene-based therapy, Nat Rev Genet, 15 (2014) 541-555.

[68] J.B. Bramsen, M.B. Laursen, A.F. Nielsen, T.B. Hansen, C. Bus, N. Langkjaer, B.R. Babu, T. Hojland, M. Abramov, A. Van Aerschot, D. Odadzic, R. Smicius, J. Haas, C. Andree, J. Barman, M. Wenska, P. Srivastava, C. Zhou, D. Honcharenko, S. Hess, E. Muller, G.V. Bobkov, S.N. Mikhailov, E. Fava, T.F. Meyer, J. Chattopadhyaya, M. Zerial, J.W. Engels, P. Herdewijn, J. Wengel, J. Kjems, A large-scale chemical modification screen identifies design rules to generate siRNAs with high activity, high stability and low toxicity, Nucleic Acids Res, 37 (2009) 2867-2881.

[69] A. Khvorova, J.K. Watts, The chemical evolution of oligonucleotide therapies of clinical utility, Nat Biotechnol, 35 (2017) 238-248.

[70] A. Akinc, M.A. Maier, M. Manoharan, K. Fitzgerald, M. Jayaraman, S. Barros, S. Ansell, X. Du, M.J. Hope, T.D. Madden, B.L. Mui, S.C. Semple, Y.K. Tam, M. Ciufolini, D. Witzigmann, J.A. Kulkarni, R. van der Meel, P.R. Cullis, The Onpattro story and the clinical translation of nanomedicines containing nucleic acid-based drugs, Nat Nanotechnol, 14 (2019) 1084-1087.

[71] F. Yuan, M. Dellian, D. Fukumura, M. Leunig, D.A. Berk, V.P. Torchilin, R.K. Jain, Vascular permeability in a human tumor xenograft: molecular size dependence and cutoff size, Cancer Res, 55 (1995) 3752-3756.

[72] S. Barua, S. Mitragotri, Challenges associated with Penetration of Nanoparticles across Cell and Tissue Barriers: A Review of Current Status and Future Prospects, Nano Today, 9 (2014) 223-243.

[73] D.W. Northfelt, F.J. Martin, P. Working, P.A. Volberding, J. Russell, M. Newman, M.A. Amantea, L.D. Kaplan, Doxorubicin encapsulated in liposomes containing surface-bound polyethylene glycol: pharmacokinetics, tumor localization, and safety in patients with AIDS-related Kaposi's sarcoma, The Journal of Clinical Pharmacology, 36 (1996) 55-63.

[74] D. Peer, J.M. Karp, S. Hong, O.C. Farokhzad, R. Margalit, R. Langer, Nanocarriers as an emerging platform for cancer therapy, Nature nanotechnology, 2 (2007) 751.

[75] M.E. Davis, Z.G. Chen, D.M. Shin, Nanoparticle therapeutics: an emerging treatment modality for cancer, Nat Rev Drug Discov, 7 (2008) 771-782.

[76] R.A. Petros, J.M. DeSimone, Strategies in the design of nanoparticles for therapeutic applications, Nat Rev Drug Discov, 9 (2010) 615-627.

[77] A.K. Iyer, G. Khaled, J. Fang, H. Maeda, Exploiting the enhanced permeability and retention effect for tumor targeting, Drug discovery today, 11 (2006) 812-818.

[78] F. Danhier, O. Feron, V. Préat, To exploit the tumor microenvironment: passive and active tumor targeting of nanocarriers for anti-cancer drug delivery, Journal of controlled release, 148 (2010) 135-146.

[79] A. Wicki, D. Witzigmann, V. Balasubramanian, J. Huwyler, Nanomedicine in cancer therapy: challenges, opportunities, and clinical applications, J Control Release, 200 (2015) 138-157.

[80] L. Zhang, F.X. Gu, J.M. Chan, A.Z. Wang, R.S. Langer, O.C. Farokhzad, Nanoparticles in medicine: therapeutic applications and developments, Clin Pharmacol Ther, 83 (2008) 761-769.

[81] K. Zhou, Y. Wang, X. Huang, K. Luby-Phelps, B.D. Sumer, J. Gao, Tunable, ultrasensitive pH-responsive nanoparticles targeting specific endocytic organelles in living cells, Angewandte Chemie International Edition, 50 (2011) 6109-6114.

[82] D. Wang, T. Wang, J. Liu, H. Yu, S. Jiao, B. Feng, F. Zhou, Y. Fu, Q. Yin, P. Zhang, Acid-activatable versatile micelleplexes for PD-L1 blockade-enhanced cancer photodynamic immunotherapy, Nano letters, 16 (2016) 5503-5513.

[83] H. Yu, Z. Cui, P. Yu, C. Guo, B. Feng, T. Jiang, S. Wang, Q. Yin, D. Zhong, X. Yang, pH- and NIR light-responsive micelles with hyperthermia-triggered tumor penetration and cytoplasm drug release to reverse doxorubicin resistance in breast cancer, Advanced Functional Materials, 25 (2015) 2489-2500.

[84] T. Wang, D. Wang, H. Yu, M. Wang, J. Liu, B. Feng, F. Zhou, Q. Yin, Z. Zhang, Y. Huang, Intracellularly acid-switchable multifunctional micelles for combinational photo/chemotherapy of the drug-resistant tumor, ACS nano, 10 (2016) 3496-3508.

[85] X. Xu, J. Wu, Y. Liu, P.E. Saw, W. Tao, M. Yu, H. Zope, M. Si, A. Victorious, J. Rasmussen, D. Ayyash, O.C. Farokhzad, J. Shi, Multifunctional Envelope-Type siRNA Delivery Nanoparticle Platform for Prostate Cancer Therapy, ACS Nano, 11 (2017) 2618-2627.

[86] X. Xu, J. Wu, Y. Liu, M. Yu, L. Zhao, X. Zhu, S. Bhasin, Q. Li, E. Ha, J. Shi, Ultra-pH-responsive and tumor-penetrating nanoplatform for targeted siRNA delivery with robust anti-cancer efficacy, Angewandte Chemie International Edition, 55 (2016) 7091-7094.

[87] X. Xu, P.E. Saw, W. Tao, Y. Li, X. Ji, M. Yu, M. Mahmoudi, J. Rasmussen, D. Ayyash, Y. Zhou, O.C. Farokhzad, J. Shi, Tumor Microenvironment-Responsive Multistaged Nanoplatform for Systemic RNAi and Cancer Therapy, Nano Lett, 17 (2017) 4427-4435.

[88] H.J. Li, J.Z. Du, J. Liu, X.J. Du, S. Shen, Y.H. Zhu, X. Wang, X. Ye, S. Nie, J. Wang, Smart Superstructures with Ultrahigh pH-Sensitivity for Targeting Acidic Tumor Microenvironment: Instantaneous Size Switching and Improved Tumor Penetration, ACS Nano, 10 (2016) 6753-6761.

[89] S. Shen, H.J. Li, K.G. Chen, Y.C. Wang, X.Z. Yang, Z.X. Lian, J.Z. Du, J. Wang, Spatial Targeting of Tumor-Associated Macrophages and Tumor Cells with a pH-Sensitive Cluster Nanocarrier for Cancer Chemoimmunotherapy, Nano Lett, 17 (2017) 3822-3829.

[90] H.J. Li, J.Z. Du, X.J. Du, C.F. Xu, C.Y. Sun, H.X. Wang, Z.T. Cao, X.Z. Yang, Y.H. Zhu, S. Nie, J. Wang, Stimuli-responsive clustered nanoparticles for improved tumor penetration and therapeutic efficacy, Proc Natl Acad Sci U S A, 113 (2016) 4164-4169.

[91] P. Kuppusamy, H. Li, G. Ilangovan, A.J. Cardounel, J.L. Zweier, K. Yamada, M.C. Krishna, J.B. Mitchell, Noninvasive imaging of tumor redox status and its modification by tissue glutathione levels, Cancer research, 62 (2002) 307-312.

[92] S. Takae, K. Miyata, M. Oba, T. Ishii, N. Nishiyama, K. Itaka, Y. Yamasaki, H. Koyama, K. Kataoka, PEG-detachable polyplex micelles based on disulfide-linked block catiomers as bioresponsive nonviral gene vectors, Journal of the American Chemical Society, 130 (2008) 6001-6009.

[93] Y. Zhu, J. Zhang, F. Meng, C. Deng, R. Cheng, J. Feijen, Z. Zhong, cRGD-functionalized reduction-sensitive shell-sheddable biodegradable micelles mediate enhanced doxorubicin delivery to human glioma xenografts in vivo, J Control Release, 233 (2016) 29-38.

[94] Y. Zhu, X. Wang, J. Zhang, F. Meng, C. Deng, R. Cheng, J. Feijen, Z. Zhong, Exogenous vitamin C boosts the antitumor efficacy of paclitaxel containing reduction-sensitive shell-sheddable micelles in vivo, J Control Release, 250 (2017) 9-19.

[95] S. Yin, J. Huai, X. Chen, Y. Yang, X. Zhang, Y. Gan, G. Wang, X. Gu, J. Li, Intracellular delivery and antitumor effects of a redox-responsive polymeric paclitaxel conjugate based on hyaluronic acid, Acta Biomater, 26 (2015) 274-285.

[96] J. Liu, W. Liu, I. Weitzhandler, J. Bhattacharyya, X. Li, J. Wang, Y. Qi, S. Bhattacharjee, A. Chilkoti, Ring-opening polymerization of prodrugs: a versatile approach to prepare well-defined drug-loaded nanoparticles, Angewandte Chemie International Edition, 54 (2015) 1002-1006.

[97] F. Lin, D. Wen, X. Wang, R.I. Mahato, Dual responsive micelles capable of modulating miRNA-34a to combat taxane resistance in prostate cancer, Biomaterials, 192 (2019) 95-108.

[98] Q. Bai, J. Liu, J. Tang, Z. Li, X. Zheng, Q. Chen, Redox-Responsive Polymeric RNAi Based on Multivalent Conjugation of siRNA for Improved Intracellular Delivery, Bioconjug Chem, 30 (2019) 2777-2781.

[99] Z. Zhou, J. Tang, Q. Sun, W.J. Murdoch, Y. Shen, A multifunctional PEG–PLL drug conjugate forming redox-responsive nanoparticles for intracellular drug delivery, Journal of Materials Chemistry B, 3 (2015) 7594-7603.

[100] S.S. Dunn, S. Tian, S. Blake, J. Wang, A.L. Galloway, A. Murphy, P.D. Pohlhaus, J.P. Rolland, M.E. Napier, J.M. DeSimone, Reductively responsive siRNA-conjugated hydrogel nanoparticles for gene silencing, J Am Chem Soc, 134 (2012) 7423-7430.

[101] M. Zhao, A. Biswas, B. Hu, K.I. Joo, P. Wang, Z. Gu, Y. Tang, Redox-responsive nanocapsules for intracellular protein delivery, Biomaterials, 32 (2011) 5223-5230.

[102] J. Dai, S. Lin, D. Cheng, S. Zou, X. Shuai, Interlayer-crosslinked micelle with partially hydrated core showing reduction and pH dual sensitivity for pinpointed intracellular drug release, Angew Chem Int Ed Engl, 50 (2011) 9404-9408.

[103] K. Miyata, Y. Kakizawa, N. Nishiyama, A. Harada, Y. Yamasaki, H. Koyama, K. Kataoka, Block catiomer polyplexes with regulated densities of charge and disulfide cross-linking directed to enhance gene expression, Journal of the American Chemical Society, 126 (2004) 2355-2361.

[104] Y. Kakizawa, A. Harada, K. Kataoka, Environment-sensitive stabilization of core− shell structured polyion complex micelle by reversible cross-linking of the core through disulfide bond, Journal of the American Chemical Society, 121 (1999) 11247-11248.

[105] O.C.J. Andren, A.P. Fernandes, M. Malkoch, Heterogeneous Rupturing Dendrimers, J Am Chem Soc, 139 (2017) 17660-17666.

[106] C. Yu, L. Qian, J. Ge, J. Fu, P. Yuan, S.C. Yao, S.Q. Yao, Cell-Penetrating Poly (disulfide) Assisted Intracellular Delivery of Mesoporous Silica Nanoparticles for Inhibition of miR-21 Function and Detection of Subsequent Therapeutic Effects, Angewandte Chemie International Edition, 55 (2016) 9272-9276.

[107] X. Wang, X. Cai, J. Hu, N. Shao, F. Wang, Q. Zhang, J. Xiao, Y. Cheng, Glutathione-triggered “off–on” release of anticancer drugs from dendrimer-encapsulated gold nanoparticles, Journal of the American Chemical Society, 135 (2013) 9805-9810.

[108] D. Trachootham, J. Alexandre, P. Huang, Targeting cancer cells by ROS-mediated mechanisms: a radical therapeutic approach?, Nat Rev Drug Discov, 8 (2009) 579-591.

[109] B.C. Dickinson, C.J. Chang, Chemistry and biology of reactive oxygen species in signaling or stress responses, Nat Chem Biol, 7 (2011) 504-511.

[110] M. Diehn, R.W. Cho, N.A. Lobo, T. Kalisky, M.J. Dorie, A.N. Kulp, D. Qian, J.S. Lam, L.E. Ailles, M. Wong, B. Joshua, M.J. Kaplan, I. Wapnir, F.M. Dirbas, G. Somlo, C. Garberoglio, B. Paz, J. Shen, S.K. Lau, S.R. Quake, J.M. Brown, I.L. Weissman, M.F. Clarke, Association of reactive oxygen species levels and radioresistance in cancer stem cells, Nature, 458 (2009) 780-783.

[111] G. Saravanakumar, J. Kim, W.J. Kim, Reactive-Oxygen-Species-Responsive Drug Delivery Systems: Promises and Challenges, Adv Sci (Weinh), 4 (2017) 1600124.

[112] S.H. Lee, M.K. Gupta, J.B. Bang, H. Bae, H.J. Sung, Current progress in Reactive Oxygen Species (ROS)-Responsive materials for biomedical applications, Adv Healthc Mater, 2 (2013) 908-915.

[113] X. Xu, P.E. Saw, W. Tao, Y. Li, X. Ji, S. Bhasin, Y. Liu, D. Ayyash, J. Rasmussen, M. Huo, J. Shi, O.C. Farokhzad, ROS-Responsive Polyprodrug Nanoparticles for Triggered Drug Delivery and Effective Cancer Therapy, Adv Mater, 29 (2017).

[114] S. Lv, Y. Wu, K. Cai, H. He, Y. Li, M. Lan, X. Chen, J. Cheng, L. Yin, High drug loading and sub-quantitative loading efficiency of polymeric micelles driven by donor–receptor coordination interactions, Journal of the American Chemical Society, 140 (2018) 1235-1238.

[115] X. Xin, F. Lin, Q. Wang, L. Yin, R.I. Mahato, ROS-Responsive Polymeric Micelles for Triggered Simultaneous Delivery of PLK1 Inhibitor/miR-34a and Effective Synergistic Therapy in Pancreatic Cancer, ACS applied materials & interfaces, 11 (2019) 14647-14659.

[116] X. Liu, J. Xiang, D. Zhu, L. Jiang, Z. Zhou, J. Tang, X. Liu, Y. Huang, Y. Shen, Fusogenic Reactive Oxygen Species Triggered Charge-Reversal Vector for Effective Gene Delivery, Adv Mater, 28 (2016) 1743-1752.

[117] Y. He, Y. Nie, G. Cheng, L. Xie, Y. Shen, Z. Gu, Viral Mimicking Ternary Polyplexes: A Reduction-Controlled Hierarchical Unpacking Vector for Gene Delivery, Advanced Materials, 26 (2014) 1534-1540.

[118] S. Zhai, X. Hu, Y. Hu, B. Wu, D. Xing, Visible light-induced crosslinking and physiological stabilization of diselenide-rich nanoparticles for redox-responsive drug release and combination chemotherapy, Biomaterials, 121 (2017) 41-54.

[119] X. Zeng, X. Zhou, M. Li, C. Wang, J. Xu, D. Ma, W. Xue, Redox poly(ethylene glycol)-b-poly(L-lactide) micelles containing diselenide bonds for effective drug delivery, J Mater Sci Mater Med, 26 (2015) 234.

[120] V.G. Deepagan, S. Kwon, D.G. You, V.Q. Nguyen, W. Um, H. Ko, H. Lee, D.G. Jo, Y.M. Kang, J.H. Park, In situ diselenide-crosslinked polymeric micelles for ROS-mediated anticancer drug delivery, Biomaterials, 103 (2016) 56-66.

[121] N. Qiu, X. Liu, Y. Zhong, Z. Zhou, Y. Piao, L. Miao, Q. Zhang, J. Tang, L. Huang, Y. Shen, Esterase-Activated Charge-Reversal Polymer for Fibroblast-Exempt Cancer Gene Therapy, Adv Mater, 28 (2016) 10613-10622.

[122] N. Qiu, J. Gao, Q. Liu, J. Wang, Y. Shen, Enzyme-Responsive Charge-Reversal Polymer-Mediated Effective Gene Therapy for Intraperitoneal Tumors, Biomacromolecules, 19 (2018) 2308-2319.

[123] J. Lee, E.T. Oh, H. Yoon, C.W. Kim, Y. Han, J. Song, H. Jang, H.J. Park, C. Kim, Mesoporous nanocarriers with a stimulus-responsive cyclodextrin gatekeeper for targeting tumor hypoxia, Nanoscale, 9 (2017) 6901-6909.

[124] H. Cabral, Y. Matsumoto, K. Mizuno, Q. Chen, M. Murakami, M. Kimura, Y. Terada, M.R. Kano, K. Miyazono, M. Uesaka, N. Nishiyama, K. Kataoka, Accumulation of sub-100 nm polymeric micelles in poorly permeable tumours depends on size, Nat Nanotechnol, 6 (2011) 815-823.

[125] J. Wang, W. Mao, L.L. Lock, J. Tang, M. Sui, W. Sun, H. Cui, D. Xu, Y. Shen, The Role of Micelle Size in Tumor Accumulation, Penetration, and Treatment, ACS Nano, 9 (2015) 7195-7206.

[126] Z. Dai, Q. Yao, L. Zhu, MMP2-sensitive PEG–lipid copolymers: a new type of tumor-targeted P-glycoprotein inhibitor, ACS applied materials & interfaces, 8 (2016) 12661-12673.

[127] L. Zhu, T. Wang, F. Perche, A. Taigind, V.P. Torchilin, Enhanced anticancer activity of nanopreparation containing an MMP2-sensitive PEG-drug conjugate and cell-penetrating moiety, Proc Natl Acad Sci U S A, 110 (2013) 17047-17052.

[128] J. Li, Z. Ge, S. Liu, PEG-sheddable polyplex micelles as smart gene carriers based on MMP-cleavable peptide-linked block copolymers, Chemical Communications, 49 (2013) 6974-6976.

[129] O.C. Olson, J.A. Joyce, Cysteine cathepsin proteases: regulators of cancer progression and therapeutic response, Nat Rev Cancer, 15 (2015) 712-729.

[130] C. Zhang, D. Pan, K. Luo, W. She, C. Guo, Y. Yang, Z. Gu, Peptide Dendrimer–Doxorubicin Conjugate-Based Nanoparticles as an Enzyme-Responsive Drug Delivery System for Cancer Therapy, Advanced healthcare materials, 3 (2014) 1299-1308.

[131] X. Wei, Q. Luo, L. Sun, X. Li, H. Zhu, P. Guan, M. Wu, K. Luo, Q. Gong, Enzyme-and pH-sensitive branched polymer–doxorubicin conjugate-based nanoscale drug delivery system for cancer therapy, ACS applied materials & interfaces, 8 (2016) 11765-11778.

[132] A. Chilkoti, M.R. Dreher, D.E. Meyer, D. Raucher, Targeted drug delivery by thermally responsive polymers, Adv Drug Deliv Rev, 54 (2002) 613-630.

[133] A.S. Hoffman, 4. Poly(NIPAAm) revisited - it has been 28 years since it was first proposed for use as a biomaterial: Original research article: Applications of thermally reversible polymers hydrogels in therapeutics and diagnostics, 1987; thermally reversible hydrogels: II. Delivery and selective removal of substances from aqueous solutions, 1986; a novel approach for preparation of pH-sensitive hydrogels for enteric drug delivery, 1991, J Control Release, 190 (2014) 36-40.

[134] Y.H. Bae, T. Okano, R. Hsu, S.W. Kim, Thermo-sensitive polymers as on-off switches for drug release, Die Makromolekulare Chemie, Rapid Communications, 8 (1987) 481-485.

[135] G. Chen, R. Chen, C. Zou, D. Yang, Z.-S. Chen, Fragmented polymer nanotubes from sonication-induced scission with a thermo-responsive gating system for anti-cancer drug delivery, Journal of Materials Chemistry B, 2 (2014) 1327-1334.

[136] M. Zhou, S. Liu, Y. Jiang, H. Ma, M. Shi, Q. Wang, W. Zhong, W. Liao, M.M. Xing, Doxorubicin-loaded single wall nanotube thermo-sensitive hydrogel for gastric cancer chemo-photothermal therapy, Advanced Functional Materials, 25 (2015) 4730-4739.

[137] M.R. Dreher, W. Liu, C.R. Michelich, M.W. Dewhirst, A. Chilkoti, Thermal cycling enhances the accumulation of a temperature-sensitive biopolymer in solid tumors, Cancer Res, 67 (2007) 4418-4424.

[138] W. Liu, J.A. MacKay, M.R. Dreher, M. Chen, J.R. McDaniel, A.J. Simnick, D.J. Callahan, M.R. Zalutsky, A. Chilkoti, Injectable intratumoral depot of thermally responsive polypeptide–radionuclide conjugates delays tumor progression in a mouse model, Journal of controlled Release, 144 (2010) 2-9.

[139] J.R. McDaniel, D.J. Callahan, A. Chilkoti, Drug delivery to solid tumors by elastin-like polypeptides, Adv Drug Deliv Rev, 62 (2010) 1456-1467.

[140] C. Qian, P. Feng, J. Yu, Y. Chen, Q. Hu, W. Sun, X. Xiao, X. Hu, A. Bellotti, Q.D. Shen, Z. Gu, Anaerobe-Inspired Anticancer Nanovesicles, Angew Chem Int Ed Engl, 56 (2017) 2588-2593.

[141] F. Perche, S. Biswas, T. Wang, L. Zhu, V.P. Torchilin, Hypoxia-targeted siRNA delivery, Angew Chem Int Ed Engl, 53 (2014) 3362-3366.

[142] S. Taranejoo, J. Liu, P. Verma, K. Hourigan, A review of the developments of characteristics of PEI derivatives for gene delivery applications, Journal of Applied Polymer Science, 132 (2015).

[143] J. Shi, P.W. Kantoff, R. Wooster, O.C. Farokhzad, Cancer nanomedicine: progress, challenges and opportunities, Nat Rev Cancer, 17 (2017) 20-37.

Chapter II

ROS responsive polymeric micelles for triggered simultaneous delivery of PLK1 inhibitor/miR-34a and effective synergistic therapy in pancreatic cancer

2.1 Abstract

Ineffective drug delivery and poor prognosis are two major challenges in the treatment of pancreatic ductal adenocarcinoma (PDAC). While there is significant downregulation of tumor suppressor microRNA-34a (miR-34a), which targets many oncogenes related to proliferation, apoptosis and invasion, high expression level of Polo-like kinase 1 (PLK1) is closely associated with short survival rates of pancreatic cancer patients. Therefore, the objective is to co-deliver miR-34a mimic and small molecule PLK1 inhibitor volasertib (BI6727) using poly (ethylene glycol)-poly[aspartamidoethyl (p-boronobenzyl) diethyl ammonium bromide] (PEG-B-PAEBEA) This polymer could self-assemble into micelles of ~100 nm with 10 % drug loading of volasertib and form complex with miR-34a at the N/P ratio of 18 and higher. Combination treatment of volasertib and miR-34a displays synergistic effect and superior anti-proliferative activity along with an enhanced G2/M phase arrest and suppression of colony formation, leading to cell death due to potential c-myc targeting therapeutics. Orthotopic pancreatic tumor bearing NSG mice are scanned for fluorescence by IVIS after systemic administration of micelles encapsulating volasertib and miR-34a at doses of 5 mg/kg and 1 mg/kg, respectively. Cy5.5 concentration in plasma and major organs is determined by measuring fluorescence intensity. A significant reduction in tumor volume was observed in pharmacodynamic study with negligible systemic toxicity proved by histological evaluation. In conclusion, PEG-B-PAEBEA micelles carrying volasertib and miR-34a mimic provide strong potential on pancreatic cancer treatment by improving drug delivery behaviors.

2.2 Introduction

Pancreatic ductal adenocarcinomas (PDAC) is one of the most aggressive cancers, where 85% of patients have metastatic disease making surgical interventions ineffective. High mortality of pancreatic cancer patients are due to late-stage prognosis and development of chemoresistance upon prolonged treatment with chemotherapeutic drug(s) [1]. Gemcitabine is the first line Food and Drug Administration (FDA) approved drug used alone or in combination with others to

improve the quality and lifespan of PDAC patient [2]. However, pancreatic tumors present a complex and highly obstructive microenvironment that is characterized by dysregulation of miRNAs and development of chemoresistance [3]. Alteration of miRNA expression and replenishment of anticancer miRNAs may effectively restore chemosensitivity by decreasing the expression of essential genes involved in cell growth or survival [4]. Meanwhile, polo-like kinase 1 (PLK1) emerges as a promising target due to the mediation of gemcitabine resistance and regulation of mitosis [5, 6].

MicroRNAs (miRNAs) are 17-25 nucleotides long and highly conserved and non-coding RNA products, play critical roles in the regulation of drug resistance, cancer stem cell (CSC) proliferation and cancer metabolism [7, 8]. The advantage of miRNAs lies in their ability to modulate multiple cellular pathways simultaneously, which is difficult to be accomplished using small molecules and therapeutic proteins [9]. Cellular stimuli, glucose level, and hypoxia critically orchestrate miRNA activity in various pathologies, including pancreatic cancer [10]. Among many miRNAs, miR-34a is downregulated in PDAC patients and has a key role in chemosensitization [11]. Increase in miR-34a expression level contributes to the suppression of Bcl-2, a well-known anti-apoptotic gene, leading to decrease in migration, invasion and proliferation, and enhancement in apoptosis of tumor cells [12, 13], thereby overcome drug resistance and treat PDAC more efficiently.

Polo-like kinase 1 (PLK1) plays a key role in mitosis and meiosis, and its overexpression has been found in various cancer types, including pancreatic cancer. Moreover, higher PLK1 expression correlates with tumor aggressiveness and a poor prognosis. Therefore, PLK1 is an attractive target for treating pancreatic cancer. Recently, several PLK1 inhibitors, including volasertib and GSK461364, have been investigated in various cancers. Volasertib is an ATP-competitive kinase inhibitor with higher potency and selectivity than those of its predecessor, BI 2536. Treatment with volasertib[14] results in the inhibition of G2/M cell cycle arrest in cancer cells [15, 16]. Most importantly, combination treatment with Bcl-2 and PLK1 inhibitors specifically

induces synergistic cell death due to the depletion of c-myc, a common target miR-34a and PLK1 [17]. Here, we hypothesized that combination of miR-34a and volasertib could synergistically and effectively treat PDAC.

Considering the challenges that miRNAs and hydrophobic drugs face, including off-target effects, low transfection efficiency, poor aqueous solubility and burst release, recent efforts have been focused on developing nanocarriers for delivery of both of miRNAs and hydrophobic drugs [18]. Compared with conventional drug delivery systems which have poor bioavailability, adverse side effects and low therapeutic indices [19], polymeric nanoparticle delivery systems have generated considerable commercial and translational attention due to their potential for extended drug release kinetics and enhanced stability [20]. Cationic polymers and lipids are widely used for miRNA delivery [21, 22]. Unfortunately, the highly positive charge systems with high density of amines will generate severe and intense toxicity, impeding their clinical translation.

We previously reported methoxy poly(ethylene glycol)-*block*-poly(2-methyl-2-carboxyl-propylene carbonate-*graft*-dodecanol-*graft*-tetraethylene pentamine) (mPEG-b-PCC-g-DC-g-TEPA) conjugated polycarbonate-based polymer for co-delivery of miRNA and small molecules with high drug loading and efficient complex formation with miRNA for treating type I diabetes and pancreatic cancer [23-25]. However, the polymer synthesis requires multiple steps, and polycarbonate is subjected to degradation when being modified under alkali condition. Non-specific hydrophobic interactions between the drug and polymer often lead to drug aggregation and decrease in drug-loading [26]. Moreover, the intracellular dissociation and release of miRNAs and drugs from delivery systems is well-known to be the prerequisite for effective transfection and therapy, whereas miRNA/polymer complexes are thermodynamically unstable and the drug-polymer conjugates linked with chemical bonds are even more resistant to release cargos under physiological environment. Therefore, it is highly desirable to develop a nanocarrier that can not

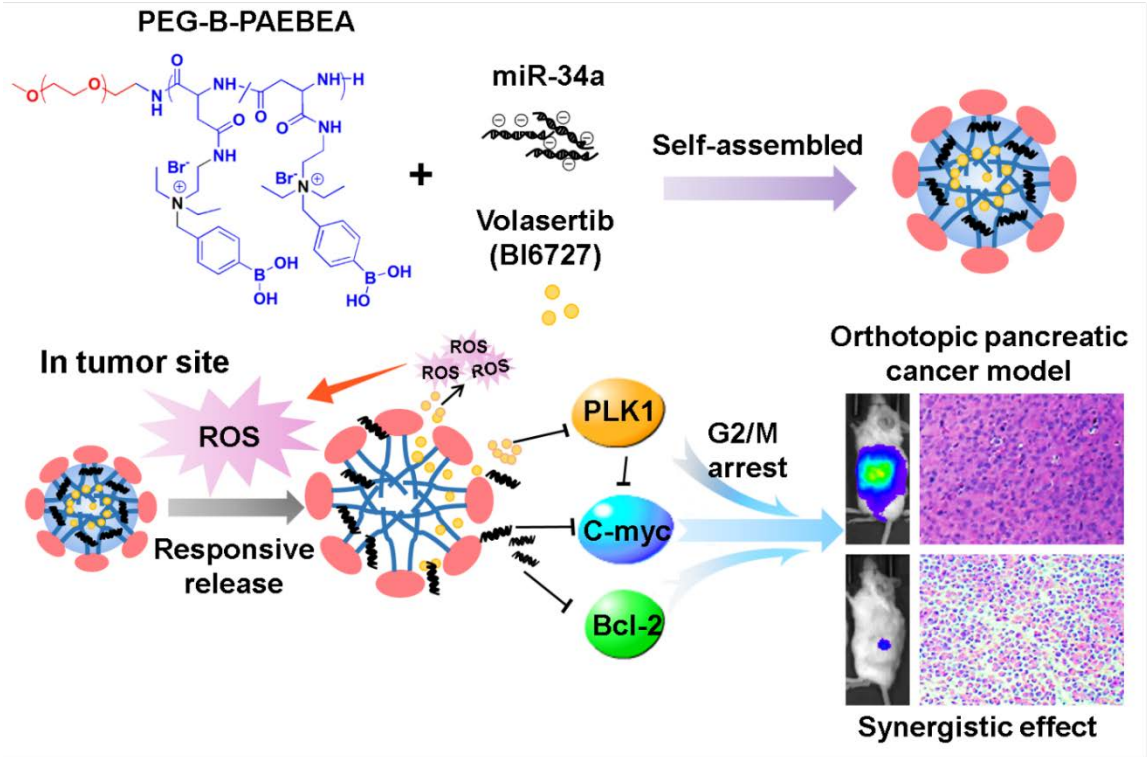

Figure 2.1 Illustration of combination therapy of small molecule PLK1 inhibitor and microRNA-34a in pancreatic cancer.

only co-load both gene and drugs, but also effectively dissociate and rapidly release the cargos in cancer cells. To date, low pH in acidic endocytic vesicles and increased level of glutathione (GSH) as well as oxidative species in cancer cells have encouraged the development of polymers which are sensitive to specific stimuli for bio-imaging and cancer treatment [27]. Inspired by these recent advances, we hypothesize the overproduced reactive oxygen species (ROS) can be exploited as a cancer related stimulus to mediate successfully cargo release from nanocarriers in the cytoplasm [28]. Taken together, we present a synthetic polymeric delivery system of miR-34a and volasertib for treating pancreatic cancer. We synthesized poly(ethylene glycol)-poly[aspartamidoethyl(p-boronobenzyl)diethyl ammonium bromide] (PEG-B-PAEBEA), which could form stable micelles

in aqueous solution with both of miR-34a and volasertib through electrostatic interaction of nucleic acid and quaternary ammonium and intense nitrogen-boron (N-B) coordination of tertiary amines and boronic acid, respectively. Upon oxidation by ROS, boronic acid would be first detached, followed by a self-immolative process to produce tertiary amines and *para*-quinone methide, leading to rapid release of miR-34a and volasertib, thereby improving the potential of their antitumor effects and minimal systemic toxicity (**Figure 2.1**). In this study, the biodistribution, therapeutic efficacy and systemic toxicity of miR-34a and volasertib loaded micelles was measured on orthotopic pancreatic tumor-bearing NSG mice by intravenous injection.

2.3 Experimental section

2.3.1 Materials

Dulbecco's Modified Eagle Medium (DMEM) high glucose medium, Dulbecco's phosphate buffered saline (DPBS) and 0.25% trypsin were purchased from Hyclone (Logan, UT). Keratinocyte-SFM medium, bovine pituitary extract, and human recombinant EGF were purchased from Gibco (Chevy Chase, MD). Heat inactivated fetal bovine serum (FBS), antibiotic-antimycotic for cell culture, RIPA buffer for cell lysis, hlat™ protease and phosphatase inhibitor cocktail (100×), Pierce™ BCA protein assay kit, H2DCFDA (D399) and FxCycle™ PI/RNase staining solution (F10797) were purchased from Thermo Fisher Scientific (Waltham, MA). HEPES buffer was purchased from Millipore Sigma (St. Louis, MO). Human PLK1 primary antibody was purchased from cell signaling technology (Danvers, MA). Human c-myc primary antibody was purchased from Proteintech (Manchester, UK). β-actin primary antibody was purchased from Santa Cruz Biotechnology (Dallas, TX). Dithiothreitol (DTT), 4×Laemmli buffer, 10×Tris/Glycine/SDS protein electrophoresis running buffer (pH 8.3) and 10×TBS buffer were purchased from Bio-Rad (Hercules, CA). Volasertib was purchased from Adooq Bioscience (Irvine, CA). miR-34a was purchased from GE Healthcare Dharmacon, Inc. (Lafayette, CO).

2.3.2 Synthesis of poly(ethylene glycol)-poly[aspartamidoethyl(p-boronic acid) benzyldiethyl ammonium bromide] (PEG-B-PAEBEA)

Step 1. Triphosgene (2.744 g, 9.24 mmol) dissolved in 10 mL of tetrahydrofuran (THF) was added to a suspension of benzyl aspartate (4.7 g, 21 mmol) in 200 mL of THF with stirring and the mixture was then heated to 50 °C. Once the suspension became clear (approximately 30 min). Then, the solvent was removed under reduced pressure. The resultant solid was recrystallized from excess hexane. Finally, 4.459 g of β-benzyl-L-aspartate N-carboxy anhydride (BLA-NCA) was obtained with a yield of 85%. ^{1}H NMR (500 MHz, $CDCl_3$, δ): 7.43 – 7.15 (m, 5H), 5.13 (s, 2H), 4.69 (t, J = 4.5 Hz, ^{1}H), 2.98 (ddd, J = 88.8, 17.8, 4.5 Hz, 2H).

Step 2. A solution of BLA-NCA (2.739 g, 11 mmol) in N,N-dimethylformamide (DMF) was added to a stirred solution of mPEG-NH2 (1.0 g, 0.2 mmol) in DMF under N2 atmosphere. The solution was heated to 40 °C and kept stirring for 72h. The resulting mixture was poured to a large amount of diethyl ether. The resulting solid was collected by filtration and dried to afford poly(ethylene glycol)-poly(beta-benzyl-L-aspartate) (PEG-PBLA) copolymer (2.99 g, 80%).

Step 3. PEG-PBLA (2 g) was first dissolved in DMF, followed by the addition of N, N-diethylethylene diamine (4 equivalent to BLA unit) and triethylamine (TEA) (4 equivalent to BLA unit). The mixture was stirred at 35 °C overnight. Afterwards, the mixture was dialyzed against distilled water and lyophilized to produce poly(ethylene glycol)-poly(beta-diisoethylamino-ethyl-aspartamide) (PEG-PAsp(DIE)), with a yield of 77%.

Step 4. In a 50 mL round bottom flask, (4-(bromomethyl)phenyl boronic acid (2.5 equivalent of DIE unit) and PEG-Pasp(DIE) (700 mg) were dissolved in DMF and stirred at 50 °C for 24h. Then, the resulting mixture was dialyzed against deionized water and the final product poly(ethylene glycol)-poly[aspartamidoethyl(*para*-boronic acid) benzyl diethyl ammonium bromide] (PEG-B-PAEBEA) was obtained as white solid after lyophilization, with a yield of 69%. The chemical

structure of PEG-B-PAEBEA was determined by ^{1}H NMR and its molecular weight and polydispersity (PDI) were determined by gel permeation chromatography (GPC) under following conditions: Styragel® HR 4E column (5 µm, 7.8×300 mm) at 40 °C and flow rate of 1 mL/min. DMF (containing 1 % lithium bromide) was used as the mobile phase and injection volume is 20 µL.

2.3.3 Cell culture

MIA PaCa-2 and Capan-1 cell lines were purchased from American Type Culture Collection (ATCC, Manassas, VA), MIA PaCa-2 resistant (MIA PaCa-2R) and Capan-1 resistant (Capan-1R) cells were generated from MIA PaCa-2 and Capan-1 by incubating with gemcitabine (GEM), respectively. All the above cell lines were maintained in high glucose DMEM medium supplemented except human pancreatic duct epithelial (HPDE) cells with 10% FBS and 1% penicillin/streptomycin at 37 °C, 5% CO_2 and 100% humidity, and were split when confluent. HPDE cells were cultured in Keratinocyte-SFM supplemented bovine pituitary extract (BPE) and human recombinant EGF in the identical atmosphere.

2.3.4 Preparation and characterization of nanoparticles

Volasertib (1 mg/mL) dissolved in acetone (100 µL) was added drop by drop to acetone solution of the copolymer (1 mg) under stirring at the room temperature. To remove the residual acetone, the samples were evaporated under reduced pressure. These nanoparticles were then used for complex formation with miR-34a or scrambled miRNA by mixing at an equal volume and vortexing gently for 30s followed by incubation at room temperature for 30 min. Rhodamine (Rho) labeled nanoparticles were prepared by dissolving Rho and volasertib in acetone, which was then mixed with the polymer solution under stirring. FITC labeled nanoparticles were fabricated by forming complex between FITC-labeled miRNA and nanoparticles. Particle size distribution and ζ potential were determined by dynamic light scattering (DLS) using a Malvern Zetasizer

(Worcestershire, UK) at 25 °C. Surface morphology of these nanoparticles was determined by transmission electron microscopy (TEM, Burlington, NC). The encapsulation efficiency (EE) and drug loading (DL) of volasertib were calculated using the following formulas:

EE (%) = Amount of volasertib encapsulated/Amount of volasertib added × 100% (1)

DL (%) = Amount of volasertib encapsulated/Amount of polymer × 100% (2)

2.3.5 miRNA binding ability

The miRNA complexation efficiency was assessed by agarose gel retardation assay. Nanoparticles were prepared at various N/P ratios, and miRNA was used as a control. 20 μL of nanoparticles were mixed with 6 μL of 6×loading buffer, and then the mixture was loaded onto 0.8% (w/v) agarose gel containing 0.5 μg/mL of ethidium bromide (EB). Electrophoresis was performed at a constant voltage of 110 V for 20 min in 1×TBE running buffer. The migration of miRNA bands was visualized and photographed with a using GelDoc Ez system (Bio-Rad, Hercules, CA).

2.3.6 ROS-triggered degradation of PEG-B-PAEBEA and release of miRNA

PEG-B-PAEBEA (5 mg) was dissolved in D_2O (1 mL) with 15 mM H_2O_2 solution at 37 °C. At given time points (1 h and 24 h), the solution was detected by ^1H NMR. To confirm the ROS responsiveness release of miRNA, nanoparticles at mass ratio of 32 were incubated with final H_2O_2 concentrations at 0.25, 0.5, 0.75 and 1.5 mM, respectively. Those solutions were then subjected to the electrophoresis as descried above after incubation for 1 h at 37 °C. Naked miRNA were used as a control.

2.3.7 Critical micelle concentration (CMC)

Critical micelle concentration (CMC) was determined with fluorescent spectroscopy using pyrene as a hydrophobic fluorescent probe [27]. Briefly, 1 mL of micelle samples were prepared in DI water with concentration ranges from 1×10^{-7} to 0.5 mg/mL and pyrene stock solution (1.2×10^{-6} M) was added to micelle samples. The emission fluorescent intensity of 384 nm and 373 nm was

recorded with an excitation wavelength of 334 nm. The intensity ratio (I384/I373) was plotted against the logarithm of micelle concentrations.

2.3.8 Fluorescence resonance energy transfer

For fluorescence resonance energy transfer (FRET) determination, FITC and Rhodamine were employed as the donor and acceptor, respectively. The dual-labeled nanoparticles carrying FITC labeled miR-34a and volasertib were fabricated by using Rho-labeled polymer. The emission spectra of FITC-miRNA and dual-labeled nanoparticles from 500–700 nm were scanned at an excitation wavelength of 490 nm (donor) using a fluorescence spectrometer.

2.3.9 Measurement of ROS production

ROS produced by cells were detected using 2',7'-dichlorofluorescin diacetate (DCFDA), which can passively diffuse across cell membranes. DCFDA is deacetylated by esterases to dichlorofluorescein (DCFH) and subsequently reacts with ROS to generate the green fluorophore, DCF [52]. MIA PaCa-2R cells were seeded in 12 well plates for 24 h, incubated with free volasertib and nanoparticles carrying ether miR-34a, volasertib or their combination. The concentration of volasertib and miR-34a were fixed at 50 and 100 nM. After 24 h, cells were removed from growth media, resuspended in pre-warmed PBS containing 5μM DCFDA and incubated 30 min at 37°C. Then the cells were washed with PBS for three times and resuspended in serum-free media. Fluorescence was respectively measured by flow cytometry (Becton, Dickinson, NJ) with excitation at 490 nm and emission at 520 nm.

2.3.10 Cytotoxicity, synergistic effect and apoptosis

Cytotoxicity of volasertib, miR-34a, and their combination was determined by MTT assay. MIA PaCa-2, MIA PaCa-2R, Capan-1 and Capan-1R cells were plated at a density of 5,000 cells/well in a 96-well plate for 24 h incubation. Then, free volasertib and formulations containing volasertib, or the combination of volasertib and miR-34a were added to 96-well plates with

volasertib concentration ranging from 10 to 1000 nM and miR-34a concentration from 10 to 200 nM, respectively. After 48 h of incubation, 5 mg/mL MTT solution was added and cells were cultured for another 3 h. The supernatant was discarded and 200 µL DMSO was added to each well. Cell viability was determined by a Spectrophotometer. The combination index (CI) and dose reduced index (DRI) were calculated using CompuSyn 1.0 software (ComboSyn, Inc., USA). In addition, $CI < 1$, $CI = 1$ and $CI > 1$ indicated synergistic, additive and antagonistic effects, respectively. To demonstrate ROS-responsive cytotoxicity, cells were treated with dithiothreitol (DTT, 5mM), a potent ROS scavenger, for 6 h prior to incubation with formulations.

For apoptosis assay, MIA PaCa-2R cells were seeded in 12 well plates for 24 h, incubated with nanoparticles carrying ether miR-34a, volasertib or their combination. We also used scrambled miRNA complexed nanoparticles as well as free volasertib as controls. Volasertib and miR-34a were fixed at 50 and 100 nM concentrations, respectively. These cells were incubated for 24 h, washed with PBS for three times, and stained with Annexin V-Cy5/PI apoptosis kit according to the manufacturer's protocol. The early and late apoptosis rates were calculated by flow cytometry (Becton, Dickinson, NJ).

2.3.11 Colony formation assay

MIA PaCa-2R cells were transfected with volasertib, miR-34a, and their combination for 24 h using scrambled miRNA as control. Transfected cells were reseeded in the 12-well plate at 1000 cells per well. Cells were cultured for 14 days, then plates were washed with PBS, fixed with formalin, stained with 5% crystal violet for 30 min, washed with tapping water and photographed.

2.3.12 Cell cycle

2×10^5 MIA PaCa-2R cells were seeded in a 6-well plate for 24 h and incubated with volasertib, miR-34a, and their combination, respectively using scrambled miRNA as a negative control. After 48 h, cells were harvested through trypsinization, fixed by 70 % ethanol, washed three times by

PBS, centrifuged and then the supernatant was decanted, leaving a pellet of cells in each sample tube. Then, 0.5 mL of FxCycle™ PI/RNase staining solution was added to each sample tube and incubated for 15 min at room temperature while protecting from light. Finally, flow cytometry was utilized to analyze the samples using excitation at 532 nm and emission at 585 nm.

2.3.13 3D spheroid tumor model

MIA PaCa-2R cells (4×10^3 cells in 40 µL per well) in DMEM medium with 10 % FBS were seeded onto Perfecta3D® 96-Well Hanging Drop Plates (3D Biomatrix, Inc., Ann Arbor MI) in triplicate and incubated at 37 °C, 5% CO_2. On 4th day, the spheroids were then treated with nanoparticles carrying either miR-34a, volasertib or their combination. Cells treated with PBS, scrambled miRNA and free volasertib were used as controls. Morphologies of tumor spheroids were visualized under a microscope on day 2, 4 and 6 to check the cytotoxic efficacy of different formulations.

2.3.14 Cell migration in vitro

Inhibition of cell migration was evaluated by scratch wound healing assay and Transwell® assay, respectively. For scratch wound healing assay, MIA PaCa-2R cells (2×10^5 per well) were plated onto a 12-well plate. Then, cells were treated with nanoparticles carrying either miR-34a, volasertib or their combination. Cells treated with PBS, scrambled miRNA and free volasertib were used as controls. At 24h post treatment, a wound was created in each well using 200 µL tips, dislodged cells were washed with PBS and treatment were re-added for 24 h and 48 h, respectively. Cell migration assay was performed using Transwell® chambers in MIA PaCa-2R cell lines. MIA PaCa-2R cells were cultured at a density of 4×10^5 cells/well in 6-well plates for 24 h prior to use. The cells were treated with nanoparticles carrying miR-34a, volasertib or their combination. Cells treated with PBS, scrambled miRNA and free volasertib were used as controls. These formulations were incubated in 2 mL of culture media without serum for 6 h, followed by two washes with PBS

and incubation in DMEM medium with 10% FBS for an additional 24 h. The cells were harvested and 200 µL of cell suspension in DMEM medium was added into the upper chamber of Transwell®. Subsequently, 1 mL of DMEM with 20 % FBS as the chemoattractant was added into the lower Transwell® chamber and the cells were incubated for 24 h. Then, cells that did not migrate through the pores were carefully removed using a cotton-tipped swab. The filters were fixed in 4% paraformaldehyde, dried in room temperature, and stained with crystal violet.

2.3.15 Real time RT-PCR

HPDE, MIA PaCa-2, MIA PaCa-2R, Capan-1 and Capan-1R cells were cultured in 6-well plates at a density of 2×10^5 cells/well for 24 h, transfected with volasertib or miR-34a for 24 h. Cells were then subjected to extraction of total RNA using RNAeasy isolation kit (Qiagen, Valencia, CA). Reverse transcription reaction of total RNA to cDNA was carried out using miScript II Reverse Transcription kit and Taqman® Reverse Transcription reagents (Thermo Fisher, Waltham, MA), respectively. miR-34a and PLK1 mRNA levels and c-myc were quantitatively assayed in a real-time PCR system (Roche, Basel, Switzerland) using miScript SYBR Green dye universal master mix, miR-34a primer as well as primers of PLK1 and c-myc on a Light Cycler 480 (Roche, Indianapolis). U6 was used as a housekeeping gene and relative amount of miR-34a, PLK1 and c-myc was calculated using the crossing point (Cp) value. Primers were designed as: PLK1 FWD: 5'-CAGCAAGTGGGTGGACTATT-3', PLK1 REV: 5'- ATCAGTGGGCACAAGATGAG-3'; c-myc FWD: 5'-CACGAAACTTTGCCCATAGC-3', c-myc REV: 5'-GCAAGGAGAGCCTTTCAGAG-3'.

2.3.16 Western blot analysis

MIA PaCa-2 and MIA PaCa-2R cells in 6-well plates with a density of 2×10^5 cells/well were incubated with formulations for 24 h, followed by protein isolation with radioimmunoprecipitation assay (RIPA) buffer and determination with a BCA protein assay kit. The cell lysates were then

mixed with loading buffer, boiled buffer at 100 °C for 5 min, loaded on the wells of SDS-PAGE gel, transferred by electroporation to polyvinylidene difluoride (PVDF) membrane, incubated with blocking buffer for 1 h at room temperature, cultured with PLK1, Bcl-2 and c-myc rabbit primary antibodies as well as β-actin primary antibody overnight at 4°C and IR fluorescent dye labeled secondary antibodies was added, followed by analysis using Licor Odyssey system (LI-COR Biotechnology, Lincoln, NE). β-actin was used as the loading control.

2.3.17 Biodistribution and therapeutic studies

All the animal experiments were approved by the Institutional Animal Care and Use Committee (IACUC) of the University of Nebraska Medical Center, Omaha, USA and carried out as per the National Institutes of Health (NIH) use guidelines. The orthotopic human pancreatic cancer mouse model was developed using 6-8 week male NSG mice (24-30 g). Luciferase stably expressing MIA PaCa-2R cells (1×10^6) were mixed with Matrigel (2:1) using ice-cold instruments and syringes. Then mice were anesthetized using isoflurane in an induction chamber, and 20 µL of Matrigel-cell suspension was orthotopically injected into the pancreas tail. Tumor growth was monitored using an IVIS Spectrum In Vivo Imaging System (PerkinElmer, Hopkinton, MA) after intraperitoneal administration of 20mg/mL luciferin to mice (150µL per mouse). Three weeks after tumor injection, free Cy5.5 and Cy5.5 labeled micelles were injected to mice via the tail vein at a single of Cy5.5 at the dose of 0.1 mg/kg. To localize Cy5.5 labeled micelles, the mice were observed in the IVIS imaging system at an excitation wavelength of 640 nm and emission wavelength of 710 nm at 1, 2, 4, 8, 24 h. After *in vivo* imaging, mice were sacrificed and major organs such as tumor, heart, liver, spleen, lung and kidney were collected for *ex vivo* imaging.

For therapeutic study, mice were randomly divided into 5 groups (n=5 per group) when the bioluminescence reached 1×10^6. Formulations including were administered via tail vein with volasertib 5 mg/kg and miR-34a 1 mg/kg every three days in a total of 7 injections, according to the animal's weight. Body weights were measured every time before injection. At the 3rd day after

the 7th administration, the animals were euthanized to harvest major organs such as tumor, heart, liver, spleen, lung and kidney haematoxylin and eosin (H&E) staining, immunohistochemical and Western blot (WB) analysis.

2.3.18 Statistical analysis

Results are presented as the mean ± standard deviation (SD). One-way analysis of variance (ANOVA) was carried out to assess the statistical significance of the differences between groups. $P < 0.05$ indicated significant differences.

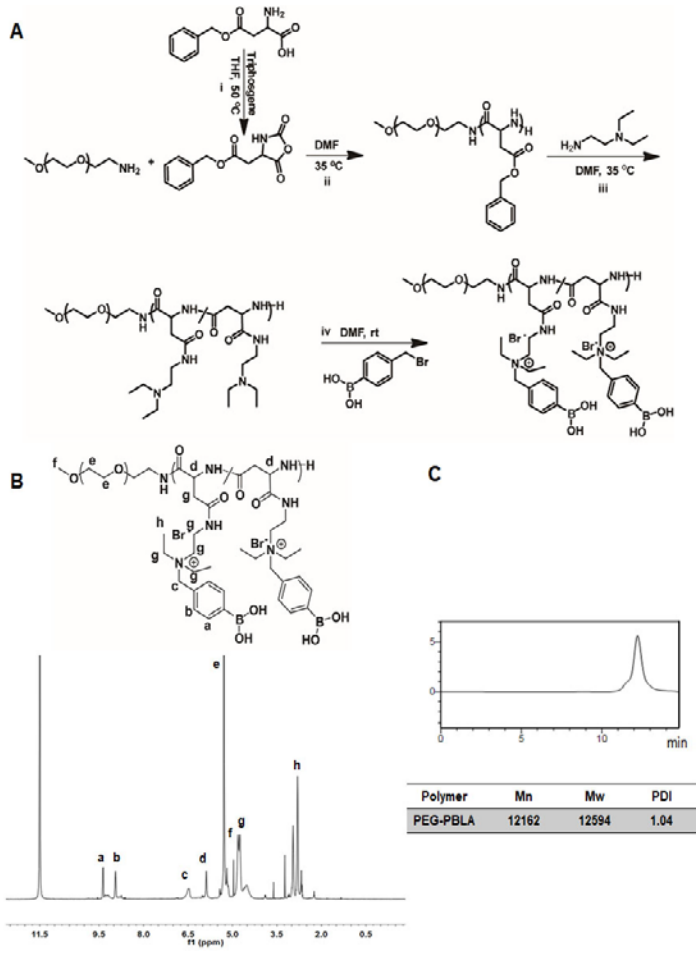

Figure 2.2 Synthesis and characterization of PEG-B-PAEBEA. (A) Synthesis scheme for PEG-B-PAEBEA. (B)1H NMR spectrum of PEG-B-PAEBEA in TFA-d6. (C) Molecular weight of PEG-PBLA confirmed by GPC.

2.4 Results

2.4.1 Copolymer synthesis and characterization

A reactive oxygen species (ROS)-labile charge-reversal polymer PEG-B-PAEBEA was synthesized by a 4-step process and characterized by ^{1}H NMR. Briefly, BLA-NCA was produced from the reaction of L-aspartic acid β-benzyl ether, followed by copolymerization with mPEG-NH_2 (Mw=5000) to produce PEG-PBLA. Afterwards, N, N-diethylethylenediamine (DEEDA) replaced the benzyl groups through aminolysis, affording PEG-PAsp(DIE). Finally, the reaction between 4-(bromomethyl)phenyl boronic acid and PEG-PAsp(DIE) gave the final product PEG-B-PAEBEA (**Figure 2.2 A-B**). The molecular weight of PEG-PBLA was 12,594 Da with PDI of 1.04 according to GPC determination (**Figure 2.2 C**). PEG-B-PAEBEA had strong interactions with the GPC column due to the positive charge, so their molecular weight could not be measured by the GPC and were calculated from their precursor PEG-PBLA. According to the ^{1}H NMR spectrum of PEG-B-PAEBEA in **Figure 2.2 B**, 15 4-methylphenyl boronic acids were attached to tertiary amines of PEG-PAsp(AIE), as based on the integrated areas of the peak at 5.28 ppm (assigned to methylene hydrogens of -PEG). Thus, the molecular weight of PEG-B-PAEBA is 14,611 Da.

2.4.2 Preparation and characterization of micelles

Volasertib loaded micelles were prepared by precipitation using PEG-B-PAEBEA and coating drug particles through N-B coordination, thereby allowing the micelles to achieve a positively charged surface for complex formation with miR-34a via ionic interaction. The mean particle size of micelles was 90.1 ± 0.3 nm with volasertib loading of 10.8 ± 0.1 %, volasertib encapsulation efficiency of 96.7 ± 0.8 %, and ζ potential of 35.5 ± 2.7 mV (**Figure 2.3 A**). The polymer effectively condensed miR-34a at N/P ratios above 18, as probed by gel electrophoresis, and the ζ potential of micelles decreased to 10.4 ± 1.6 mV with the mean particle size increased to 101.4 ± 0.7 nm. TEM of micelles presented spherical particles. Upon oxidation of the boronic acid group by ROS such as H_2O_2 solution at 0.25 mM for 1 h, miR-34a could be released from the micelles and their

morphologies were collapsed as shown in TEM image, demonstrating the ROS-responsive release of miR-34a (**Figure 2.3 B-C**). We investigated the ROS-triggered degradation of micelles by ^{1}H NMR as well. Micelles in D_2O showed only the PEG peak (**Figure 2.3 D**), however peaks of 4-hydroxymethyl phenol appeared, the intensity increased with incubation time and ζ potential altered to 3.67 ± 0.28 mV, indicating the disassembly of micelles (**Figure 2.3 D**). Additionally, elevated ROS production induced by volasertib can in turn promote the degradation of micelles,

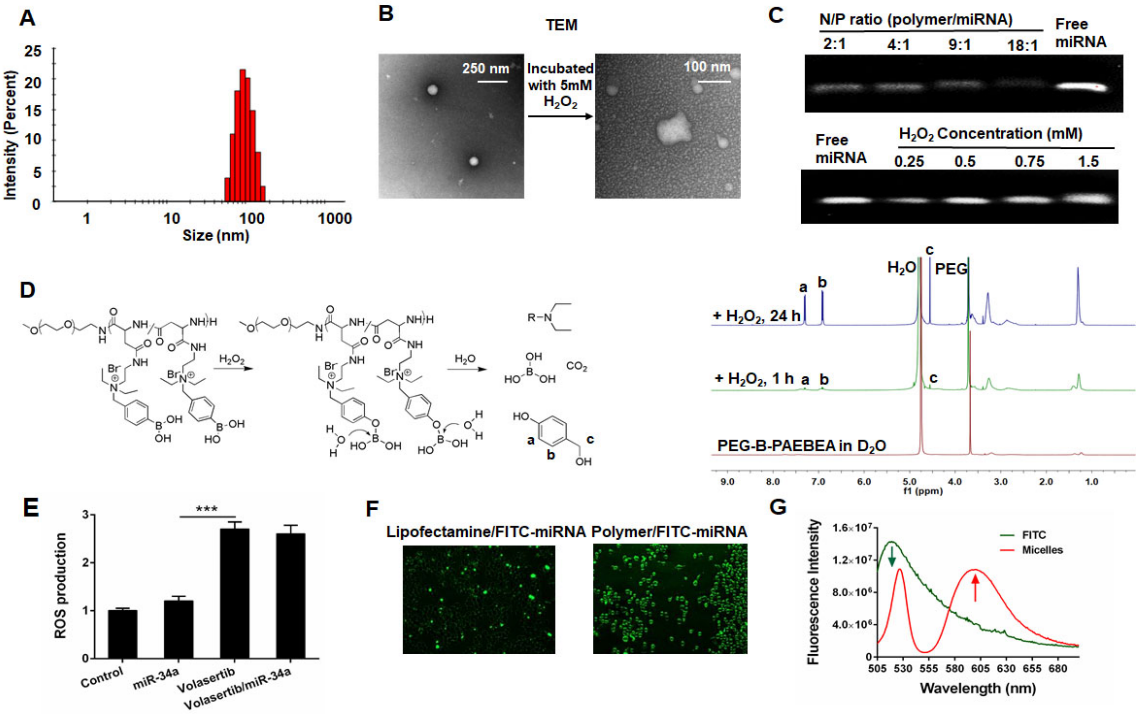

Figure 2.3 Characterization of micelles. (A) Particle size distribution and morphology of nanoparticles. (B) ROS responsiveness confirmed by a transmission electron microscope (TEM). (C) Gel electrophoresis to confirm miRNA condensation and ROS responsive miRNA release. (D)1H NMR spectra of PEG-B-PAEBEA micelles after H2O2 treatment in D2O. (E) ROS production. (F) Cellular uptake of lipofectamine/FITC-miRNA and polymer/FITC-miRNA. G) FRET effect is demonstrated via the reduction fluorescence intensity of donor at 520 nm with increased fluorescence of acceptor at 600 nm.

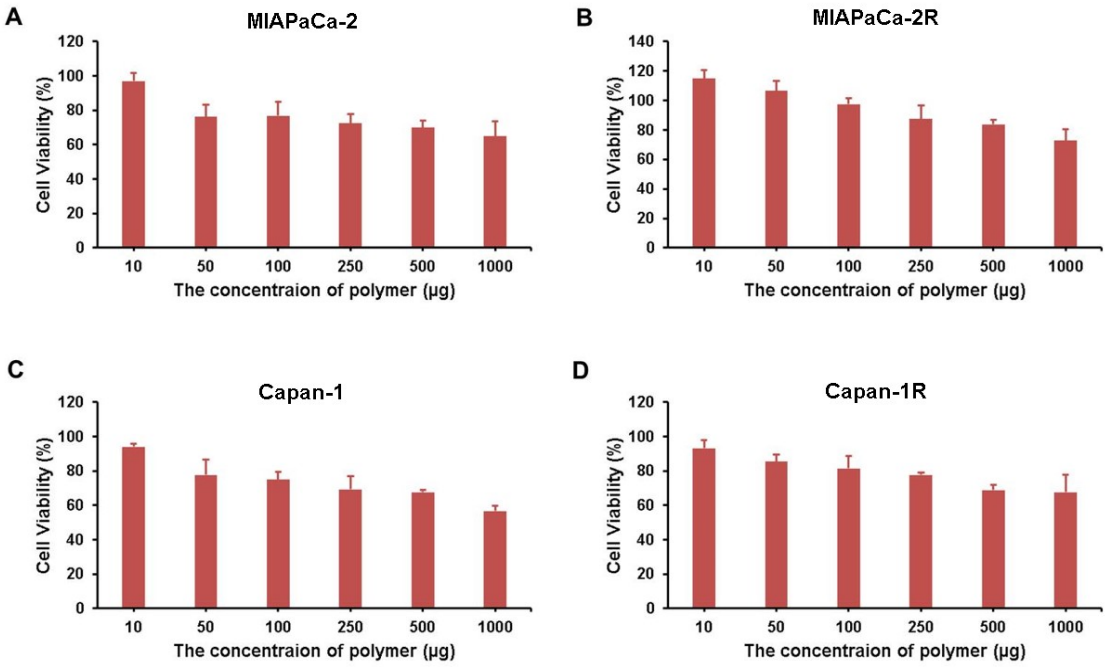

Figure 2.4 Biocompatibility of polymer in pancreatic cancer cell lines.

and further increase the release of small molecules and genes (**Figure 2.3 E**). Moreover, the polymeric micelles improved intracellular delivery of miRNA, compared to the commercial transfection reagent, lipofectamine 2000 (**Figure 2.3 F**). The critical micelle concentration (CMC) of micelles was determined to be 2.0 μg/mL using pyrene as a fluorescent probe.

To further ascertain miR-34a loading in micelles, FRET measurement was performed, where FITC was utilized as a donor conjugated to miR-34a (FITC-miR-34a), Rhodamine was employed as an acceptor loaded in micelles. The maximal fluorescence intensity at 520 nm of FITC (donor) from dual-labeled micelles carrying miR-34a and volasertib were significantly reduced, whereas the fluorescent intensity at 600 nm was increased compared to FITC-labeled miR-34a, which demonstrates an effective energy transfer from the donor to acceptor in the micelles (**Figure 2.3 G**).

2.4.3 Synergistic effect of volasertib and miR-34a and apoptosis

PEG-B-PAEBEA showed high biocompatibility and was suitable for co-delivery of volasertib and miR-34a (**Figure 2.4**). The cytotoxicity of volasertib and its combination with miR-34a on pancreatic cancer cell lines was carried out as a function of volasertib or miR-34a concentrations.

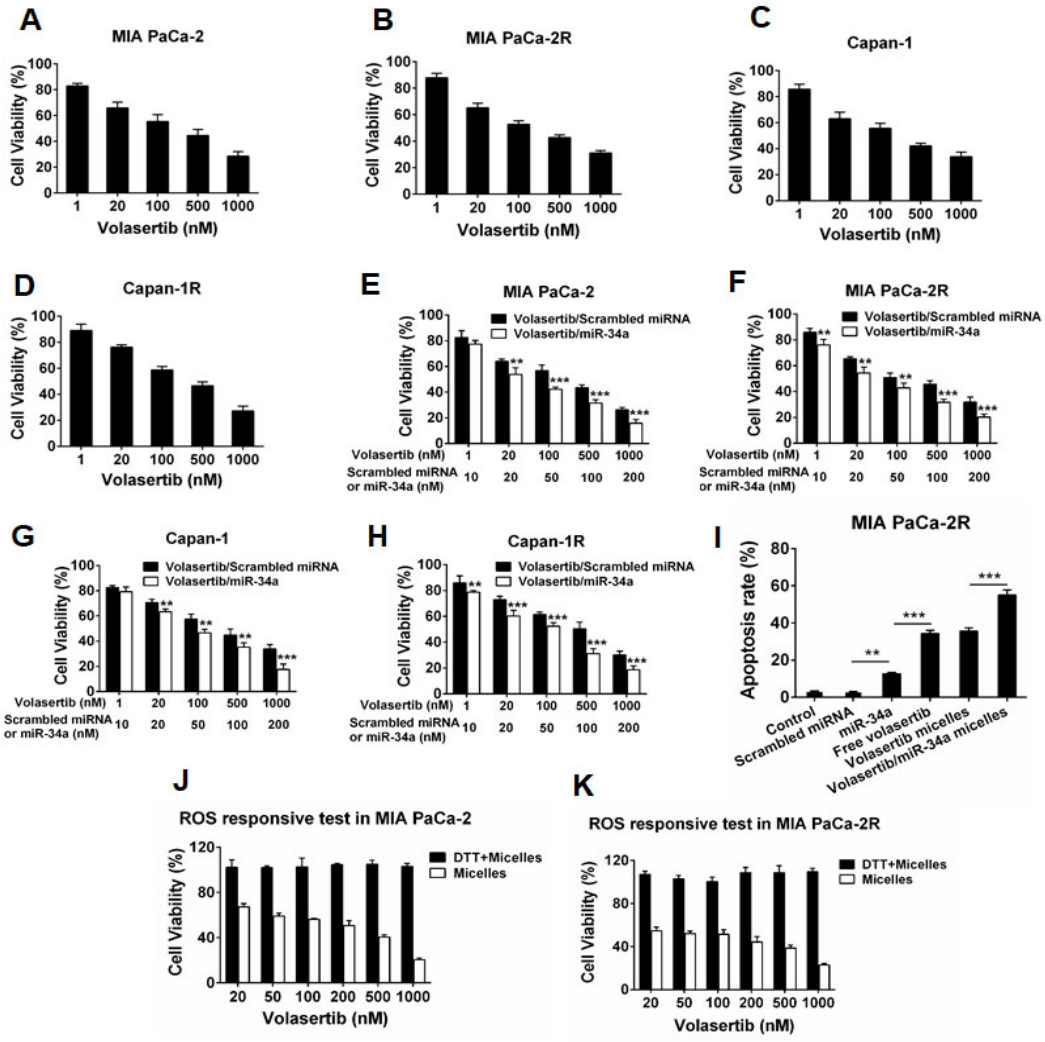

Figure 2.5 Effect of volasertib and miR-34a on pancreatic cancer. (A-D) Cytotoxicity induced by volasertib alone (E-H) Cytotoxicity caused by the combination of volasertib and miR-34a. (I) Effect of miR-34a and volasertib on apoptosis. MIA PaCa-2R cells were treated with micelles loaded with miR-34a, volasertib or their combination. Results are presented as the mean ± S.D. (n= 3). (J and K) Effect of ROS inhibition triggered by DTT on cytotoxicity in pancreatic cancer cells.

As shown in **Figure 2.5 A-D**, cell viability after transfection with volasertib was dose-dependent, and the capability of killing cancer cells by volasertib remained in the nanomolar level. Most importantly, the IC_{50} value of volasertib in combination with miR-34a was decreased by ~2-4.5 fold, compared to volasertib alone and the combination of volasertib and scrambled miRNA (**Figure 2.5 E-H**). Meanwhile, CI values obtained after combination treatment of volasertib and miR-34a were 0.1-0.7 (less than 1), indicating the synergistic effect of the small molecule and miRNA. Quantitative apoptosis analysis by flow cytometry using Annexin V-Cy5/PI apoptosis detection kits also indicated that combination of volasertib and miR-34a with total apoptotic cells of 55 % exhibited higher apoptotic activity in contrast to other groups (**Figure 2.5 I** and **2.6**). Accordingly, micelles carrying miR-34a and volasertib were capable of inducing apoptosis with high efficiency. However, once the ROS was eliminated by a scavenger dithiothreitol (DTT), micelles carrying miR-34a and volasertib displayed no efficiency compared to the group without DTT pretreatment, which also suggested the ROS responsive release of volasertib and miR-34a contributed to the therapeutic effect in pancreatic cancer cells (**Figure 2.5 J-K**).

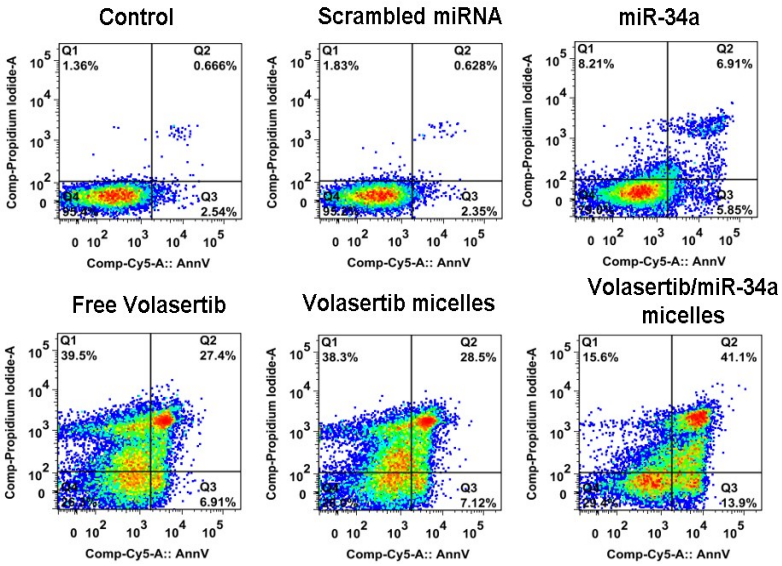

Figure 2.6 Flow cytometry analysis of apoptosis induced by miR-34a and volasertib.

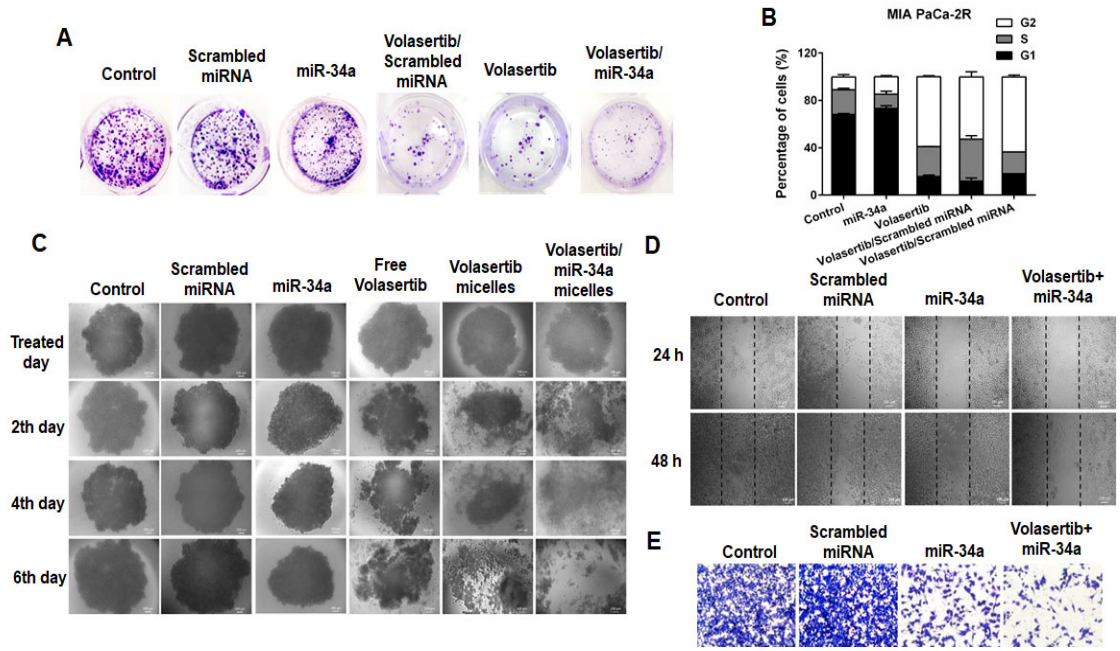

Figure 2.7 Colony formation assay, cell cycle, effect on tumor spheroids and migration assays. (A) Colony assay after treatment of MIA PaCa-2R cells with micelles carrying miR-34a, volasertib or their combination. The cells treated with micelles carrying scrambled miRNA and volasertib were also used control. (B) Cell cycle analysis in MIA PaCa-2R cells. (C) Effect of different formulations on 3D tumor spheroids. Migration inhibition investigated by scratch wound healing assay (D) and transwell chamber assay (E), respectively.

2.4.4 Colony assay and cell cycle

To determine whether the combination of volasertib and miR-34a has greater effect on long-term anticancer therapy, we studied volasertib, miR-34a and their combination using scrambled miRNA as a negative control in MIA PaCa-2R cell line with final concentration of 100 nM for volasertib and 100 nM for miR-34a, respectively. A significant decrease in the density of colony was observed with the combination treatment compared to small molecule volasertib alone (**Figure 2.7 A**). The lower colonies indicated an improved therapeutic efficacy of the combination of volasertib and miR-34a, due to their synergistic effect.

PLK1 regulates the cell division cycle during late G_2 and M phase and volasertib is a highly potent PLK1 inhibitor, resulting in G_2/M cell cycle arrest followed by programmed cell death in cancer cell lines. Combination of volasertib and miR-34a demonstrated the strongest ability in arresting MIA PaCa-2R cells in the G_2/M phase among all tested samples. Volasertib and combination group progressively induced G_2/M arrest in MIA PaCa-2R cells, with significantly parallel decrease of G_1 population (**Figure 2.7 B** and **2.8**).

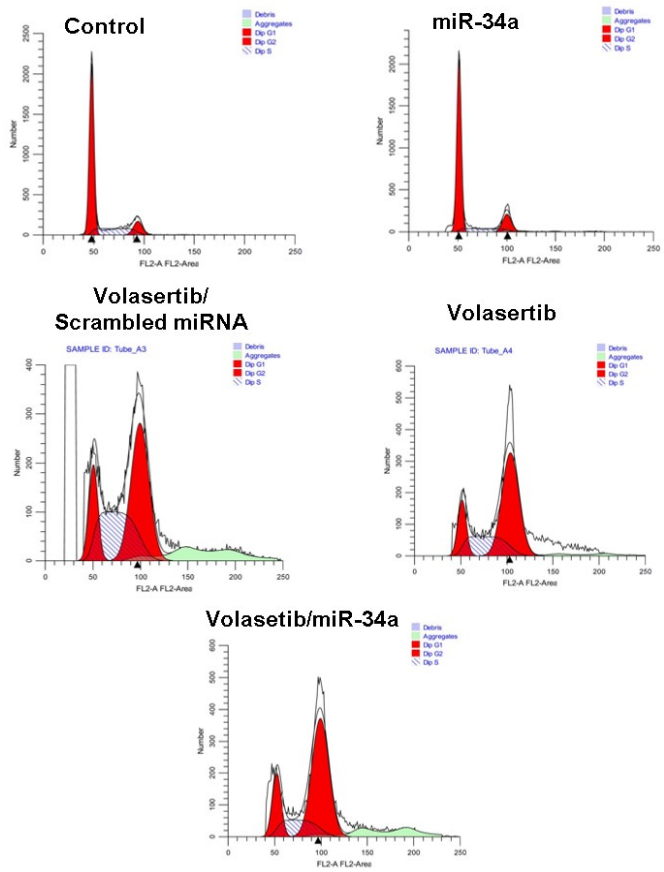

Figure 2.8 Flow cytometry analysis of cell cycle in MIA PaCa-2R cells

2.4.5 Therapeutic efficacy in 3D tumor spheroids and Migration inhibition

The 3D tumor spheroid sizes in control and scrambled miRNA groups were increased after treatment. In contrast, miR-34a could slightly decrease the size of tumor spheroid. Notably, free volasertib and micelles encapsulating volasertib exhibited similar results in inhibiting the growth

of tumor spheroids, while micelles formulating miR-34a and volasertib could significantly reduce the spheroid size and consequently lead to the collapse of tumor spheroids (**Figure 2.7 C**). These results indicated that miR-34a and volasertib loaded micelles displayed significant inhibition on tumor spheroid-growth.

On the other hand, the migration of cancer cells was predominant element leading to cancer recurrence. Compared to PBS control group and scrambled miRNA did not suppress cell migration and partially closed the wound after 48 h. In contrast, miR-34a and combination of miR-34a and

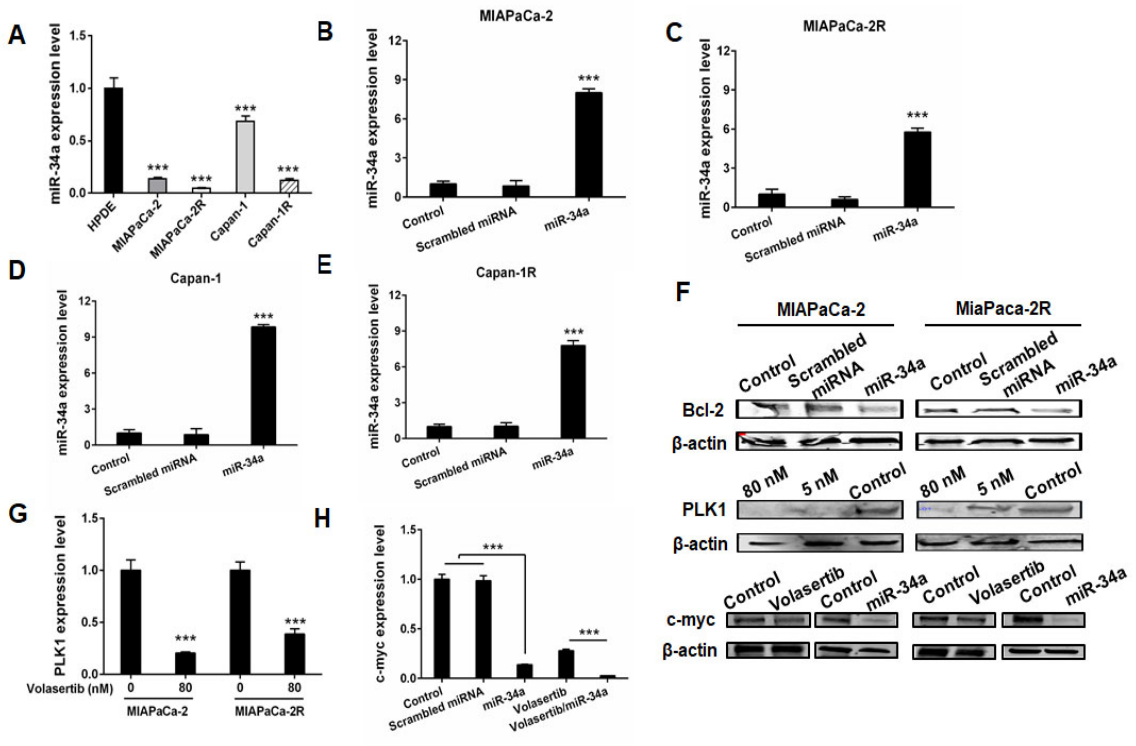

Figure 2.9 Molecular mechanism for the synergistic effect of volasertib and miR-34a. (A-E) miR-34a expression level determined by qPCR after treatment of HPDE, MIA PaCa-2, MIA PaCa-2R, Capan-1 and Capan-1R cell lines. (F) Western blotanalysis of Bcl-2, PLK1 and c-myc in MIA PaCa-2 and MIA PaCa-2R cell lines. (G and H) PLK1 and c-myc mRNA expression levels determined by qPCR. PBS was used as control (n=3, $^{*}p < 0.05$, $^{**}p < 0.01$ and $^{***}p < 0.001$).

volasertib displayed little migration after 24 h and caused reduction of migration after 48 h (**Figure 2.7 D-E**), thereby indicating the efficient intracellular delivery of miR-34a to cancer cells.

2.4.6 Molecular mechanisms of volasertib and miR-34a

miR-34a expression was significantly lower in pancreatic cancer cell lines compared to normal pancreatic cancer HPDE cell line (**Figure 2.9 A**). After transfection with miR-34a mimics, miR-34a expression level was enhanced by 6 to 10- fold in MIA PaCa-2 cells (**Figure 2.9 B-E**). On the other hand, PLK1 expression level was profoundly suppressed in MIA PaCa-2 cells after incubation with volasertib in 5 and 80 nM, respectively, while higher concentration (80 nM) was needed to inhibit PLK1 expression level in MIA PaCa-2R cells (**Figure 2.9 F** and **G**).

Bcl-2 has shown to have a dominant role in the survival of cancer cells. miR-34a downregulated Bcl-2 expression, further leading to inhibition of proliferation and enhancement of apoptosis in cancer cells (**Figure 2.9 F**). The treatment of volasertib, miR-34a and their combination contributed to significant suppression of c-myc expression as well in pancreatic cancer cell lines (**Figure 2.9 F** and **H**), indicating that c-myc was the common target of volasertib and miR-34a, leading to the synergistic effect of volasertib and miR-34a in pancreatic cancer.

2.4.7 Biodistribution studies

Following systemic administration to NSG mice harboring orthotopic pancreatic tumors, we compared the delivery and retention of free Cy5.5 and Cy5.5 labeled micelles to evaluate whether micelles could accumulate in solid tumors. Due to the short half-life of Cy5.5 [29], the NIR signal intensity was dimmer and disappeared rapidly in mice injected with free Cy5.5. In contrast, robust fluorescence intensity was obtained at the tumor sites within 4 h of Cy5.5 labeled micelles injection, following which the signal intensity was sustained for 24 h (**Figure 2.10 A**). In addition, the liver, kidney and spleen were also major sites of micelles distribution (**Figure 2.10 B-D**).

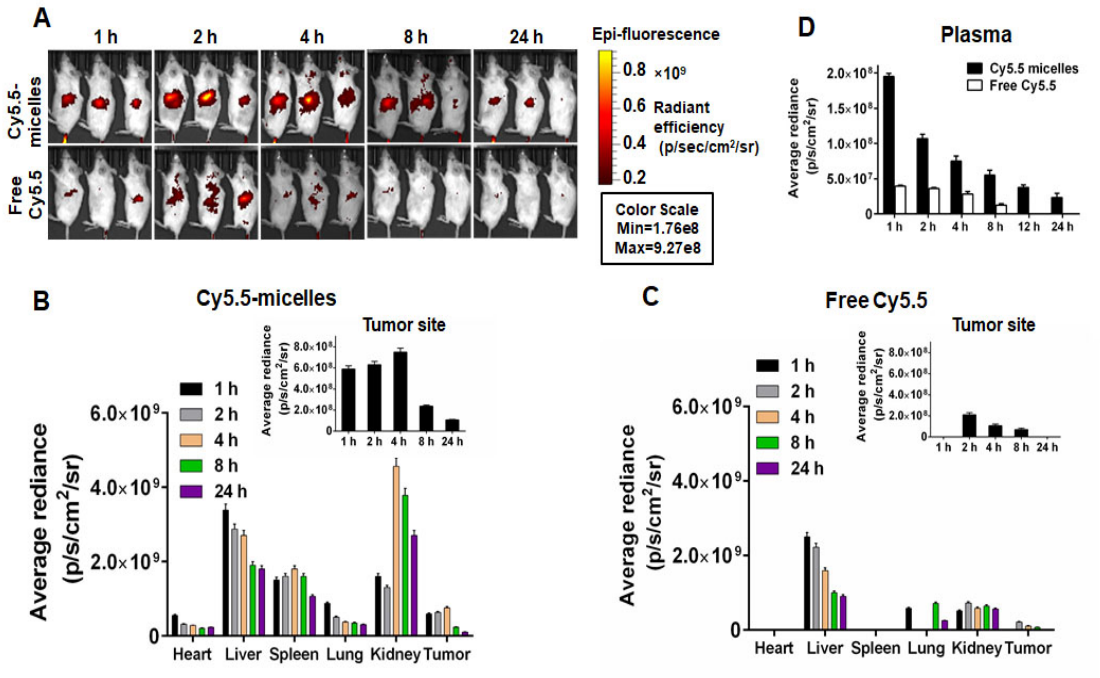

Figure 2.10 Biodistribution of micelles in vivo. (A) Real-time biodistribution of free Cy5.5 and Cy5.5 labeled micelles at 1, 2, 4, 8, 24 h (n=3). Quantified accumulation of (B) Cy5.5 labeled micelles and (C) free Cy5.5 in major organs, including heart, liver, spleen, lung, kidney and tumor (n=3). (D) Quantified accumulation of Cy5.5 labeled micelles and free Cy5.5 in plasma (n=3). In plasma, Cy5.5 signal intensity in Cy5.5-micelles injected mice may be from both Cy5.5-micelles and cleaved Cy5.5 dye.

2.4.8 Antitumor activity

Systemic administration was repeated every 3 days for up to 7 repetitions. Orthotopic tumor growth was monitored by IVIS bioluminescence imaging, demonstrating significantly slower tumor growth by treatment with combination micelles compared to saline, free volasertib, miR-34a, volasertib loaded micelles (**Figure 2.11 A** and **B**). This su1ggested that combination of miR-34a and volasertib elicit a potent antitumor efficacy. No reduction in body weight or morbidity was observed in mice (**Figure 2.11 C**), indicating that micellar formulations of volasertib and miR-34a

were well tolerated. The pathological changes in mouse vital organs were compared among the groups and representative micrographs of H&E staining proved negligible systemic toxicity of the formulations as no damage or inflammation was observed (**Figure 2.12**).

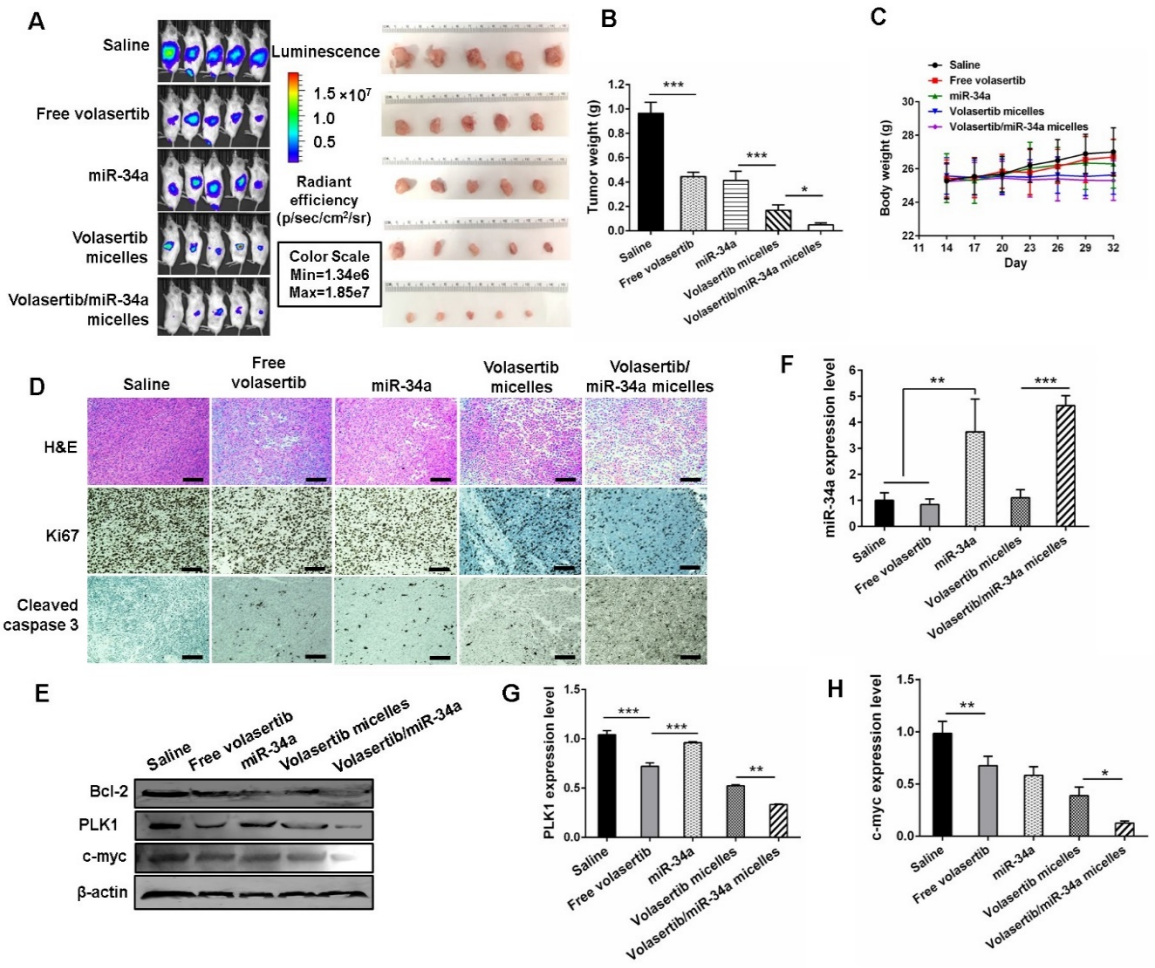

Figure 2.11 Antitumor efficiency in vivo. (A) Bioluminescence images of tumors and isolated tumor images at the end of the experiment. (B) Tumor weight after treatment with the various formulations (n = 5, $^{*}P < 0.05$, $^{**}P < 0.01$ and $^{***}P < 0.001$). (C) Body weight. (D) H&E staining, Ki67 and cleaved caspase 3 analysis of the tumor specimens. (E) Bcl-2, PLK1 and c-myc expression determined by Western blot assay. (F) miR-34a, (G) PLK1 and (H) c-myc expression level in tumor was determined by PCR assay (n = 3, $^{**}P < 0.01$ and $^{***}P < 0.001$).

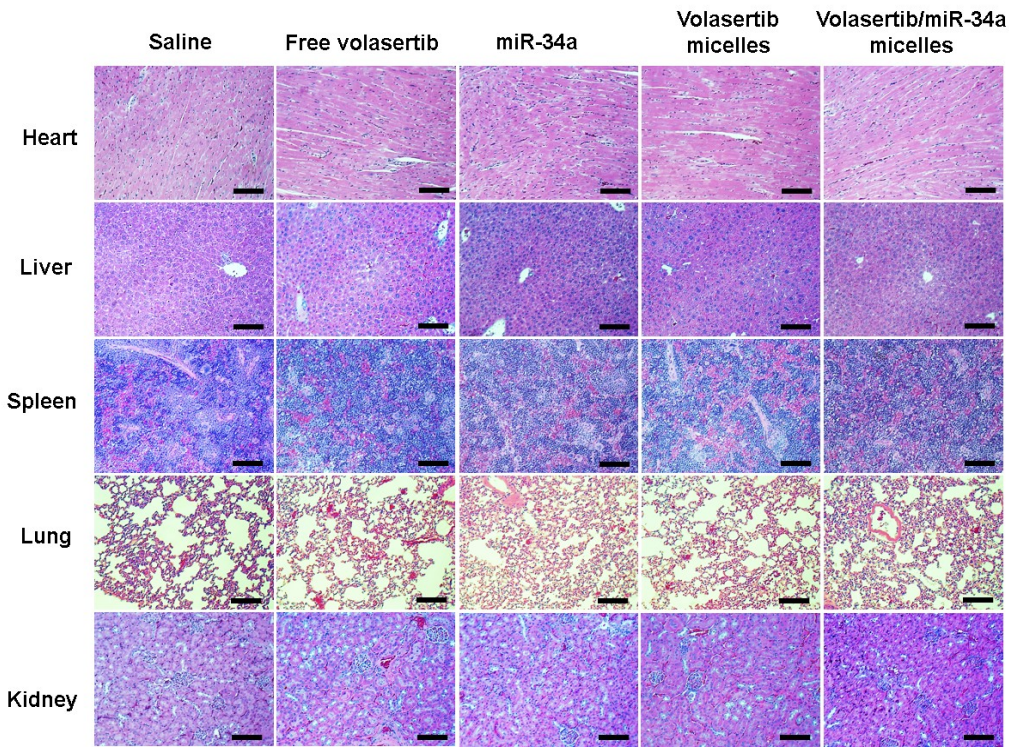

Figure 2.12 Representative histological images from retrieved tissues

Tumor tissue sections from different treatment groups were examined by H&E staining and immunohistochemistry (IHC) staining. In comparison with the morphological characteristics of H&E stained tissue sections of saline-treated tumors that contained dense carcinoma cells, tumor cell density in combination micelles-treated tumors was significantly decreased with necrotic tumor cell areas (**Figure 2.11 D**). Utilizing an IHC staining for the detection of cleaved caspase 3, we observed notable apoptotic cell death in combination micelles-treated mice, compared to free volasertib, miR-34a and volasertib loaded micelles, respectively. Representative IHC images are shown in **Figure 2.11 D**. Ki-67 is a marker of proliferation and its staining showed marked differences between different treatment groups. There was remarkable decrease in the number of Ki-67 positive proliferating cells in the tumor of the mice treated with combination micelles than other groups (**Figure 2.11 D**). Therefore, effective induction of the apoptotic cell death and profound inhibition of tumor cell proliferation contributed to the antitumor effect in mice. As

depicted in **Figure 2.11 F**, miR-34a was considerably upregulated in miR-34a complexed micelles and the group treated with micelles loaded with volasertib and miR-34a and that is ascertained the downregulation of Bcl-2 and c-myc in tumor tissues by Western blot and PCR analysis (**Figure 2.11 E**, **G** and **H**). We further confirmed this by quantifying the Western blot bands of **Figure 2.11 E** by using ImageJ 1.5a (Java 1.8.0_112 (64 bit)) and the results are shown in **Figure 2.13**. Moreover, the downregulation of PLK1 induced by volasertib contributed notable c-myc suppression in tumor sites as well. According to those results, the combination of miR-34a and volasertib can restore miR-34a expression level, sensitize the cells to chemotherapy, further exhibit synergistic effect in pancreatic cancer via c-myc, leading to tumor growth suppression and apoptosis.

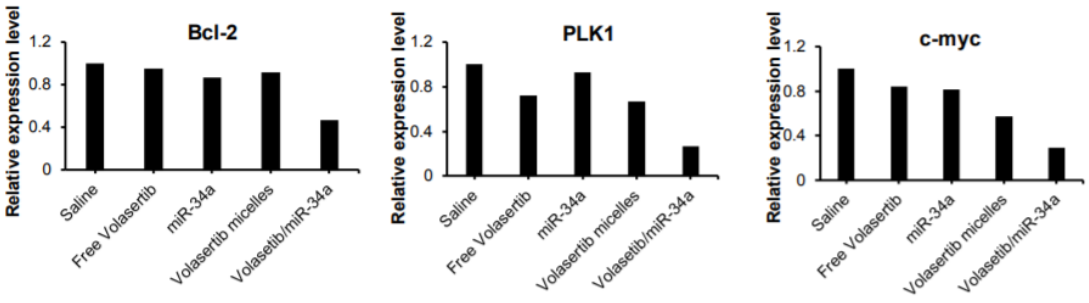

Figure 2.13 Quantification of Western blot bands for Bcl-2, PLK1 and c-myc expression by ImageJ 1.5a (Java 1.8.0_112 (64 bit)) of tumors isolated from mice.

2.5. Discussion

Several nanocarriers have been reported to enhance drug delivery to the tumor after systemic administration. However, most of the current nanoparticle platforms are rarely used for co-delivery of small molecules or oligonucleotides. Previously, we developed nanocarriers capable of carrying small molecules and miRNA simultaneously and evaluated their delivery efficacy in subcutaneous and orthotopic tumor mouse models. Compared to polycarbonate which we used in our previous

studies, polyaspartate has the following advantages: 1) it is stable during synthesis and post-modification; 2) it is compatible with ring-opening polymerization (ROP) protocols with functional alcohols; 3) one-step synthesis of monomer for copolymerization; 4) it avoids a two-step reaction that is deprotection with H2 and subsequent coupling in the presence of EDC/HOBt for replacement of pendent benzyl groups by simply mixing polyaspartate and tertiary amines; 5) micelles can be formed by simply dissolving lyophilized polymer in aqueous solution, making it a highly attractive platform for drug delivery.

Smart polymers capable of responding to the stimuli intrinsic to a tumor environment have emerged as efficient nanocarriers for the treatment of cancer [30]. Elevated rates of ROS have been detected in most cancers, and the levels of intracellular ROS in cancer cells are unique biological stimuli that can be utilized for efficient and targeted drug delivery to cancer cells [28, 31]. Boronic acid has been extensively used for detection of H_2O_2 in vitro and in vivo, and the integration of these functional moieties in the polymeric backbone has been reported [32, 33]. This mechanism depends on the oxidation-triggered hydrolysis of the boronic ester to a phenol and subsequent degradation of nanoparticles [33], leading to the release of therapeutic agents. Meanwhile, phenyl boronic acid (PBA) is also known as Lewis acid, which renders donor-acceptor interaction, also called coordination bonding with various amines. The donor-acceptor bond energy is much stronger than non-specific hydrophobic interactions, and undesired drug aggregation can be evitable during this process [26].

Volasertib with two tertiary amines in the piperazine group could be encapsulated by PEG-B-PAEBEA via specific nitrogen-boronic coordination instead of hydrophobic interaction [26]. More importantly, upon the oxidation of boronic acid group of PEG-B-PAEBEA, the positive quaternary amines could alter to tertiary amines with no loading capacity (**Figure 2.3 D**) [26, 32], facilitating the release of miR-34a and volasertib simultaneously (**Figure 2.1**). With the elimination of ROS by DTT a well-known ROS scavenger [34], volasertib micelles exhibited no effect to cancer cells

(**Figure 2.4 J-K**) [35, 36], further indicating the release of volasertib is in a ROS-dependent manner. Additionally, volasertib could boost ROS levels which in turn accelerated the degradation of PEG-B-PAEBEA (**Figure 2.1** and **Figure 2.3 E**), thus a positive feedback loop was established to enhance the antitumor efficacy while minimize systemic toxicity.

The potential challenges facing NPs include rapid clearance by the mononuclear phagocyte system (MPS), vehicle-related cytotoxicity, and elicitation of cytokine response caused by the activation of toll-like receptors (TLRs) [37, 38]. However, the rational design of the polymer/carrier could be used for addressing these limitations. For example, micelles with particle size below 100 nm modified by PEG on the surface can prolong the circulation by decreasing serum protein adsorption and preventing MPS recognition [39, 40]. The micelles designed in this study were decorated by PEG as the hydrophilic surface with particle size around 100 nm, providing them a great chance for extended circulation and tumor accumulation.

By whole-body fluorescence imaging, mice injected with free Cy5.5 showed maximal tumor fluorescence at 2 h followed by rapid clearance with time. The positive quandary amine of Cy5.5 might increase its binding to plasma proteins, therefore biodistribution of free Cy5.5 showed little liver and kidney accumulation with low tumor retention at 8 h [41, 42]. In contrast, mice treated with Cy5.5-conjugated micelles showed excellent tumor accumulation of micelles even at 24 h post systemic administration, demonstrating that the Cy5.5 was not removed from micelles and the high intensity in the tumor was resulted from high accumulation of micelles, not free Cy5.5.

High expression of PLK1 and low expression of miR-34a is associated with short survival rate in pancreatic cancer patients [14, 43, 44]. PLK1 is essential for stabilizing Myc family oncoproteins and miR-34a can affect cell proliferation through repression of Myc [45]. PLK1-Myc feedforward activation loop participates in PDAC progression and Myc amplification in pancreatic cancers predicts poor prognosis and resistance to therapy [17, 46, 47]. Altogether, c-myc downregulation can contribute to the inhibition of pancreatic cancer development [14, 47]. PLK1 inhibitor

volasertib could not only downregulate PLK1 to arrest cell cycle of tumor cells, but also reduce downstream c-myc phosphoraylation then inhibit c-myc transcription [46]. Meanwhile, miR-34a can target c-myc and Bcl-2 directly [45, 48]. To date, volasertib and miR-34a was tested alone in clinical trial, but their combination has not been evaluated yet [6, 49]. Herein, we investigated efficacy of combination of those two anticancer agents encapsulated by PEG-B-PAEBEA in orthotopic pancreatic tumor-bearing mice. Due to the synergistic effect of volasertib and miR-34a, downregulating of PLK1 while upregulating miR-34a resulted in significant suppression of their common target c-myc and pronounced tumor inhibition, which suggests the potential of combination of volasertib and miR-34a could be translated as a strategy in future pancreatic cancer therapy [17]. Moreover, H&E staining validated the formulations were well tolerated and did not display any signs of tissue or cellular damage such as ballooning degeneration of hepatocytes, increased alveolar wall thickness or cellular infiltration in lung tissue, myocardial fibrillar loss and vacuolation in heart tissues, edema, tubular vacuolization or tubular dilation with hemorrhagic areas in the kidney, or increased numbers of granulocytes in the spleen (**Figure 2.12**) [50, 51]. Those results support that our ROS-triggered polymeric micellar system has potential to overcome the limitations and adverse effects of gene and anticancer drug delivery.

In conclusion, we have demonstrated a ROS-labile polymer PEG-B-PAEBEA which was strongly positive charged can be self-assembled to micelles and effectively packaged volasertib and miR-34a into micelles but became neutral charged once triggered by intracellular ROS. The micelles successfully delivered volasertib and miR-34a in a controlled manner so that they can be released into the tumor sites accurately, resulting in high tumor regression compared to single drug-loaded micelles. Without complicated polymer design or drug modification, PEG-B-PAEBEA provided a facile and robust strategy with high biocompatibility for the encapsulation of hydrophobic drugs and genes.

2.6 Reference

[1] Y. Jia, D. Gu, J. Wan, B. Yu, X. Zhang, E.G. Chiorean, Y. Wang, J. Xie, The role of GLI-SOX2 signaling axis for gemcitabine resistance in pancreatic cancer, Oncogene, (2018).

[2] A. Adamska, A. Domenichini, M. Falasca, Pancreatic ductal adenocarcinoma: current and evolving therapies, International journal of molecular sciences, 18 (2017) 1338.

[3] B. Baradaran, R. Shahbazi, M. Khordadmehr, Dysregulation of key microRNAs in pancreatic cancer development, Biomedicine & Pharmacotherapy, 109 (2019) 1008-1015.

[4] S. Singh, D. Chitkara, V. Kumar, S.W. Behrman, R.I. Mahato, miRNA profiling in pancreatic cancer and restoration of chemosensitivity, Cancer letters, 334 (2013) 211-220.

[5] B. Song, X.S. Liu, S.J. Rice, S. Kuang, B.D. Elzey, S.F. Konieczny, T.L. Ratliff, T. Hazbun, E.G. Chiorean, X. Liu, Plk1 phosphorylation of orc2 and hbo1 contributes to gemcitabine resistance in pancreatic cancer, Molecular cancer therapeutics, 12 (2013) 58-68.

[6] R.E.A. Gutteridge, M.A. Ndiaye, X. Liu, N. Ahmad, Plk1 inhibitors in cancer therapy: from laboratory to clinics, Molecular cancer therapeutics, 15 (2016) 1427-1435.

[7] R. Garzon, G. Marcucci, C.M. Croce, Targeting microRNAs in cancer: rationale, strategies and challenges, Nature reviews Drug discovery, 9 (2010) 775.

[8] V. Rottiers, A.M. Näär, MicroRNAs in metabolism and metabolic disorders, Nature Reviews Molecular Cell Biology, 13 (2012) 239.

[9] V. Kumar, V. Kumar, A.K. Chaudhary, D.W. Coulter, T. McGuire, R.I. Mahato, Impact of miRNA-mRNA Profiling and Their Correlation on Medulloblastoma Tumorigenesis, Molecular Therapy-Nucleic Acids, 12 (2018) 490-503.

[10] W. Lu, C. Logsdon, J. Abbruzzese, Cancer Metabolism and its Therapeutic Implications, Journal of Cell Science & Therapy, 4 (2013) 143-152.

[11] X.J. Li, Z.J. Ren, J.H. Tang, MicroRNA-34a: a potential therapeutic target in human cancer, Cell Death &Amp; Disease, 5 (2014) e1327.

[12] H. Ling, M. Fabbri, G.A. Calin, MicroRNAs and other non-coding RNAs as targets for anticancer drug development, Nature Reviews Drug Discovery, 12 (2013) 847.

[13] G.T. Bommer, I. Gerin, Y. Feng, A.J. Kaczorowski, R. Kuick, R.E. Love, Y. Zhai, T.J. Giordano, Z.S. Qin, B.B. Moore, p53-mediated activation of miRNA34 candidate tumor-suppressor genes, Current biology, 17 (2007) 1298-1307.

[14] H. Gibori, S. Eliyahu, A. Krivitsky, D. Ben-Shushan, Y. Epshtein, G. Tiram, R. Blau, P. Ofek, J.S. Lee, E. Ruppin, Amphiphilic nanocarrier-induced modulation of PLK1 and miR-34a leads to improved therapeutic response in pancreatic cancer, Nature communications, 9 (2018) 16.

[15] D. Rudolph, M. Steegmaier, M. Hoffmann, M. Grauert, A. Baum, J. Quant, C. Haslinger, P. Garin-Chesa, G.R. Adolf, BI 6727, a Polo-like kinase inhibitor with improved pharmacokinetic profile and broad antitumor activity, Clinical cancer research, 15 (2009) 3094-3102.

[16] P. Schöffski, A. Awada, H. Dumez, T. Gil, S. Bartholomeus, P. Wolter, M. Taton, H. Fritsch, P. Glomb, G. Munzert, A phase I, dose-escalation study of the novel Polo-like kinase inhibitor volasertib (BI 6727) in patients with advanced solid tumours, European journal of cancer, 48 (2012) 179-186.

[17] D. Xiao, M. Yue, H. Su, P. Ren, J. Jiang, F. Li, Y. Hu, H. Du, H. Liu, G. Qing, Polo-like kinase-1 regulates Myc stabilization and activates a feedforward circuit promoting tumor cell survival, Molecular cell, 64 (2016) 493-506.

[18] X. Xin, X. Pei, X. Yang, Y. Lv, L. Zhang, W. He, L. Yin, Rod-Shaped Active Drug Particles Enable Efficient and Safe Gene Delivery, Advanced Science, 4 (2017) 1700324.

[19] S. Senapati, A.K. Mahanta, S. Kumar, P. Maiti, Controlled drug delivery vehicles for cancer treatment and their performance, Signal Transduction and Targeted Therapy, 3 (2018) 7.

[20] C.J. Cheng, G.T. Tietjen, J.K. Saucier-Sawyer, W.M. Saltzman, A holistic approach to targeting disease with polymeric nanoparticles, Nature Reviews Drug Discovery, 14 (2015) 239.

[21] S.C. Semple, A. Akinc, J. Chen, A.P. Sandhu, B.L. Mui, C.K. Cho, D.W. Sah, D. Stebbing, E.J. Crosley, E. Yaworski, I.M. Hafez, J.R. Dorkin, J. Qin, K. Lam, K.G. Rajeev, K.F. Wong, L.B. Jeffs, L. Nechev, M.L. Eisenhardt, M. Jayaraman, M. Kazem, M.A. Maier, M. Srinivasulu, M.J. Weinstein, Q. Chen, R. Alvarez, S.A. Barros, S. De, S.K. Klimuk, T. Borland, V. Kosovrasti, W.L. Cantley, Y.K. Tam, M. Manoharan, M.A. Ciufolini, M.A. Tracy, A. de Fougerolles, I. MacLachlan, P.R. Cullis, T.D. Madden, M.J. Hope, Rational design of cationic lipids for siRNA delivery, Nature biotechnology, 28 (2010) 172-176.

[22] J. Schulze, S. Kuhn, S. Hendrikx, M. Schulz-Siegmund, T. Polte, A. Aigner, Spray-Dried Nanoparticle-in-Microparticle Delivery Systems (NiMDS) for Gene Delivery, Comprising Polyethylenimine (PEI)-Based Nanoparticles in a Poly (Vinyl Alcohol) Matrix, Small, 14 (2018) 1701810.

[23] Y. Peng, D. Wen, F. Lin, R.I. Mahato, Co-delivery of siAlox15 and sunitinib for reversing the new-onset of type 1 diabetes in non-obese diabetic mice, Journal of Controlled Release, (2018).

[24] V. Kumar, G. Mondal, P. Slavik, S. Rachagani, S.K. Batra, R.I. Mahato, Codelivery of small molecule hedgehog inhibitor and miRNA for treating pancreatic cancer, Molecular pharmaceutics, 12 (2015) 1289-1298.

[25] A. Mittal, D. Chitkara, S.W. Behrman, R.I. Mahato, Efficacy of gemcitabine conjugated and miRNA-205 complexed micelles for treatment of advanced pancreatic cancer, Biomaterials, 35 (2014) 7077-7087.

[26] S. Lv, Y. Wu, K. Cai, H. He, Y. Li, M. Lan, X. Chen, J. Cheng, L. Yin, High drug loading and sub-quantitative loading efficiency of polymeric micelles driven by donor–receptor coordination interactions, Journal of the American Chemical Society, 140 (2018) 1235-1238.

[27] F. Lin, D. Wen, X. Wang, R.I. Mahato, Dual responsive micelles capable of modulating miRNA-34a to combat taxane resistance in prostate cancer, Biomaterials, (2018).

[28] G.-Y. Liou, P. Storz, Reactive oxygen species in cancer, Free radical research, 44 (2010) 479-496.

[29] Y. Zhang, J. Wei, S. Liu, J. Wang, X. Han, H. Qin, J. Lang, K. Cheng, Y. Li, Y. Qi, Inhibition of platelet function using liposomal nanoparticles blocks tumor metastasis, Theranostics, 7 (2017) 1062.

[30] S. Mura, J. Nicolas, P. Couvreur, Stimuli-responsive nanocarriers for drug delivery, Nature materials, 12 (2013) 991.

[31] M.S. Shim, Y. Xia, A reactive oxygen species (ROS)-responsive polymer for safe, efficient, and targeted gene delivery in cancer cells, Angewandte Chemie International Edition, 52 (2013) 6926-6929.

[32] C. Qiao, J. Yang, Q. Shen, R. Liu, Y. Li, Y. Shi, J. Chen, Y. Shen, Z. Xiao, J. Weng, Traceable Nanoparticles with Dual Targeting and ROS Response for RNAi-Based Immunochemotherapy of Intracranial Glioblastoma Treatment, Advanced Materials, 30 (2018) 1705054.

[33] C. Tapeinos, A. Pandit, Physical, Chemical, and Biological Structures based on ROS-Sensitive Moieties that are Able to Respond to Oxidative Microenvironments, Advanced Materials, 28 (2016) 5553-5585.

[34] J. Kováčik, B. Klejdus, M. Bačkor, Nitric oxide signals ROS scavenger-mediated enhancement of PAL activity in nitrogen-deficient Matricaria chamomilla roots: side effects of scavengers, Free Radical Biology and Medicine, 46 (2009) 1686-1693.

[35] R. Jin, Z. Liu, Y. Bai, Y. Zhou, X. Chen, Multiple-Responsive Mesoporous Silica Nanoparticles for Highly Accurate Drugs Delivery to Tumor Cells, ACS Omega, 3 (2018) 4306-4315.

[36] F. Zhang, S.S. Lau, T.J. Monks, The cytoprotective effect of N-acetyl-L-cysteine against ROS-induced cytotoxicity is independent of its ability to enhance glutathione synthesis, Toxicological Sciences, 120 (2010) 87-97.

[37] D.E. Owens III, N.A. Peppas, Opsonization, biodistribution, and pharmacokinetics of polymeric nanoparticles, International journal of pharmaceutics, 307 (2006) 93-102.

[38] S. Wilhelm, A.J. Tavares, Q. Dai, S. Ohta, J. Audet, H.F. Dvorak, W.C. Chan, Analysis of nanoparticle delivery to tumours, Nature reviews materials, 1 (2016) 16014.

[39] S. Kommareddy, M. Amiji, Antiangiogenic gene therapy with systemically administered sFlt-1 plasmid DNA in engineered gelatin-based nanovectors, Cancer gene therapy, 14 (2007) 488.

[40] H. Qi, H. Zhou, Q. Tang, J.Y. Lee, Z. Fan, S. Kim, M.C. Staub, T. Zhou, S. Mei, L. Han, Block copolymer crystalsomes with an ultrathin shell to extend blood circulation time, Nature communications, 9 (2018) 3005.

[41] X. Ji, N. Kong, J. Wang, W. Li, Y. Xiao, S.T. Gan, Y. Zhang, Y. Li, X. Song, Q. Xiong, A Novel Top-Down Synthesis of Ultrathin 2D Boron Nanosheets for Multimodal Imaging-Guided Cancer Therapy, Advanced Materials, 30 (2018) 1803031.

[42] M. Song, T. Liu, C. Shi, X. Zhang, X. Chen, Bioconjugated manganese dioxide nanoparticles enhance chemotherapy response by priming tumor-associated macrophages toward M1-like phenotype and attenuating tumor hypoxia, ACS nano, 10 (2015) 633-647.

[43] L. Li, L. Yuan, J. Luo, J. Gao, J. Guo, X. Xie, MiR-34a inhibits proliferation and migration of breast cancer through down-regulation of Bcl-2 and SIRT1, Clinical and experimental medicine, 13 (2013) 109-117.

[44] W. Weichert, M. Schmidt, J. Jacob, V. Gekeler, J. Langrehr, P. Neuhaus, M. Bahra, C. Denkert, M. Dietel, G. Kristiansen, Overexpression of Polo-like kinase 1 is a common and early event in pancreatic cancer, Pancreatology, 5 (2005) 259-265.

[45] N. Christoffersen, R. Shalgi, L. Frankel, E. Leucci, M. Lees, M. Klausen, Y. Pilpel, F. Nielsen, M. Oren, A.H. Lund, p53-independent upregulation of miR-34a during oncogene-induced senescence represses MYC, Cell death and differentiation, 17 (2010) 236.

[46] C. Murga-Zamalloa, A. Polk, W. Hanel, P. Chowdhury, N. Brown, A.C. Hristov, N.G. Bailey, T. Wang, T. Phillips, S. Devata, Polo-like-kinase 1 (PLK-1) and c-myc inhibition with the dual kinase-bromodomain inhibitor volasertib in aggressive lymphomas, Oncotarget, 8 (2017) 114474.

[47] V.J.S.-A. Lobo, L.C. Fernández, E. Carrillo-de-Santa-Pau, L. Richart, I. Cobo, J. Cendrowski, U. Moreno, N. del Pozo, D. Megías, B. Bréant, c-Myc downregulation is required for preacinar to acinar maturation and pancreatic homeostasis, Gut, 67 (2018) 707-718.

[48] Q. Ji, X. Hao, M. Zhang, W. Tang, M. Yang, L. Li, D. Xiang, J.T. DeSano, G.T. Bommer, D. Fan, MicroRNA miR-34 inhibits human pancreatic cancer tumor-initiating cells, PloS one, 4 (2009) e6816.

[49] M.S. Beg, A.J. Brenner, J. Sachdev, M. Borad, Y.-K. Kang, J. Stoudemire, S. Smith, A.G. Bader, S. Kim, D.S. Hong, Phase I study of MRX34, a liposomal miR-34a mimic, administered twice weekly in patients with advanced solid tumors, Investigational new drugs, 35 (2017) 180-188.

[50] M. Zhang, B. Xiao, H. Wang, M.K. Han, Z. Zhang, E. Viennois, C. Xu, D. Merlin, Edible ginger-derived nano-lipids loaded with doxorubicin as a novel drug-delivery approach for colon cancer therapy, Molecular Therapy, 24 (2016) 1783-1796.

[51] B. Xiao, M. Zhang, E. Viennois, Y. Zhang, N. Wei, M.T. Baker, Y. Jung, D. Merlin, Inhibition of MDR1 gene expression and enhancing cellular uptake for effective colon cancer treatment using dual-surface-functionalized nanoparticles, Biomaterials, 48 (2015) 147-160.

[52] C.-W. Lin, K.-Y. Lu, S.-Y. Wang, H.-W. Sung, F.-L. Mi, CD44-specific nanoparticles for redox-triggered reactive oxygen species production and doxorubicin release, Acta biomaterialia, 35 (2016) 280-292.

Chapter III

Dual Responsive Micelles Capable of Modulating miRNA-34a to Combat Taxane Resistance in Prostate Cancer

3.1 Abstract

There is a direct correlation between increase in the number of cancer stem cells (CSCs) and chemoresistance that impedes successful chemotherapy. Synergistic therapy by targeting both bulk tumor cells and CSCs has shown promise in reversing chemoresistance and treating resistant prostate cancer. Herein, we demonstrated the fabrication of a pH and glutathione (GSH) sensitive nanocarrier for co-delivery of docetaxel (DTX) and rubone (RUB), a miR-34 activator for targeting CSCs, for the treatment of taxane resistant (TXR) prostate cancer. DTX loaded P-RUB (DTX/P-RUB) micelles were prepared by encapsulating DTX into pH responsive diisopropylaminoethanol (DIPAE) and GSH responsive RUB prodrug conjugated polycarbonate-based micelles. The self-assembled DTX/P-RUB micelles displayed good stability in vitro and could efficiently target to tumors by enhanced permeability and retention (EPR) effect. After endocytosis by tumor cells, the micelles underwent expansion and disassembly due to the protonation of DIPAE and GSH induced cleavage of disulfide bond in acidic endocytic vesicles, resulting in fast release of DTX and RUB. The released RUB then upregulated the intracellular miR-34a, which then affected the expression of proteins involved in chemoresistance, thus sensitizing the tumor cells towards DTX and further leading to significant inhibition of TXR tumor progression. Thus, DTX/P-RUB micelles have the potential to treat TXR prostate cancer. By taking advantage of this dual responsive strategy, the successful delivery of many other hydrophobic drugs can be achieved for cancer treatment.

3.2 Introduction

Development of chemoresistance poses a serious problem in cancer chemotherapy [1,2]. The mounting evidence indicates the increased number of cancer stem cells (CSCs) after repeated treatments mainly accounts for the acquired chemoresistance because of their inherent tumor initiating and self-renewal capacity, more chemo-resistant property and key roles in tumorigenesis, progression and metastasis [3-6]. MicroRNAs (miRNAs) regulate CSCs as well as normal stem cells and dysregulation of miRNAs in CSCs has been contributed to chemoresistance [7-11]. Tumor suppressor miR-34a recently received increasing attention and is a key negative regulator of tumorigenic prostate CSCs [7,12,13]. A chalcone derivative, 2′-hydroxy-2,4,4′,5,6′-pentamethoxychalcone, termed as rubone (RUB), was found to upregulate the intracellular miR-34a in hepatocellular carcinoma, resulting in significant tumor shrinkage [14]. Unfortunately, the in vivo delivery of oligonucleotide-based miRNA and highly hydrophobic drugs remains a challenge due to potential off-target toxicity, rapid clearance, poor cellular uptake or in vivo instability [14-17]. Over the past several decades, nanoparticles have received tremendous attention in cancer therapy for its ability to improve aqueous solubility and stability of hydrophobic drugs and nucleic acids, prolong blood circulation half-life and increase deposition in the target tissues via the enhanced permeability and retention (EPR) effect [18-22].

Although some nanoparticles have been designed to address chemoresistance [23-26], we noted that only a few have been exploited to reverse the drug resistance by targeting the CSCs by regulating the level of miRNAs with small molecules. Deng et al. reported through encapsulation of RUB in cationic micelles, the RUB exhibits higher water solubility and higher potency in antitumor activity [27]. We previously reported the co-delivery of paclitaxel and RUB through encapsulation in poly (ethylene glycol)-block-poly (2-methyl-2-carboxyl-propylene carbonate-graft-dodecanol; PEG-PCD) can be used for the treatment of taxane resistant (TXR) prostate

cancer by chemosensitizing the prostate cancer cells [28]. Compared with these conventional nanoparticles, a bio-responsive nanoplatform with excellent biocompatibility, biodegradation and high drug loading is of growing interest in recent years [29,30], especially for polymer-drug conjugate delivery system, since insufficient drug exposure due to slow drug release might induce acquired chemoresistance. It is well documented that tumor has a slightly acidic microenvironment (6.5-6.8) while the pH value is 5.5-6.5 in early endosomes and 4.5-5.5 in late endosomes/lysosomes [31,32] and the level of glutathione (GSH) is significantly elevated in tumor cells [33,34]. Thus, the design of taking advantage of the variations in either redox condition [35-37] or pH value [30,38-40] or even both [41,42] will be markedly influential on the effectiveness of nanoparticles by accelerating and maximizing the cargo release. Keeping all these in mind, we have developed a novel pH and GSH responsive nanoplatform by integrating multi-responsive property to meet the demands in combating drug resistance in the study. Our polymeric drug delivery system undergoes rapid drug release at the tumor site upon endocytosis into acidic intracellular compartments where the low pH value promotes protonation of DIPAE and the abundant GSH induces the cleavage of disulfide bond, leading to efficient drug release. As proof-of-concept, we selected the microtubule stabilizer DTX and a miR-34a activator RUB as a combination therapy for treating TXR prostate cancer [28]. Driven by delicate balance between hydrophobic (i.e., RUB and tertiary amine) and hydrophilic (i.e., PEG) segments [43] and the ionic interaction (i.e., partially ionized tertiary amines [44] and carboxylic acids) at physiological pH condition (7.4), the RUB and DIPAE conjugated polycarbonate (P-RUB) can self-assemble into micelles and encapsulate DTX into the micellar core by coprecipitation, with pH responsive property conferred by DIPAE, a tertiary amine [45–47] and GSH responsive property endowed by the attachment of RUB through 2,2′-dithiodiethanol, a disulfide containing linker [48–50]. We expect such micellar system could keep its structural integrity and selectively accumulate in TXR tumor site after administration. Upon endocytosis by tumor cells, the micelles would expand and

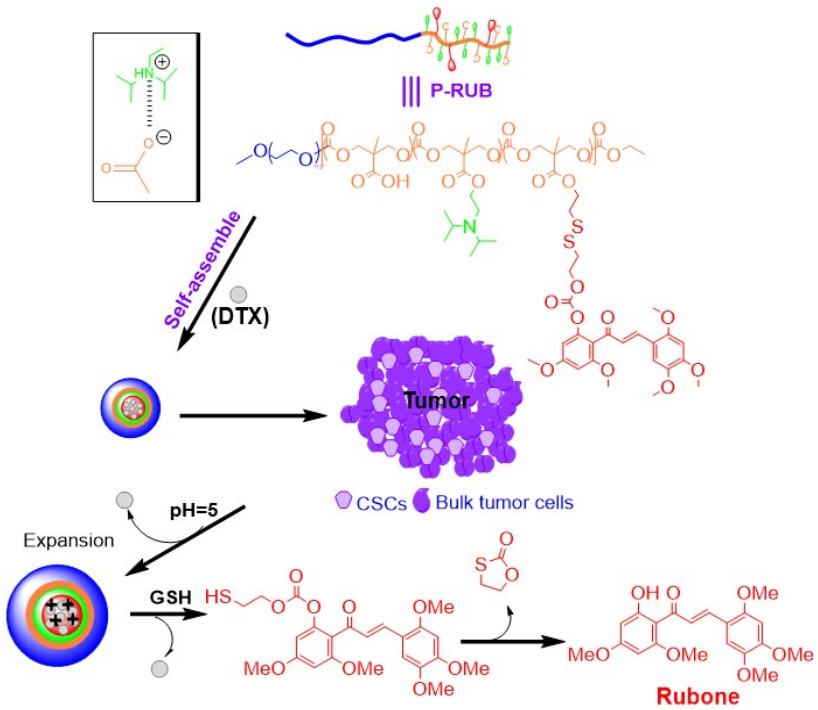

Figure 3.1 Schematic illustration of structural compositions, self-assembly and drug release of dual-sensitive DTX loaded RUB-conjugated polymeric (P-RUB) micelles.

dissociate in response to low pH value of endocytic vehicles, thus leading to ultrafast drug release by consequent sufficient exposure to GSH for the cleavage of disulfide bond, which would result in successful inhibition of TXR tumor growth. This consequence should be attributed to the protonation of ionizable amino groups and subsequent breakup of the ionic bonds in acidic endocytic vehicles (**Figure 3.1**). The design not only perfectly solves RUB loading issue (less than 7%) faced by other studies, including ourselves', but also lowers the chance of resultant chemoresistance induced by sublethal drug exposure.

3.3 Experimental session

3.3.1 Materials

4′,6′-Dimethoxy-2′-hydroxyacetophenone, 2,4,5-trimethoxybenzaldehyde were purchased from TCI America. α-Methoxy-ε-hydroxy- poly(ethylene glycol) (mPEG-OH, Mn = 5 kDa) (mPEG-OH), trimethylamine (TEA), 2-dihydroxyethyl disulfide, sodium hydroxide (NaOH), potassium hydroxide (KOH), N-(3-dimethylaminopropyl)-N′-ethylcarbodiimide hydrochloride (EDCI), 1-hydroxy-7-azabenzotriazole (HOAt), pyridine, dimethylformamide (DMF), dichloromethane (DCM), tetrahydrofuran (THF), chlorotriethylsilane (TES-Cl), imidazole, 1,8-diazabicyclo [5.4.0]undec-7-ene (DBU), benzyl bromide, 2,2′-bis(hydroxymethyl)propionic acid and triphosgene were all purchased from Sigma-Aldrich and used as received. Docetaxel (DTX) was obtained from LC Laboratories. The buffer solutions were prepared in our lab. Dialysis membrane was obtained from Spectrum Lab. All solvents were of analytical grade.

3.3.2 Synthesis of RUB-S-S-OH, P-RUB and non-responsive R-RUB

3.3.2.1 Synthesis of RUB-S-S-OH

Step 1. A mixture of 4, 6-dimethoxy-2-hydroxyacetophenone (1.0 g, 5.1 mmol), 2,4,5-trimethoxybenzaldehyde (1.0 g, 5.1 mmol) and KOH (8.0 g, 142.9 mmol) in ethanol was stirred overnight at room temperature. After removal of solvent, the residue was dissolved in CH_2Cl_2 (400 mL) and neutralized with 4 M HCl. The organic layer was separated, and the aqueous layer was extracted with CH_2Cl_2. The combined organic extracts were washed with saturated $NaHCO_3$, water and brine, dried over anhydrous Na_2SO_4, filtered and concentrated. The crude product was purified by crystallization from EtOH to afford **RUB** as a yellow solid (1.37 g, 72%). ^{1}H NMR (500 MHz, $CDCl_3$) δ 14.54 (s, 1H), 8.00 (dd, J_1 = 130.2 Hz, J_2 = 15.6 Hz, 2H), 7.26 (s, 1H), 7.12 (s, 1H), 6.52 (s, 1H), 6.03 (dd, J_1 = 74.5 Hz, J_2 = 1.9 Hz, 2H), 3.95 (s, 3H), 3.91 (s, 6H), 3.89 (s, 3H), 3.83 (s, 3H).

Step 2. Chlorotriethylsilane (1 g, 6.5 mmol) was added to a mixture of 2-hydroxyethyl disulfide (1.0 g, 6.5 mmol) and imidazole (0.46 g, 6.8 mmol) in DCM at 0 °C. The resulting mixture was stirred overnight at the room temperature, filtered to remove solid precipitate and concentrated. The residue was dissolved in CH_2Cl_2, washed with saturated $NaHCO_3$, water and brine, dried over anhydrous Na_2SO_4, filtered and concentrated. The crude product was purified by flash column chromatography (hexane: EtOAc = 1:1) to afford **compound 1** as colorless oil (0.6 g, 60%). ^{1}H NMR (500 MHz, $CDCl_3$) δ 3.89 (dt, J_1 = 13.4 Hz, J_2 = 6.3 Hz, 4H), 2.90-2.81 (m, 4H), 2.07 (t, J = 6.3 Hz, 1H), 0.97 (t, J = 7.9 Hz, 9H), 0.62 (q, J = 7.9 Hz, 6H).

Step 3. The solution of triphosgene (59 mg, 0.3 mmol) in DCM was added to the mixture of RUB (374 mg, 1.0 mmol) and DMAP (610 mg, 5 mmol) in DCM. The mixture was stirred for 1 h before the solution of **compound 1** (280.875 mg, 1.05 mmol) in CH_2Cl_2 was added. After stirring overnight, the solvents were removed and the residue was re- dissolved in CH_2Cl_2, washed with water, dried over anhydrous Na_2SO_4, filtered and concentrated. The crude product was purified by column chromatography (Hexane: EtOAc = 1:1) to afford **compound 2** as a yellow solid (0.43 g, 65%).

Step 4. A mixture of **compound 2** (0.4 g, 0.6 mmol) in ethanol with tetrabutylammonium fluoride (TBAF) was stirred at the room temperature for 1 h before neutralized with saturated $NaHCO_3$ aqueous solution. The mixture was then diluted with CH_2Cl_2 and washed with water and brine, dried over anhydrous Na_2SO_4, filtered and concentrated. The crude product was purified by silica chromatography (Hexane: EtOAc = 1:3) to afford **RUB-S-S-OH** as an orange solid (282.54 mg, 85%). ^{1}H NMR (499 MHz, CDCl3): δ 7.34 (dd, J_1 = 374.7 Hz, J_2 = 16.1 Hz, 1H), 6.86 (dd, J_1 = 145.1 Hz, J_2 = 129.0 Hz, 1H), 6.42 (dd, J_1 = 18.8 Hz, J_2 = 1.9 Hz, 1H), 4.42 (t, J = 6.6 Hz, 1H), 3.93 (s, 1H), 3.87-3.83 (m, 3H), 3.80 (s, 1H), 2.93 (t, J = 6.6 Hz, 1H), 2.86 (t, J = 6.1 Hz, 1H), 2.54 (t, J = 6.1 Hz, 1H). ^{13}C NMR (126 MHz, CDCl3): δ

191.74, 161.89, 158.99, 154.47, 152.91, 152.50, 149.95, 143.24, 140.07, 126.11, 116.12, 115.28, 111.24, 99.68, 97.11, 96.88, 66.43, 60.41, 56.46, 56.39, 56.04, 56.03, 55.65, 41.45, 36.60.

3.3.2.2 Synthesis of P-RUB

Step 1. 2, 2-bis(hydroxymethyl)propionic acid (22.51 g, 0.168 mol) and KOH (9.4 g, 0.168 mol) was dissolved in DMF by heating the solution to 100 °C. Benzyl bromide (34.34 g, 0.202 mol) was then added dropwise to the above solution and the mixture was kept stirring at 100 °C overnight. After removal of solvent, the residue was re-dissolved in EtOAc, washed with H_2O (4 x 200 mL), dried over anhydrous Na_2SO_4, filtered and concentrated. The crude product was recrystallized from toluene to afford **benzyl 2,2-bis(methylol)propionate** as a white solid (26.34 g, 70%).

Step 2. A solution of triphosgene (7.425 g, 25 mmol) in CH_2Cl_2 was added dropwise to a solution of benzyl 2, 2-bis(methylol)propionate (11.25 g, 50 mmol) and pyridine (25 mL) in CH_2Cl_2 (150 mL) at −78 °C under N_2 atmosphere over 1 h. The resulting mixture was stirred at room temperature for 2 h before being quenched with saturated ammonium chloride solution. The organic layer was separated, and the aqueous layer was extracted with CH_2Cl_2 (2 × 100 mL). The combined organic extracts were washed with 1 M HCl (3 × 150 mL), saturated sodium hydrogen carbonate aqueous solution and brine, dried over anhydrous Na_2SO_4, filtered and concentrated. The crude product was further purified by recrystallization in ethyl acetate to afford **2-methyl- 2-benzyloxycarbonyl-propylene carbonate (MBC)** as a white solid (9.37 g, 75%).

Step 3. The catalyst 1,8-diazabicyclo[5.4.0]undec-7-ene (DBU) was added to a stirred solution of mPEG-OH (1.0 g, 0.2 mmol) and MBC(1.8 g, 7.2 mmol) in CH_2Cl_2. The resulting mixture was stirred for 4 h before being quenched by benzoic acid. The mixture was then concentrated and triturated with cold isopropanol (IPA). The resulting solid was collected by filtration and dried to afford PEG-PBC (2.154 g, 85%).

Step 4. To a mixture of PEG-PBC in THF and methanol (1:1) was added 10% w/w Pd/C. The reaction was stirred for 24 h under H_2 balloon. The reaction suspension was then filtered and the filtrate was concentrated to afford **poly (ethylene glycol)-block-poly (2-methyl-2-carboxyl-propylene carbonate) (PEG-PCC)** in a yield of 97%.

Step 5. A mixture of PEG-PCC (Mw 9800, 100 mg, 0.01 mmol), RUB-S-S-OH (33.24 mg, 0.065 mmol), HOAT (67.5 mg, 0.5 mmol), 1-ethyl-3-(3-dimethylaminopropyl)carbodiimide (EDCI) (96 mg, 0.5 mmol) and triethanolamine (TEA) (60.6 mg, 0.6 mmol) in anhydrous DMF was stirred for 24 h under N_2 before diisopropylamino ethanol (73 mg, 0.5 mmol) was added. The reaction was continued for another 24 h and then triturated with cold isopropanol. The resulting solid was collected by filtration and dialyzed against acetone: methanol (1:1) to give **poly (ethylene glycol)-block-poly (2-methyl-2-carboxyl-propylene carbonate-graft-diisopropylaminoethanol-grafted-RUB-S-S-OH)** (**P-RUB)** as a yellow solid (104 mg, 73%). The successful conjugation of RUB-S-S-OH and DIPAE on P-RUB was confirmed by ^{1}H NMR spectra. 5 molecules of RUB were calculated to be conjugated on each polymer chain. The weight percentage of RUB in the conjugate was further confirmed by HPLC method (Column: Phenomenex Aqua 5U C18; temperature = 25 °C; flow rate = 0.7 mL/min; mobile phase = 4:1 vol/vol mixture of acetonitrile and water).

3.3.2.3 Synthesis of non-responsive P-RUB

Nonresponsive P-RUB was synthesized in a similar way by conjugating RUB and dodecanol to the pendant carboxylic acid groups of PEG-PCC via esterification. The chemical structure of nonresponsive P-RUB was determined by ^{1}H NMR in $CDCl_3$ and the weight percentage of RUB in the conjugate was calculated by integration of the peak and HPLC method (Column: Phenomenex Aqua 5U C18; temperature = 25 °C; flow rate = 0.7 mL/ min; mobile phase = 4:1 vol/vol mixture of acetonitrile and water).

3.3.3 Preparation and characterization of pH and GSH dual responsive P- RUB micelles

The pH and GSH responsive micelles were prepared using nano-precipitation method. Briefly, 5 mg P-RUB or Cy5.5 labeled P-RUB were first dissolved in 250 μL of acetone. The resultant clear solution was added into 1 mL of PBS under stirring for 1 h followed by evaporation of residual acetone under vacuum. DTX encapsulated P-RUB micelles were prepared using a similar way that 0.6 mg DTX was co-dissolved with 5 mg P-RUB in 250 μL of acetone. The drug loading and loading efficiency were determined using HPLC method (Column: Phenomenex Aqua 5U C18; temperature = 25 °C; flow rate = 0.7 mL/ min; mobile phase = 4:1 vol/vol mixture of acetonitrile and water) by use of a UV detector at 228 nm for DTX and 324 nm for RUB. The pH and GSH responsive property of P-RUB micelles was determined by measuring particle size and ζ potential using a Malvern Zetasizer at a 90° angle after incubation of P-RUB micelles in biomimetic environment of pH 5.0, 10 mM GSH at 37 °C. The morphology and its change of P-RUB was determined by a transmission electron microscope (TEM). In vitro RUB release from dual responsive and nonresponsive P-RUB micelles was carried out under different conditions (PBS at pH 7.4 with or without 10 mM GSH, acetate buffer at pH 5.0 with or without 10 mM GSH). For DTX release, the dialysis bags (MWCO: 14000 Da) were loaded with DTX/R-RUB micelles and were then dipped into a large excess of buffer solutions and gently shaken at 37 °C at a speed of 100 rpm (n = 3). At predetermined time points, 100 μL of solution was taken out. The buffers were changed periodically to maintain the sink condition. RUB and DTX concentrations were determined by HPLC under the following conditions: Phenomenex Aqua 5μ C18 column (250 × 4.6 mm) at 25 °C and flow rate of 0.7 mL/min. A mixture of acetonitrile and water (4:1 vol/vol) was used as the mobile phase, injection volume was 20 μL and wavelengths were 229 and 325 nm for DTX and RUB, respectively.

3.3.4 Determination of critical micelle concentration (CMC)

The CMC of P-RUB micelles was determined using pyrene as a fluorescent probe. P-RUB

micelles were prepared as aforementioned and diluted to different concentrations (1×10^{-5} ~0.5 mg/mL). Then pyrene in acetone (1.2×10^{-6} M) was added to P-RUB solutions and shook for 24 h at the room temperature. The fluorescence emission spectra of P-RUB micelles were recorded by using a spectrofluorometer with an excitation wavelength at 334 nm. The ratio of emission intensity (I384/I373) was plotted against the logarithm of P-RUB mass concentrations.

3.3.5 Cellular internalization and subcellular fate

DU145-TXR and PC3-TXR cells were kindly provided by Dr. Evan T. Keller from the University of Michigan in 2010. These cells were cultured in 100 nM containing complete RPMI 1460 medium supplemented with 10% of fetal bovine serum (FBS) and 1% antibiotics and antimycotics. Both these cell lines were cultured at 37 °C under a humidified atmosphere with 5% CO_2 supply. For cellular internalization studies, these cell lines (5×10^4) were first seeded in a coverslip chamber respectively and cultured for 24 h. Then, the cells were incubated with fresh media containing Cy5.5 labeled P-RUB micelles for 6 h at 37 °C in dark. We also used Cy5.5-labeled non-responsive P-RUB micelles as a positive control. The cells were then washed with ice cold PBS thrice and fixed with 4% paraformaldehyde. Finally, the cells were stained with 4′,6-diamidino-2-phenylindole) (DAPI) and visualized using the confocal laser scanning microscopy (CLSM). To track intracellular molecular delivery, PC3-TXR and DU145-TXR (5×10^4) were first seeded in a coverslip chamber respectively and cultured for 24 h. Then, the cells were incubated with fresh media containing Cy5.5 labeled P-RUB micelles as well as Cy5.5 labeled nonresponsive P-RUB micelles for 6 h at 37 °C in dark, followed by the stain of Lysotracker, Hoechst 44432 and immediately imaged by CLSM.

3.3.6 RT-PCR and western blot analysis

The total RNA was isolated from DU145-TXR and PC3-TXR cells using miRNeasy

isolation kits (Qiagen, Valencia, CA) after incubation with different concentrations of P-RUB for 48 h. Then, total RNA was reverse transcribed to cDNA using TaqMan qRT-PCR kit (Life Technologies, Carlsbad, CA). cDNA was amplified on real-time PCR using SYBR Green dye universal master mix and miR-34a primer on a Light Cycler 480 (Roche, Indianapolis). U6 was used as a housekeeping gene and relative amount of miR-34as was calculated using the crossing point (Cp) value.

To determine protein expression, the cells (3×10^5) treated with P-RUB (5, 10, 25, 50 μM) for 48 h were lysed with RIPA buffer. The extracted protein concentration in each sample was determined by BCA assay and then adjusted to the same level and transferred to poly- vinylidene difluoride (PVDF) membrane. After incubation with primary antibody (1:500) at 4 °C overnight, IR fluorescent dye labeled secondary antibodies (925-68074 or 925-32213, Li-COR) was added, followed by analysis using Licor Odyssey system (LI-COR Biotechnology, Lincoln, NE). The antibodies purchased from Santa Cruz Biotechnology were used in the study include anti-P-gp, anti-Elk-1 (sc-355), anti-SIRT1 (sc- 15404), anti-TAp73 (sc-7957), anti-Bax (sc-6236), anti-β-actin (sc- 1616).

3.3.7 Inhibition of CSC proliferation by P-RUB micelles

DU145-TXR and PC3-TXR cells (2.5×10^5/well) were seeded in 6 well plates. After 24 h, both of the cell lines were treated with P-RUB micelles containing 5, 10 and 25 μM of RUB and incubated for 48 h. Then, the cells were harvested and analyzed for $ALDH^+$ stained by Aldehyde assay kit per the manufacturer's instruction (Stemcell Technologies, Vancouver, Canada) and further analyzed using an FACSCalibur flow cytometer. GFP-positive and DEAB-treated cells were used to set up a gated region.

3.3.8 Drug effect on cell cycle of PC3, DU145, DU145-TXR and PC3-TXR

DU145-TXR and PC3-TXR cells (15×10^4/well) were seeded in a 6-well plate,

respectively and cultured for 24 h, the medium was replaced with 100 μL of fresh media containing different treatments, DTX (60 nM for PC3-TXR, 180 nM for DU145 TXR), P-RUB (10 μM for PC3-TXR, 20 μM for DU145-TXR), and DTX/P-RUB (30 nM/5 μM, 90 nM/10 μM) respectively. After 24 h incubation, the cells were stained with PI/RNase solution and evaluated with a flow cytometer. Effect of DTX on DU145 and PC3 cell cycle arrest was also determined.

3.3.9 Cytotoxicity of P-RUB and DTX/P-RUB in 2D and 3D models

For cell viability in a two-dimensional (2D) model, DU145-TXR and PC3-TXR cells (6×10^3/well) were seeded in 96 well plate, respectively and cultured for 24 h, the medium was replaced with 100 μL of fresh media containing different treatments as follows: DTX, RUB, P-RUB and DTX/P- RUB (5, 10, 25, 50 μM). After 48 h incubation, cell viability was evaluated by MTT assay. For cell viability in 3D model, DU145-TXR cells (8×10^4/well) suspended in 500 μL media was added to a 24-well plate with 200 μL of 100% Matrigel as basement. After 48 h, the old medium was replaced with the fresh growth medium containing DTX (180 nM), P-RUB (20 μM), DTX/P-RUB (90 nM/10 μM), nonresponsive P-RUB(20 μM), and nonresponsive DTX/P-RUB (90 nM/10 μM), which was replaced every other 2 days for 10 days before analyzing the therapeutic efficacy.

3.3.10 Biodistribution and anticancer efficacy

All animal study was performed under the guidelines of Institutional Animal Care and Use Committee (IACUC) at the University of Nebraska Medical Center (Omaha, NE). To monitor the tumor growth, luciferase expressing PC3-TXR cells were obtained by transducing the cells with lentiviral particles encoding GFP and luciferase. Orthotopic PC3-TXR bearing nude mouse model was established by making a midline incision in the lower abdomen of 8 weeks old male nude mice to expose the dorsal prostate lobe, where 30 μL of PBS containing 1 million cells was injected.

Three weeks after tumor cell injection, mice with orthotopic tumor were injected with Cy5.5 labeled DTX/P-RUB micelles through a tail vein. The fluorescence signal (excitation: 640 nm; emission: 710 nm) was detected by using IVIS imaging system (PerkinElmer, Hopkinton, MA) at 1, 3, 6, 12, 24, 48 h. After the final imaging at 24 h and 48 h, the mice were sacrificed. Tumors and major organs including kidney, heart, spleen, lung and liver were harvested for further *ex vivo* imaging. To assess RUB concentration in the tumor, equivalent doses of Cy5.5 labeled P-RUB and free RUB were intravenously injected into orthotopic prostate cancer bearing mice. Tumors were harvested at 24h and 48h, respectively, followed by homogenization. The homogenate was centrifuged at 12,000×g at 20 °C for 10 min. The supernatant was aspirated out and air dried at 40 °C. Afterwards, 250 μL of acetonitrile and 50 μL of ammonium hydroxide were added to the tubes and stirred for 20 min. Finally, RUB concentration in the tumors was determined by LC-MS/MS using Analyst® software on a QTRAP 4000 mass spectrometer. The separation was achieved on a Shimadzu HPLC, with a Waters C_{18} column (150 × 3.9 mm, 4 μm) with isocratic elution of water and acetonitrile at a ratio of 35:65 v/v as a mobile phase at 0.5 mL/min flow rate. An injection volume of 10 μL was used for sample analysis by LC-MS/MS. The mass spectrometer was operated in the positively multiple reaction monitoring (MRM) for RUB and internal standard. The following MRM transitions were monitored: m/z 375.3 for RUB and m/z 197.1 for 2,4,4-trimethoxybenzaldehye. RUB concentration was calculated using a $1/x^2$ quadratic regression over a concentration range of 5.0–5000 ng/mL with constant internal standard.

For antitumor efficacy, once the bioluminescence intensity was reached 6×10^6, the mice were randomly divided into 6 groups, with 6 mice in each group. Then the mice were intravenously injected with various formulations, including PBS, DTX+RUB, P-RUB, DTX/P-RUB, DTX/PEG-PCD and nonresponsive DTX/P-RUB micelles (DTX 5 mg/kg and RUB 25 mg/kg) every other 2 days for 18 days. Tumor bioluminescence and body weights of the mice were recorded once a

week. At 2nd day after the final injection, the mice were sacrificed. Then miR-34a level in tumors from each group was determined using miRNeasy isolation and RT-PCR (Qiagen, Valencia, CA). Besides, the major organs and tumors were collected and fixed in 10% of formalin solution overnight for following hematoxylin and eosin (H&E) staining and immunohistochemistry for SIRT1, Ki-67 and cleaved caspase-3. Representative immunohistochemical images were analyzed using ImageJ to quantify fluorescence intensity. We also determined SIRT1 protein expression in tumor tissues by Western blot analysis.

3.3.11 Statistical analysis

All the data were presented as the average value ± standard deviation (SD). The statistical comparison was carried out by one-way ANOVA and a P value < 0.05 was considered to be statistically significant.

3.4 Results

3.4.1 Synthesis and characterization of P-RUB and non-responsive P-RUB

Dual responsive P-RUB was synthesized via a multi-step process and characterized by ^{1}H NMR (**Figure 3.2**). Briefly, RUB was synthesized via aldol reaction, and then a disulfide containing linker was conjugated to RUB by the formation of carbonate bond, yielding RUB-S-S-OH. After that MBC was obtained and copolymerized with mPEG-OH (Mw = 5000) to produce PEG-PBC, followed by the removal of benzyl protecting groups to produce PEG-PCC with pendant carboxylic acids. Finally, PEG-PCC was treated with RUB-S-S-OH and DIPAE to afford P-RUB. Polycarbonate was selected as a block polymer because of its convenience for chemical functionality, its biodegradability, its biocompatibility and non-toxic consequent products (an alcohol and carbon dioxide). About 17% of the carboxylic acids reacted with RUB-S-S-OH and 47% with DIPAE based on NMR spectrum. The unreacted carboxylic acids provide opportunity for further attachment of other components (targeting ligand and chemotherapeutics). Besides, the

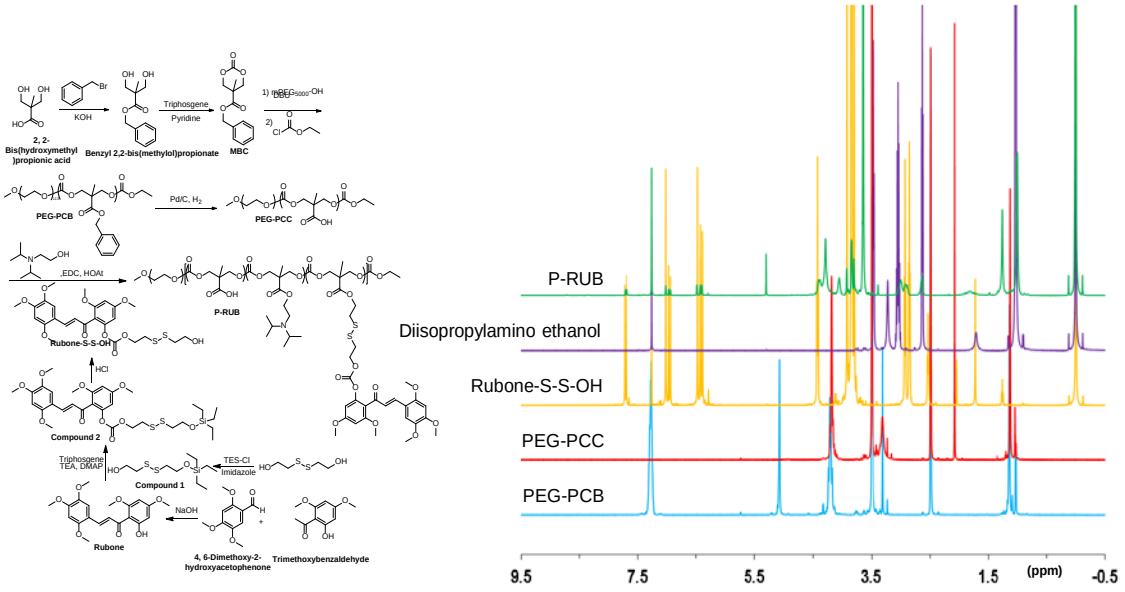

Figure 3.33 Synthesis and characterization of dual responsive P-RUB. Synthetic scheme and ^{1}H-NMR spectrum of dual sensitive poly(ethylene glycol)-block-poly(2-methyl-2-carboxyl-propylene carbonate-graft-rubone-graft-diisopropylamino ethanol (P-RUB). The black arrow indicates the presence of rubone-S-S-OH and diisopropylamino ethanol in poly(ethylene glycol)-

partially ionized carboxylic acids (pKa = 5) and DIPAE (pKa = 9) [43] at physiologic pH condition (7.4) would form ionic interaction, thus stabilizing the micellar system. RUB content in the conjugate was calculated to be 12.5 wt% as based on the integration of peak at 3.65 ppm (CH_2 of mPEG) and peak at 7.72, 7.03, 6.94,6.49, 6.4(aromatic proton on RUB-S-S-OH) in the NMR spectrum. For use as a positive control, we also synthesized nonresponsive P-RUB by conjugating RUB and dodecanol to the polycarbonate backbone. Non-responsive P-RUB was synthesized in a similar way except that RUB and dodecanol were used to react with PEG-PCC, which was characterized afterwards by ^{1}H NMR as well (**Figure 3.3**).

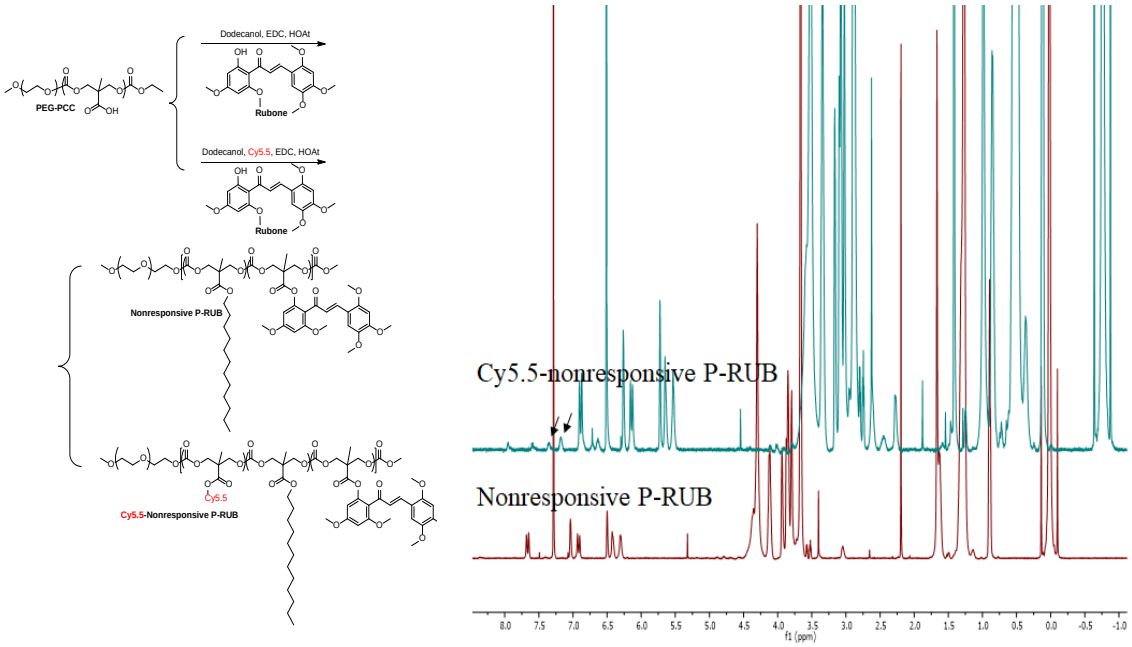

Figure 3.196 Synthesis and characterization of non-responsive P-RUB. Synthetic scheme and ^{1}H-NMR spectrum of no label or Cy5.5 labeled nonresponsive poly(ethylene glycol)-block-poly(2-methyl-2-carboxyl-propylenecarbonate-graft-rubone-graft-dodecanol)---(abbreviated as Cy5.5-labeled nonresponsive P-RUB).

3.4.2 Particle size and surface morphology of DTX/P-RUB micelles

P-RUB micelles and DTX encapsulated dual responsive and non-responsive micelles were prepared by nanoprecipitation method. The resultant responsive micelles had sizes of 45.07 ± 0.49 nm and 49 ± 0.26 nm, respectively, determined by dynamic light scattering (DLS) and showed spherical morphology by TEM （**Figure 3.4 A**）. Determined by HPLC method, the content loaded in the polymeric micelle core was relatively high (9%). The polymeric micelles prepared from PEG-PCC showed a larger size of 250 nm. The hydrophobicity of tertiary amine and RUB greatly stabilized the micellar structure, resulting in little change in the particle size of P-RUB micelles when pH was above 6.5 for 120 h (**Figure 3.4 B**), implying its ability of maintaining the structural integrity in the bloodstream and tumor microenvironment. When

Table 3.161 Particle size distribution, polydispersity (PDI), zeta-potential (ζ) and loading capacity (LC) of P-RUB micelles.

Polymers	Size (nm)	PDI	ζ (mV)	Loading Capacity (%w/w)	
				Rubone	DTX
P-RUBs	45.07±0.49	0.08 ± 0.005	pH 7.4 0.8 ± 0.333 pH 6.5 2.5 ± 0.837	12.5	--
DTX/P-RUBs	49.11±0.26	0.088 ± 0.005		12.5	9
Nonresponsive DTX/P-RUBs	71.84±0.1	0.09 ± 0.03	pH 7.4 -5.28 ± 1.44 pH 6.5 -5.56 ± 0.88	13.8	9.9

pH value was decreased to 5.0, micelles swelled to above 400 nm in 2h (**Figure 3.4 B**). Meanwhile, we noticed that ζ potential increased from 0.8 ± 0.33 mV to 2.5 ± 0.84 mV when we decreased the pH from 7.4 to 6.5. In contrast, the ζ potential of non-responsive P-RUB micelles was −5.2 ± 1.44 mV at pH 7.4 and −5.56 ± 0.88 mV at pH 6.5 (**Table 3.1**). We thus assume that P-RUB micelles expanded due to the protonation of DIPAE in acidic environment since a gradual positive surface charge increment was found. TEM and DLS were utilized to prove the acid-induced dissociation and expansion of P-RUB micelles under different conditions. As shown in **Figure 3.4 E and F**, at pH 7.4, P-RUB micelles showed spherical morphology with a diameter around 30 nm (TEM). Upon acidification to pH 5.0, the micelles dissociated as indicated by decreased counting rate by DLS and big spherical particles was observed with a diameter of around 280 nm by TEM. Meanwhile, the particle size of the micelles significantly increased (from 49 nm to 900 nm) when incubated with 10 mM GSH for 0.5 h at 5.0 (**Figure 3.4 C and D**), implying the dissociation of micelles, the subsequent cleavage of disulfide bond and aggregation formation. Furthermore, this process took much longer (12 h) when the pH was 7.4. This phenomenon strongly suggests the facilitated entry of GSH to the micellar core due to the expansion of micelles by protonation of DIPAEs at low environmental pH value of 5.0. The critical micelle concentration (CMC) of P-RUB was determined to be 9.12 μg/mL using pyrene as a fluorescent probe. Due to the poor aqueous

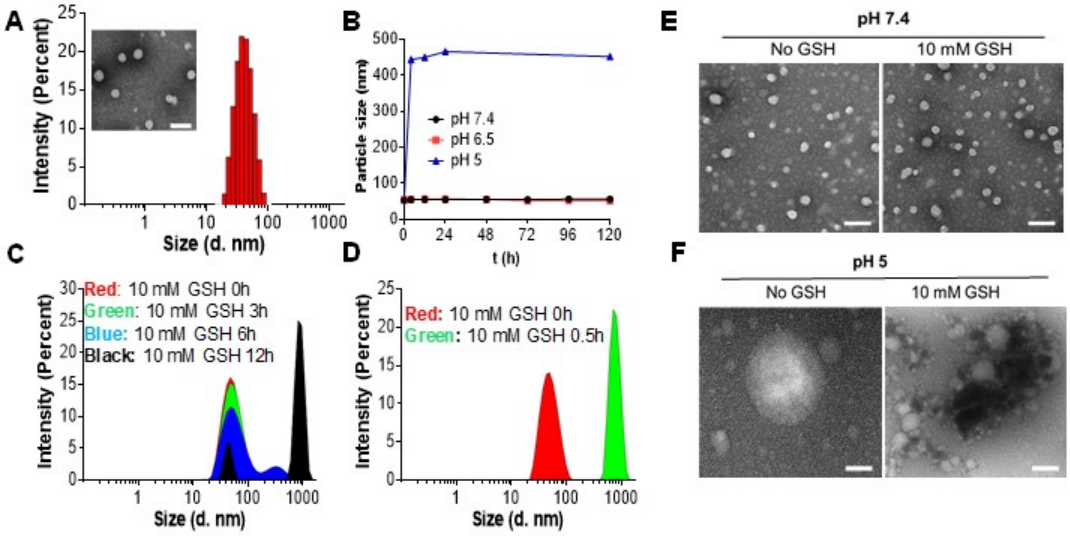

Figure 3.569 Characterization of dual-sensitive P-RUB micelles. A) Particle size distribution and TEM images of DTX/P-RUB micelles; B) Change in particle size of P-RUB micelles after incubation at pH 5, 6.5 and 7.4; particle size variation of P-RUB micelles before or after incubation for 3, 6 and 12h in 10 mM GSH at C) pH 7.4 and D) pH 5.0; TEM images at pH 7.4 E) and pH 5 (F) with or without GSH. Scale bar = 100 nm.

solubility of pyrene, it tends to diffuse into the hydrophobic core of micelles, resulting in photo-physical property changes.

3.4.3 Drug release

To achieve an ideal therapeutic effect, it is important for DTX/P-RUB micelles to undergo drug release soon after endocytosis by cancer cells. The drug release profiles of DTX/P-RUB micelles were then investigated, while using nonresponsive DTX/P-RUB micelles were used as a positive control. In agreement with the redox sensitive design, only less than 5% of RUB was released from P-RUB at both physiological pH of 7.4 and lysosomal pH of 5.0 within 24 h. Thus, RUB should not be released before P-RUB micelles are endocytosed by tumor cells. Upon the addition of GSH, RUB release was accelerated due to the cleavage of disulfide bond, especially at pH 5 as above

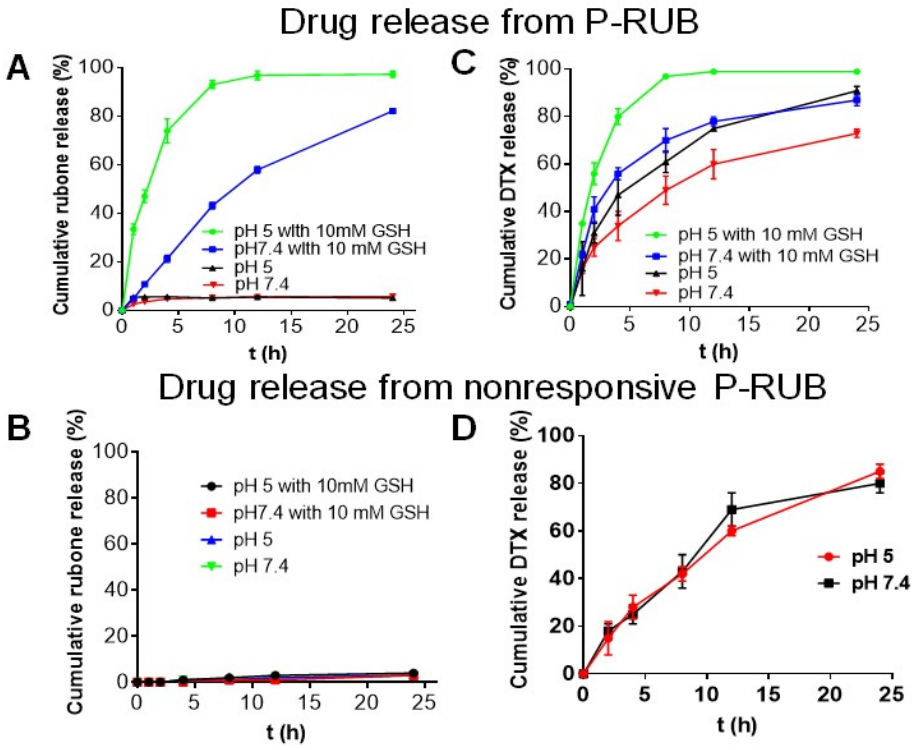

Figure 3.801 Drug release study. Effect of pH and GSH on rubone release from dual responsive (A) and nonresponsive P-RUB micelles (B); Effect of pH and/or GSH on DTX release from dual responsive (C) and nonresponsive P-RUB micelles (D).

95% of RUB was released within 8 h, when compared to that at pH 7.4, at which it requires more than 24 h (**Figure 3.5 A**). In contrast, there was little release of RUB from non-responsive P-RUB micelles regardless of change in pH from 7.4 to 5 and GSH (**Figure 3.5 B**). These results suggest that rapid increase in RUB release from the dual responsive P-RUB micelles may be due to the protonation of DIPAEs, leading to the disassembly of micelles, resulting in complete exposure of disulfide bonds to GSH. In addition, DTX was expected to kill the bulk and chemo-sensitized tumor cells. Thus, *in vitro* release behavior of DTX from DTX/P-RUB micelles was also determined. As shown in **Figure 3.5 C**, the incubation of micelles with 10 mM GSH at pH 5

resulted in 95% of DTX release within 8 h and 99% of DTX after 12 h, while the intracellular reductive circumstance (10 mM GSH) or acidic endocytic vesicles (pH = 5-6) individually facilitates DTX release, with 87% and 91%, respectively. Without these triggers, 72% of DTX was released at pH 7.4 after 24 h. It again indicates the expansion and disassembly of micelles induced by disulfide bond cleavage and protonation of tertiary amines can accelerate drug release regardless of its delivery by encapsulation or conjugation. We also determined DTX release from nonresponsive P-RUB micelles at pH7.4 and 5. There was little influence of pH on its release from these micelles (**Figure 3.5 D**).

3.4.4 Cellular uptake and intracellular distribution

To determine the cellular uptake and monitor subcellular distribution of P-RUB, Cy5.5 labeled P-RUB and Cy5.5 labeled nonresponsive P-RUB were synthesized (**Figure 3.3 and 3.6**) and further made into micelles in aqueous solution. As the results from confocal laser scanning microscopic

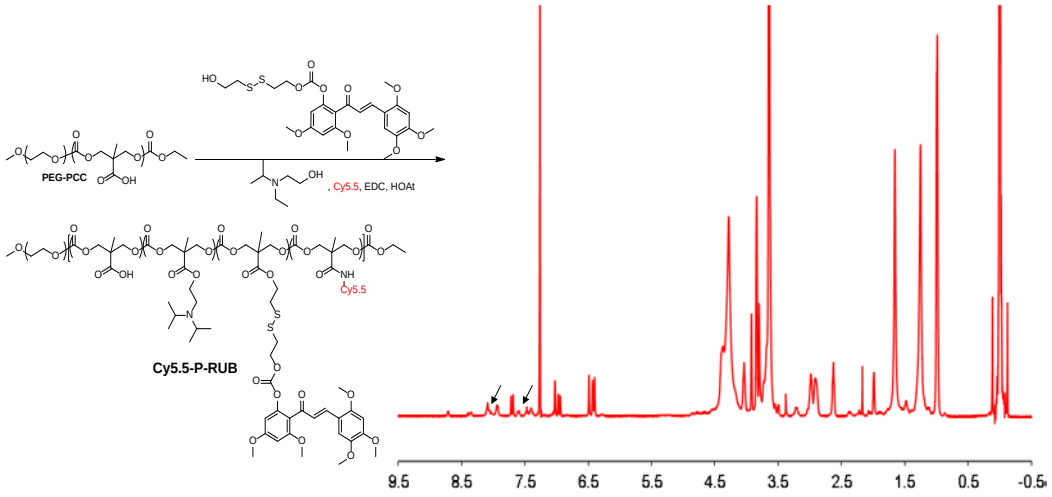

Figure 3.993 Synthesis and characterization of Cy5.5 labeled P-RUB. Synthetic scheme and ^{1}H-NMR spectrum of Cy5.5 labeled poly(ethylene glycol)-block-poly(2-methyl-2-carboxyl-propylene carbonate-graft-rubone-graft-diisopropylamino ethanol) ---

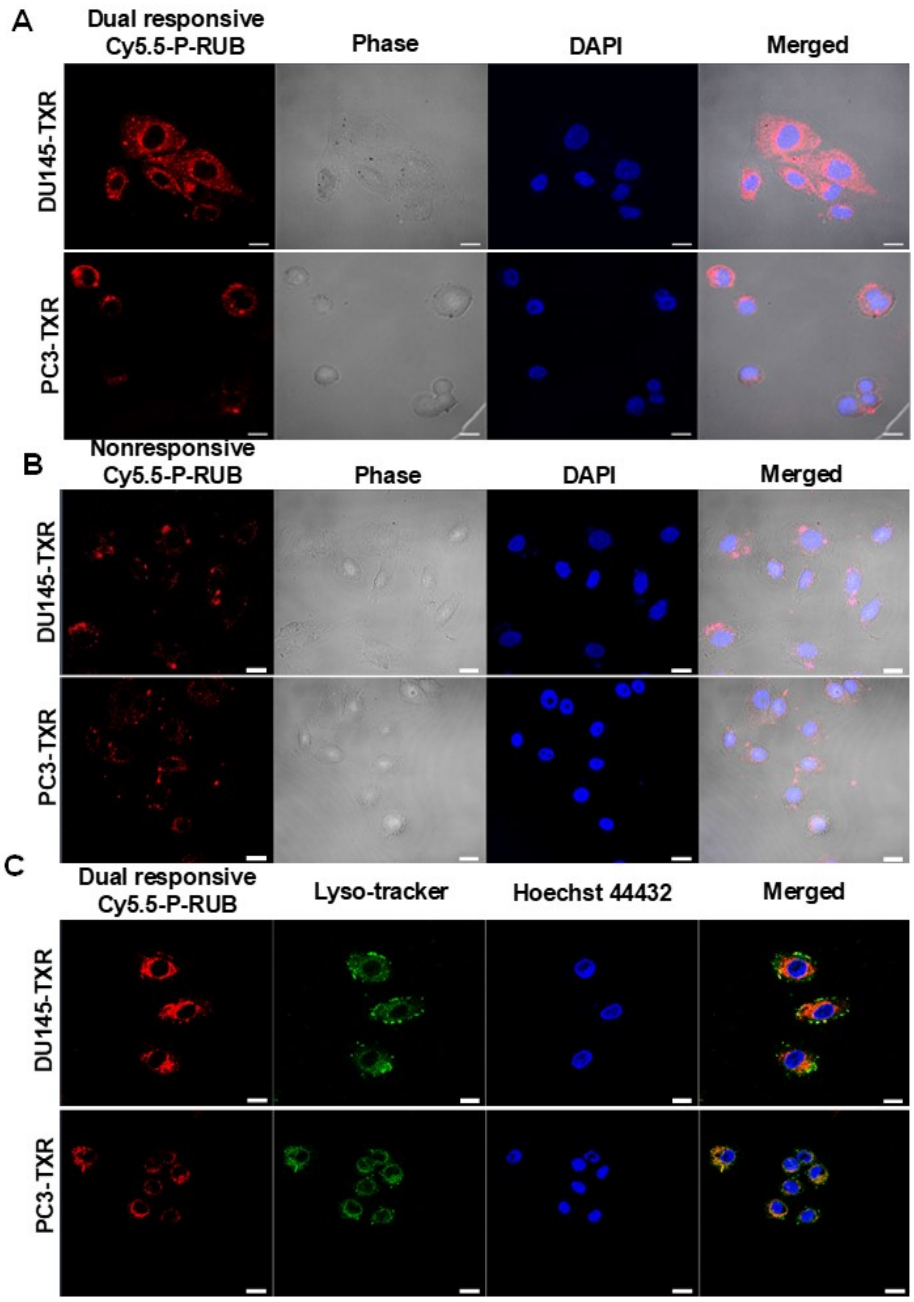

Figure 3.1105 Study of cellular uptake and intracellular distribution. A) Cellular uptake of Cy5.5 labelled DTX/P-RUB (Cy5.5-P-RUB) and B) Cy5.5 labelled nonresponsive DTX/P-RUB in DU145-TXR and PC3-TXR cells by confocal laser scanning microscopy (CLSM) (scale bar 20 μm); C) subcellular distribution of Cy5.5 labelled DTX/P-RUB micelles in DU145-TXR and PC3-TXR cells by CLSM (scale bar 20 μm).

(CLSM) shown in **Figure 3.7 A**, Cy5.5-labeled P-RUB micelles were efficiently taken up by DU145-TXR and PC3-TXR cells, with uniform intracellular distribution in both cell lines. We also determined the cellular uptake of Cy5.5 labeled non-responsive P-RUB micelles and found to be poorly taken up by these cell types, as evidenced by weaker fluorescent staining (**Figure 3.7 B**). Through the observation of micelles and intracellular lysosomes by lysotracker staining, we found that Cy5.5-labeled P-RUB micelles were mostly endocytosed (**Figure 3.7 C**). Furthermore, some polymers have escaped from the lysosome after 6 h.

3.4.5 In vitro antitumor activity

The cytotoxicity of DTX, RUB, P-RUB and DTX/P-RUB micelles and non-responsive DTX/P-RUB were evaluated on DU145-TXR and PC3-TXR by 3-(4,5-dimethylthiazol-2-yl)-2,5-diphenyl tetrazolium bromide (MTT) assay. As shown in **Figure 3.8 A**, comparable growth inhibition capability of free DTX, RUB, P-RUB, nonresponsive P-RUB and nonresponsive DTX/P-RUB micelles were observed on PC3-TXR cells, and 10 μM of P-RUB was needed in the combination therapy for the treatment of DU145-TXR cells to achieve the same proliferation inhibitory effect as 5 μM of free RUB did. Though RUB inhibited the proliferation of DU145-TXR cells by 40%, we noticed that DTX, P-RUB alone, non-responsive P-RUB did not show much antitumor effects on PC3-TXR and DU145-TXR cells and, indicating the combination therapy of DTX and P-RUB can efficiently overcome the chemoresistance of prostate cancer cell lines by the upregulation of miR-34a in the cancer cells. We also determined the effect of non-responsive DTX/P-RUB micelles on the cell viability of DU145, PC-3, DU145-TXR and PC3-TXR cells and found dose-dependent inhibition of these cell proliferation on PC-3 and DU145 cells and limited inhibitory effect on DU145-TXR and PC3-TXR cells (**Figure 3.8 A**).

To further demonstrate the usefulness of dual responsive P-RUB micelles, we used buthionine sulphoxime (BSO) to deplete intracellular GSH and Nigericin to inhibit the endosomal

acidification. As shown in **Figure 3.8 A**, blocking of both GSH and acidification of endosomes significantly decreased the cell killing ability of DTX/P-RUB micelles on PC3-TXR and DU145-TXR cells. Cell viability was higher when GSH was blocked by buthionine sulphoximine than that by Nigericin (**Figure 3.8 A**).

To better simulate the complex tumor microenvironment, we generated hanging top 3D model spheroids of DU145-TXR cells. There was significant reduction in spheroid size when the tumor spheroids were treated with DTX, P-RUB and DTX/P-RUB micelles, with almost complete disruptions of the spheroids with DTX/P-RUB micelle treatment. This suggests DTX/P-RUB

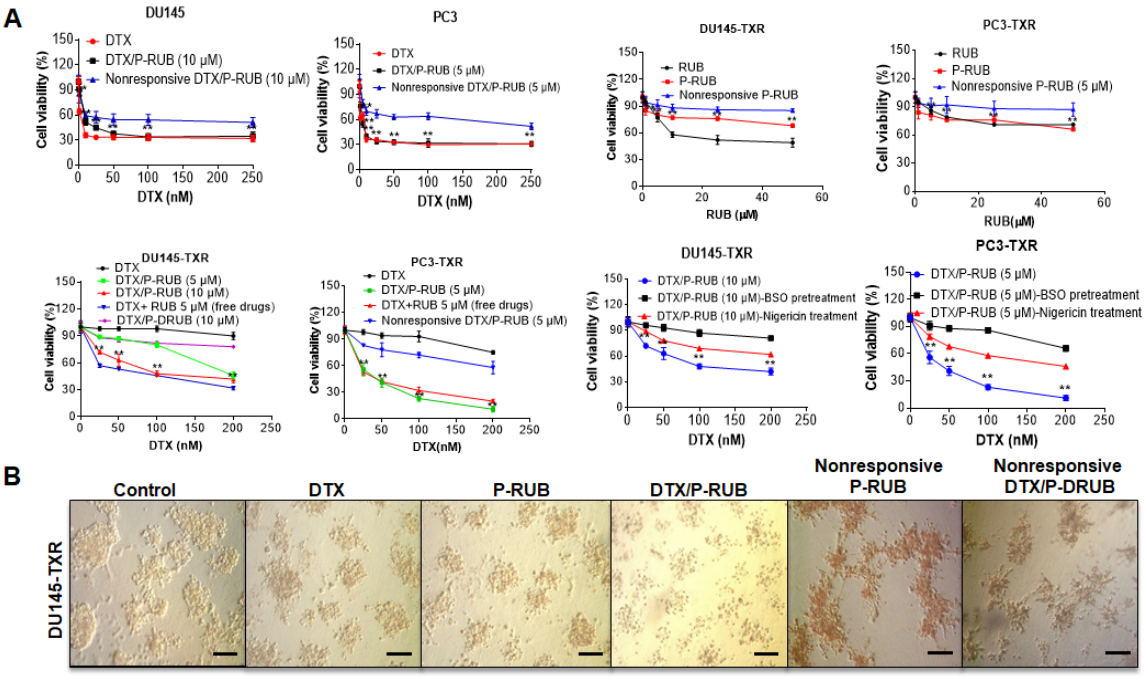

Figure 3.1348 Antitumor effect on chemoresistant prostate cancr. A) Cell viability vs concentration curve for free drugs and various formulations on DU145-TXR and PC3-TXR, respectively. Data are presented as the mean ± S.D (n=3; *, P < 0.05; **, P< 0.01); B) fluorescent microscope images of 3D spheroids for cell cytotoxicity assay of DU145-TXR treated with DTX, P-RUB ,DTX/P-RUB, P-DRUB and nonresponsive DTX/P-DRUB, while non-treated spheroids were used as the control (scale bar 200 μm).

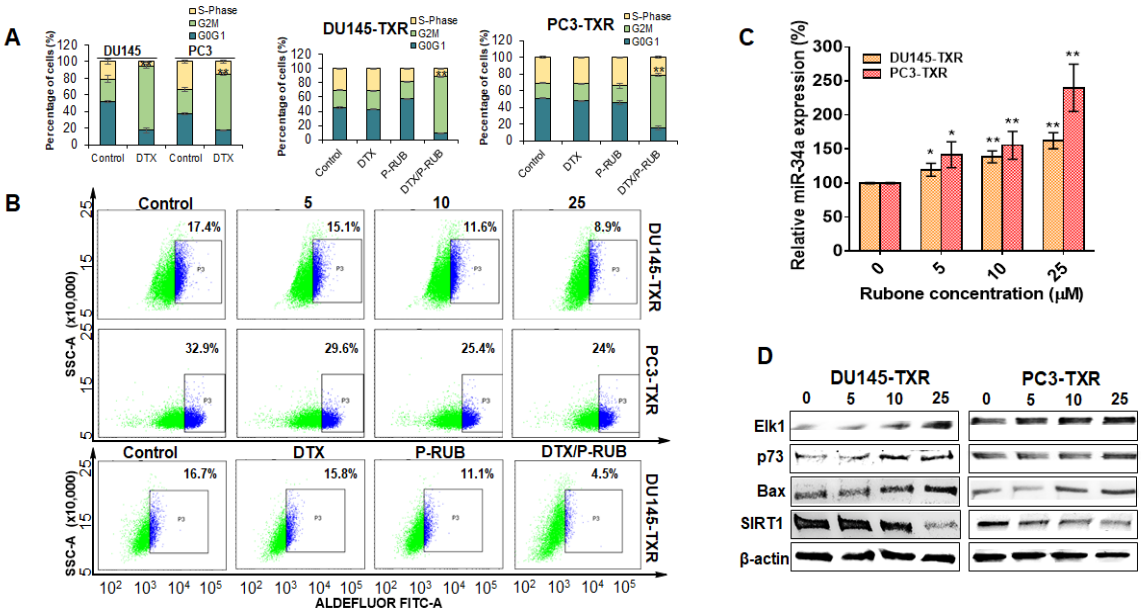

Figure 3.1591 Cell cycle, and mechanism of overcoming chemoresistance. A) Cell cycle analysis on DU145, PC3, DU145-TXR and PC3-TXR cells after incubation with DTX, P-RUB micelles and DTX/P-RUB micelles for 24h; B) change in ALDH-positive subpopulation on DU145-TXR and PC3-TXR cells after treatment with P-RUB micelles containing different concentrations (**μM)** of RUB alone or with DTX for 48h; C) western blot analysis for p-glycoprotein (p-gp); D) RT-PCR analysis for miR-34a and E) western blot for Elk1, p73, Bax and SIRT1 on DU145-TXR and PC3-TXR cells after incubation with P-RUB containing different concentrations (**μM**) of RUB for 48h. Data were given as mean ± SD (n=3; *, P <

micelles were more potent in inhibiting the cell proliferation than single treatment compared to non-treated control (**Figure 3.8 B**). We also determined the effect of nonresponsive P-RUB and DTX/P-RUB micelles on these tumor spheroids and found relatively weaker disruption of tumor spheroids.

3.4.6 Effect on cell cycle arrest and CSC proliferation

Since the combination therapy of DTX and P-RUB showed good potency in inhibiting the

proliferation of DU145-TXR and PC3-TXR cells, we determined how the formulation regulates the cell cycle of these cell lines. As shown in **Figure 3.9 A**, major population of the cells (~55%) was in G0/G1 phase in the control, DTX and P-RUB treated groups. Meanwhile, we also noticed that the cells at S phase increased a little (~5%) with the treatment of P-RUB micelles. Treatment with DTX/P-RUB micelles significantly increased the cell percentage at G2/ M phase in DU145-TXR and PC3-TXR cells (from ~22% to ~60%), indicating P-RUB micelles can chemo-sensitize DU145-TXR and PC3-TXR cells towards DTX, resulting in subsequent cell killing by DTX. This resemble the results we observed from DTX treated DU145 and PC3 cells that the major population (almost 70%) of these taxane sensitive cells was arrested in the G2/M phase (**Figure 3.9 A**).

As the CSCs contribute to chemoresistance of prostate cancer, efficacy in the inhibition of the ALDH-1 high subpopulation by P-RUB micelles was determined by Aldeflour staining of $ALDH^+$ cells. The ALDH-1 high subpopulation constitutes approximately 17.4% and 32.9% of the whole cells on DU145-TXR and PC3-TXR cells (**Figure 3.9 B**). The treatment of P-RUB micelles on these cell lines successfully decreased the ALDH-1-high subpopulation in a dose dependent manner to 8.9% and 24%, which suggests that P-RUB micelles can reverse the chemoresistance of prostate cancer cells against DTX with increased CSC proliferation. In addition, DTX/P-RUB micelles can further decrease the ALDH1-high subpopulation of DU145-TXR cells to 4.5%. Collectively, our results demonstrated that combination therapy of DTX and P-RUB significantly reversed chemoresistance and decreased the CSC population of drug resistant prostate cancer cells.

3.4.7 miR-34a and protein regulation by P-RUB micelles

Since RUB is a miR-34a activator, P-RUB is expected to upregulate miR-34a in the tumor cells. Therefore, we treated DU145-TXR and PC3-TXR cell lines with P-RUB micelles and determined their effect by RT- PCR (**Figure 3.9 C**). P-RUB micelles could successfully upregulate the level

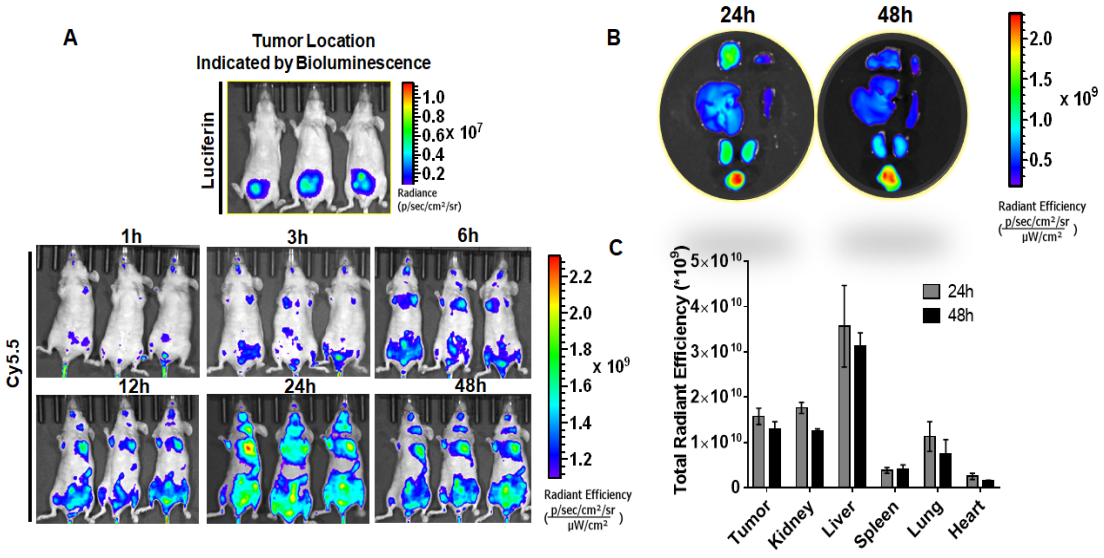

Figure 3.1834 Biodistribution of micelles *in vivo*. A) Fluorescent images of Cy5.5 labeled DTX/P-RUB micelles at different time points (red circles indicate where the tumors are by bioluminescence); B) ex vivo fluorescent image at 24 and 48h post injection; C) quantitative analysis of fluorescence in major organs and tumors at 24 and 48h post i.v. administration of DTX/P-RUB micelles.

of miR-34a on both cell lines in a dose dependent manner. Increasing RUB concentration resulted in significant increase in miR-34a expression on both cell lines compared to the group without treatment of P-RUB micelles and it is much more significant on PC3-TXR (**Figure 3.9 C**). Afterwards, we evaluated the expression of proteins relative to miR-34a following the treatment of P-RUB micelles. Compared to the control group, miR-34a inducers, Elk1 and p73 were upregulated on both cell lines. On the other hand, drug resistance and tumor growth related SIRT1 expression was repressed and the level of apoptotic Bax protein was increased by P-RUB micelles (**Figure 3.9 D**). The results are consistent with the upregulation of miR-34a in DU145-TXR and PC3-TXR from RT- PCR. In other words, P-RUB micelles first upregulated the expression of Elk1 and p73, which then induced miR-34a expression in the tumor cells.

3.4.8 Biodistribution

The tumor targeting ability of DTX/P-RUB micelles was studied on orthotopic PC3-TXR tumor bearing nude mice. The Cy5.5 labeled DTX/P-RUB micelles were first injected into mice via the tail vein and time dependent fluorescence emission images of Cy5.5 at 710 nm were taken at different time points: 0, 1, 3, 6, 12, 24 and 48 h. Fluorescent signals were observed at 1 h post injection (**Figure 3.10**). As time elapsed, the fluorescent intensity increased with time and then reached the maximum at 24 h at the tumor sites post administration. A relatively high photon flux was still recorded at 48 h post injection despite of metabolism and clearance. Thereafter, a further tissue distribution of DTX/P- RUB micelles was studied by ex vivo imaging of tumors and other major organs such as heart, lung, liver, spleen and kidney. As shown in **Figure 3.10 B** and **C**, DTX/P-RUB micelles showed more accumulation in the tumor, liver and kidneys than in spleen, heart and lungs, suggesting that DTX/ P-RUB micelles can efficiently deliver DTX and RUB to the orthotopic prostate tumors after systemic administration. Since Cy5.5 was chemically linked to P-RUB but not to RUB, we could not carry out the quantitative analysis of free RUB and Cy5.5 labeled P-RUB using a fluorimeter at 24 h and 48 h post systemic administration. Instead, we determined RUB concentration in the tumor after extraction

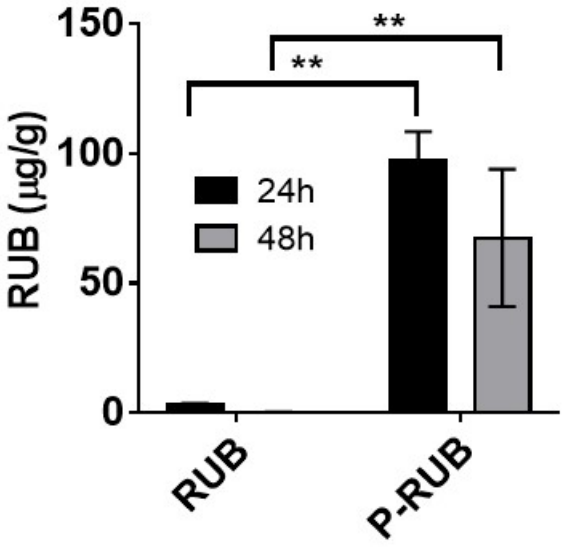

Figure 3.2075 Quantitation of RUB by LC-MS/MS. Quantitative analysis of RUB in major organs and tumors at 24 and 48h post i.v. administration of DTX/P-RUB micelles. (n=3; **, P< 0.01)

using LC/MS/MS. The results shown in **Figure 3.11** correlate well with fluorescence analysis shown in **Figure 3.10**: P-RUB micelles preferentially accumulated in the tumor. RUB concentration from Cy5.5 labeled P-RUB micelle treated tumor sample was much higher than that from the free drug treated tumor samples, possibly due to the rapid distribution, elimination and metabolism of chalcone and its derivatives including RUB. Thus, our micelles not only efficiently deliver drugs to the tumor and release the drugs upon stimulation by pH and GSH, but also protect RUB from metabolism before it reaches the tumor.

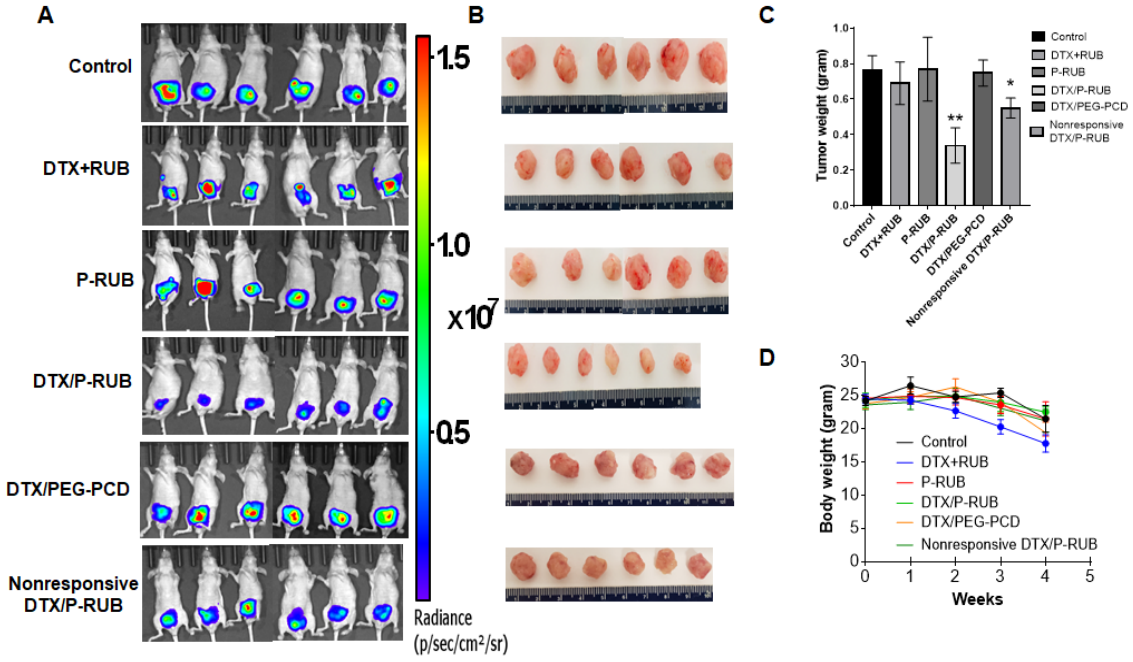

Figure 3.2298 Antitumor efficacy *in vivo*. A) Tumor growth as measured by bioluminescence (120 mg/kg luciferin), B) Size of excised tumors and C) tumor weight at the end of treatment; D) body weight change of orthotopic PC3-TXR tumor bearing nude mice after intravenous administration of PBS, DTX+RUB (free drugs), P-RUB micelles, DTX/P-RUB micelles, DTX/PEG-PCD micelles and nonresponsive DTX/P-RUB micelles. Data were given as mean ± SD (n=6; *, $P < 0.05$; **, $P < 0.01$).

3.4.9 In vivo anticancer efficacy

Inspired by the ability of DTX/P-RUB micelles in combating TXR, the *in vivo* anticancer efficacy of DTX/P-RUB micelles was determined on PC3-TXR orthotopic prostate tumor bearing nude mice. Various formulations (PBS, DTX + RUB, P-RUB micelles, DTX/P-RUB micelles, DTX/PEG-PCD micelles and nonresponsive DTX/P-RUB micelles) were intravenously injected into mice every other 2 days for 18 days. As shown in **Figure 3.12 A** and **B, C**, rapid tumor growth in mice treated with free drugs due to their rapid clearance from the body. The single treatment of P-RUB micelles failed to inhibit the tumor growth, which is consistent with the results obtained in vitro. However, the average tumor volume in DTX/P-RUB micelles treated mice were the smallest compared to the rest of the groups at the end of treatment ($P < 0.05$), showing the highest antitumor activity against PC3-TXR cells. DTX/PEG-PCD micelles did not show any therapeutic effect on PC3-TXR tumor growth. However, nonresponsive DTX/P-RUB micelles could decrease the tumor burden of mice, but not as effective as the dual responsive DTX/P-RUB micelles. It can be contributed to several reasons, including its efficient delivery of DTX and RUB to tumor sites as well as GSH and pH triggered release of DTX and RUB after endocytosis. Among all the groups, we noted that the free drug group caused obvious body weight loss due to the severe systemic toxicity of DTX, not RUB. miR-34a was greatly upregulated in P-RUB micelles and DTX/P-RUB micelles treated groups and this was supported by the downregulation of SIRT1 in tumor tissues in immunohistochemical and western blot analysis (**Figure 3.13 A and B**). Meanwhile, the level of cleaved caspase-3 that indicates cell apoptosis and proliferation was significantly increased and the number of Ki-76 positive proliferating tumor cells was decreased when treated with DTX/P-RUB micelles (**Figure 3.13 C**). We also quantified the % of SIRT1, Ki-67 and cleaved caspase-3 positive cells by ImageJ. The % of SIRT1 and Ki-67 positive cells was statistically lower, but % of cleaved caspase-3 positive cells was higher in the tumor samples of mice treated with DTX/P-RUB micelles compared to those treated with the mixture of DTX and RUB or P-RUB treated groups (**Figure 3.13 D**).

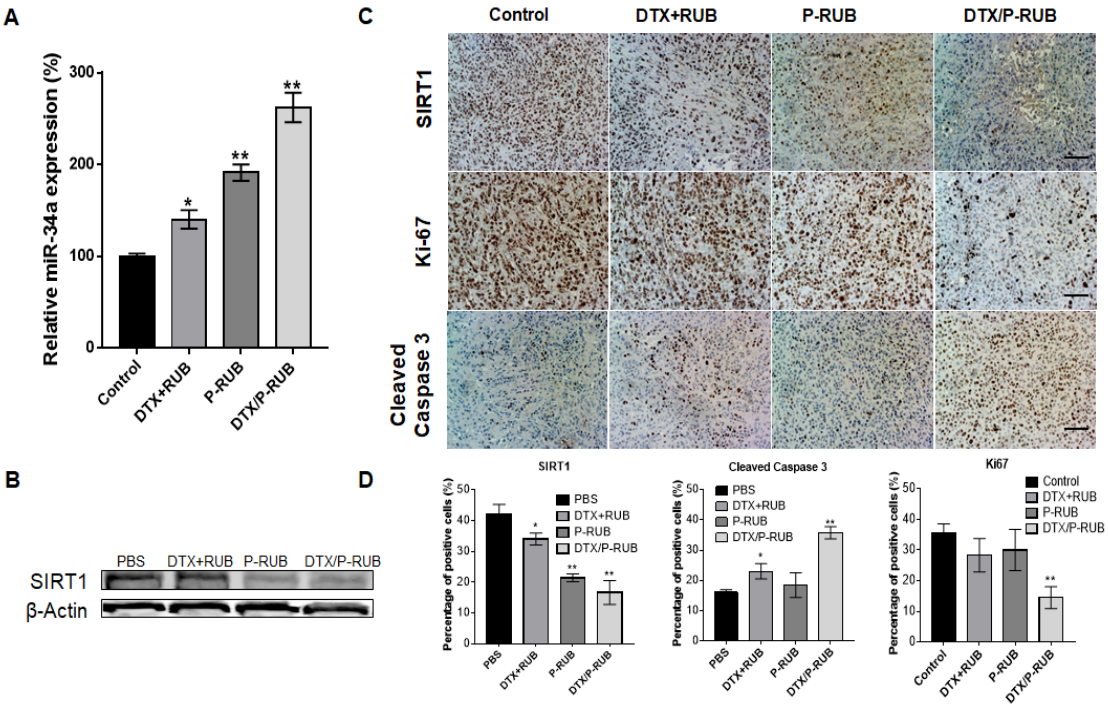

Figure 3.2459 Effect of DTX/P-RUB micelles on miR-34a and gene expression in tumors. A) miR-34a expression in tumors by RT-PCR (n=3; *, P < 0.05; **, P< 0.01); B) Western blot analysis for SIRT-1 expression; C) immunohistochemical analysis of SIRT-1, Ki-67, and cleaved caspase 3 (scale bar = 200μm) and D) quantification of SIRT-1, Ki-67 and cleaved caspase 3-positive cells.

In DTX/P-RUB micelles treated group, fewer cells were observed in hematoxylin and eosin (H&E) staining of the tumors, and there is no obvious histopathological abnormality in other organs such as kidney, heart, lung and heart in all groups (**Figure 3.14**). These results collectively indicate that DTX/P-RUB micelles can effectively suppress the tumor progression while reducing the systemic toxicity of DTX.

3.5 Discussion

While chemotherapeutic drugs such as DTX and PTX are effective in killing proliferating

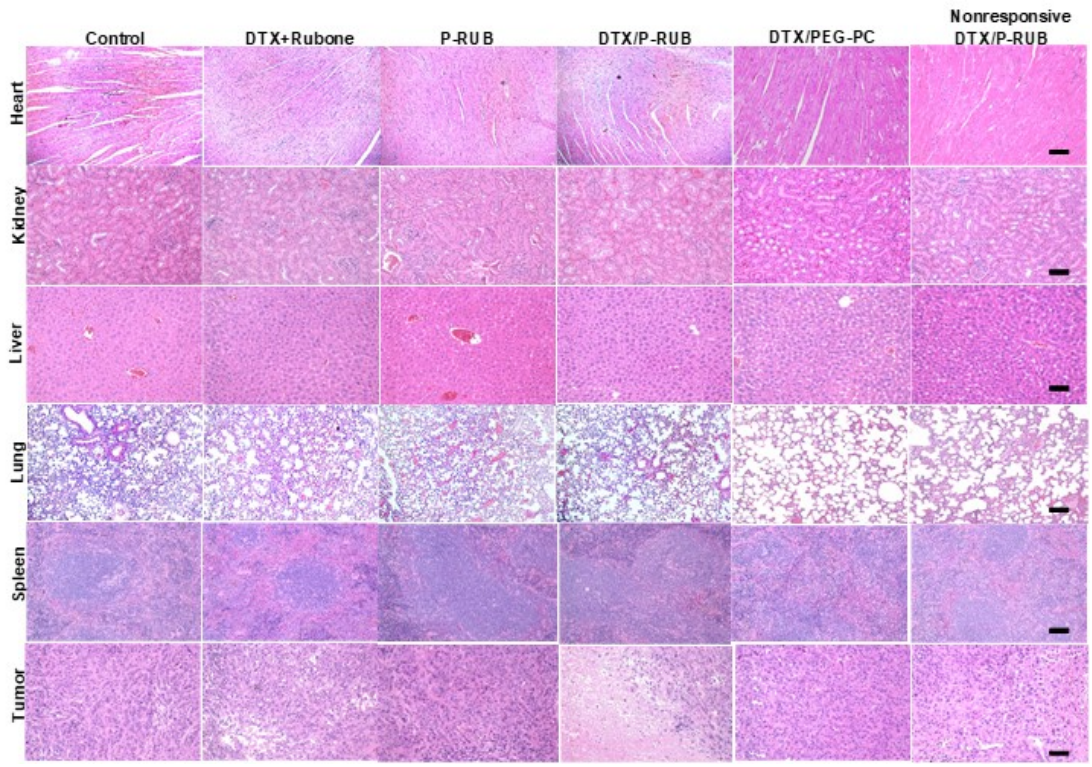

Figure 3.2522 Representative histological images from retrieved tissues. Hematoxylin and eosin (H&E) staining of major organs after systemic administration of P-RUB alone or with DTX into PC3-TXR cell implanted orthotopic prostate cancer bearing nude mice. Co-solvent formulation of DTX and rubone were also injected into tumor bearing nude mice and used as the positive control (scale bar = 200 μm).

prostate cancer cells, they fail to inhibit CSC proliferation owing to multidrug resistance (MDR) [1,51,52]. Thus, cancer patients face a big threat from chemoresistance that ultimately leads to subsequent metastasis and relapse. The complicated mechanism of chemoresistance lies on drug segregation [53–55], altered cellular pathway [56–58], insufficient drug influx due to high expression of P- glycoprotein (P-gp) for drug efflux [59], dysregulation of miRNAs [15], reduced apoptosis and proliferation of CSCs [60,61]. miR-34a and its downstream targets (SIRT1 [62], LEF1 [63], TCF7 [64], AR [65] and Notch-1 [66]) have been found to influence CSC proliferation, metastasis and chemoresistance of cancers. Considering the challenges faced by nucleic acid-based

drugs, including potential immunogenicity, in vivo instability, off target effect and high cytotoxicity [15,17], small molecules having similar function as miR-34a are often regarded as better candidates for cancer treatment due to their stability and ease of production. Thus, the simultaneous administration of a recently discovered small molecule miR-34a activator named RUB and DTX are expected to synergistically and efficiently inhibit tumor growth by killing both CSCs and bulk tumor cells. Although the hydrophobicity of the drugs is the major obstacle in application, the delivery by nanocarriers can effectively improve their aqueous solubility, enhances their therapeutic efficacy and reduces their adverse toxicities. However, recent need to improve the biological specificity in therapy has driven the efforts to the development of nanoparticles that respond to pH alteration, redox potential and reactive oxygen species (ROS) [67,68] through the spatiotemporal control of drug delivery. Despite great efforts devoted to the development of nanoparticles to overcome chemoresistance and most of them focused on how to increase of the accumulation of drugs by avoiding efflux by P-gp [25,69], including the application of Pluronics [70], not much attention has been paid to develop multifunctional pH-responsive micelles that can regulate miRNA expression by small molecule drugs while bypassing P-gp at the same time.

In this study, we developed dual responsive polymer conjugated RUB and DOX encapsulated (DOX/P-RUB) micelles that respond to intracellular pH and GSH levels to accelerate and maximize the drug release. We demonstrated that P-RUB micelles were able to upregulate miR-34a expression in p53 null prostate cell lines, PC3-TXR and DU154-TXR, through upregulating ElK1 and p73 expression (**Figure 3.9**). RUB release was accelerated by addition of GSH within 24 h which attributed to the cleavage of disulfide bond, whereas less than 5% of RUB was detected without GSH (**Figure 3.5**). We also synthesized non- responsive P-RUB by conjugating RUB and dodecanol to the pendant carboxylic acid groups of PEG-PCC. There was little release of RUB from these nonresponsive micelles at pH 7.4 and 5. Moreover, change in pH had little influence on

DTX release from these nonresponsive micelles (**Figure 3.5**).

There was significant expansion and dissociation of dual responsive P-RUB micelles at pH 5 (**Figure 3.4**). Meanwhile, DIPAE plays an important role in other aspects as well: 1) at pH 7.4, the positively charged con- jugated DIPAE (pKa: ~8.5) interact with negatively charged carboxylic acids (pKa: ~5), leading to stabilization of micellar structure; 2) due to the increased degree of protonation of tertiary amine at acidic pH value, P-RUB micelles expanded and dissociated, resulting in rapid drug release (**Figure 3.5**). In addition, DTX encapsulated P-RUB micelles (DTX/P- RUB) were proven to efficiently inhibit the cell proliferation in 2D and 3D models (**Figure 3.8**).

We previously reported the co-delivery of PTX and RUB using poly (ethylene glycol)-block-poly(2-methyl-2-carboxyl-propylene carbonate- graft-dodecanol (PEG-PCD) micelles for the treatment of TXR prostate cancer. In our previous study, RUB was physically encapsulated into PEG-PCD copolymeric micelles with poor drug loading, and release of both PTX and RUB was dependent on hydrophobic interaction and their release was mainly via passive diffusion. In contrast, in the present study the therapeutic effect of DTX and RUB depends on pH-dependent rapid drug release due to protonation and cleavage of disulfide bond. Moreover, RUB is covalently conjugated to the polymer with higher drug loading.

P-RUB studied here is a copolymer that is not only able to encapsulate other hydrophobic drugs, but also responsive to pH value and elevated intracellular GSH level to ensure rapid rate to reach the therapeutic window of drugs. Moreover, the similar idea can be applied to other delivery systems. For example, the reactive oxygen species (ROS) responsive targeting delivery system can be constructed by conjugating other drugs with thioether linkers and specific ligands to improve the tumor specificity. Therefore, the nontoxic polycarbonate with pendent carboxylic acid platform constructed here has the potential to come up with a pool of promising strategies that increase specificity and efficacy of chemotherapy and reduce their cytotoxicity to treat cancer and to other

analogous pathologies.

3.6 Reference

[1] C. Holohan, S. Van Schaeybroeck, D.B. Longley, P.G. Johnston, Cancer drug resistance: an evolving paradigm, Nat Rev Cancer 13(10) (2013) 714-26.

[2] B. Seruga, A. Ocana, I.F. Tannock, Drug resistance in metastatic castration-resistant prostate cancer, Nat Rev Clin Oncol 8(1) (2011) 12-23.

[3] E. Batlle, H. Clevers, Cancer stem cells revisited, Nat Med 23(10) (2017) 1124-1134.

[4] R. Brown, E. Curry, L. Magnani, C.S. Wilhelm-Benartzi, J. Borley, Poised epigenetic states and acquired drug resistance in cancer, Nat Rev Cancer 14(11) (2014) 747-53.

[5] T. Shibue, R.A. Weinberg, EMT, CSCs, and drug resistance: the mechanistic link and clinical implications, Nat Rev Clin Oncol 14(10) (2017) 611-629.

[6] H. Clevers, The cancer stem cell: premises, promises and challenges, Nat Med 17(3) (2011) 313-9.

[7] P. Bu, K.Y. Chen, J.H. Chen, L. Wang, J. Walters, Y.J. Shin, J.P. Goerger, J. Sun, M. Witherspoon, N. Rakhilin, J. Li, H. Yang, J. Milsom, S. Lee, W. Zipfel, M.M. Jin, Z.H. Gumus, S.M. Lipkin, X. Shen, A microRNA miR-34a-regulated bimodal switch targets Notch in colon cancer stem cells, Cell Stem Cell 12(5) (2013) 602-15.

[8] M. Garofalo, C.M. Croce, Role of microRNAs in maintaining cancer stem cells, Adv Drug Deliv Rev 81 (2015) 53-61.

[9] W.L. Hwang, J.K. Jiang, S.H. Yang, T.S. Huang, H.Y. Lan, H.W. Teng, C.Y. Yang, Y.P. Tsai, C.H. Lin, H.W. Wang, M.H. Yang, MicroRNA-146a directs the symmetric division of Snail-dominant colorectal cancer stem cells, Nat Cell Biol 16(3) (2014) 268-80.

[10] F. Li, R.I. Mahato, miRNAs as targets for cancer treatment: therapeutics design and delivery. Preface, Adv Drug Deliv Rev 81 (2015) v-vi.

[11] C. Liu, R. Liu, D. Zhang, Q. Deng, B. Liu, H.P. Chao, K. Rycaj, Y. Takata, K. Lin, Y. Lu, Y. Zhong, J. Krolewski, J. Shen, D.G. Tang, MicroRNA-141 suppresses prostate cancer stem cells and metastasis by targeting a cohort of pro-metastasis genes, Nat Commun 8 (2017) 14270.

[12] C. Liu, K. Kelnar, B. Liu, X. Chen, T. Calhoun-Davis, H. Li, L. Patrawala, H. Yan, C. Jeter, S. Honorio, J.F. Wiggins, A.G. Bader, R. Fagin, D. Brown, D.G. Tang, The microRNA miR-34a inhibits prostate cancer stem cells and metastasis by directly repressing CD44, Nat Med 17(2) (2011) 211-5.

[13] K. Kojima, Y. Fujita, Y. Nozawa, T. Deguchi, M. Ito, MiR-34a attenuates paclitaxel-resistance of hormone-refractory prostate cancer PC3 cells through direct and indirect mechanisms, Prostate 70(14) (2010) 1501-12.

[14] Z. Xiao, C.H. Li, S.L. Chan, F. Xu, L. Feng, Y. Wang, J.D. Jiang, J.J. Sung, C.H. Cheng, Y. Chen, A small-molecule modulator of the tumor-suppressor miR34a inhibits the growth of hepatocellular carcinoma, Cancer Res 74(21) (2014) 6236-47.

[15] Y. Chen, D.Y. Gao, L. Huang, In vivo delivery of miRNAs for cancer therapy: challenges and strategies, Adv Drug Deliv Rev 81 (2015) 128-41.

[16] A. Ganju, S. Khan, B.B. Hafeez, S.W. Behrman, M.M. Yallapu, S.C. Chauhan, M. Jaggi, miRNA nanotherapeutics for cancer, Drug Discov Today 22(2) (2017) 424-432.

[17] Z. Zhou, X. Liu, D. Zhu, Y. Wang, Z. Zhang, X. Zhou, N. Qiu, X. Chen, Y. Shen, Nonviral cancer gene therapy: Delivery cascade and vector nanoproperty integration, Adv Drug Deliv Rev 115 (2017) 115-154.

[18] T. Feng, X. Ai, G. An, P. Yang, Y. Zhao, Charge-Convertible Carbon Dots for Imaging-Guided Drug Delivery with Enhanced in Vivo Cancer Therapeutic Efficiency, ACS Nano 10(4) (2016) 4410-20.

[19] E. Blanco, H. Shen, M. Ferrari, Principles of nanoparticle design for overcoming biological barriers to drug delivery, Nat Biotechnol 33(9) (2015) 941-51.

[20] Q. Hu, W. Sun, C. Wang, Z. Gu, Recent advances of cocktail chemotherapy by combination drug delivery systems, Adv Drug Deliv Rev 98 (2016) 19-34.

[21] T. Sun, Y.S. Zhang, B. Pang, D.C. Hyun, M. Yang, Y. Xia, Engineered nanoparticles for drug delivery in cancer therapy, Angew Chem Int Ed Engl 53(46) (2014) 12320-64.

[22] G.H. Petersen, S.K. Alzghari, W. Chee, S.S. Sankari, N.M. La-Beck, Meta-analysis of clinical and preclinical studies comparing the anticancer efficacy of liposomal versus conventional non-liposomal doxorubicin, J Control Release 232 (2016) 255-64.

[23] W. Cheng, J. Nie, N. Gao, G. Liu, W. Tao, X. Xiao, L. Jiang, Z. Liu, X. Zeng, L. Mei, A Multifunctional Nanoplatform against Multidrug Resistant Cancer: Merging the Best of Targeted Chemo/Gene/Photothermal Therapy, Advanced Functional Materials 27(45) (2017).

[24] P. Zhao, W. Yin, A. Wu, Y. Tang, J. Wang, Z. Pan, T. Lin, M. Zhang, B. Chen, Y. Duan, Dual-Targeting to Cancer Cells and M2 Macrophages via Biomimetic Delivery of Mannosylated Albumin Nanoparticles for Drug-Resistant Cancer Therapy, Advanced Functional Materials 27(44) (2017).

[25] T. Wei, C. Chen, J. Liu, C. Liu, P. Posocco, X. Liu, Q. Cheng, S. Huo, Z. Liang, M. Fermeglia, S. Pricl, X.J. Liang, P. Rocchi, L. Peng, Anticancer drug nanomicelles formed by self-assembling amphiphilic dendrimer to combat cancer drug resistance, Proc Natl Acad Sci U S A 112(10) (2015) 2978-83.

[26] Y. Liu, C. Chen, P. Qian, X. Lu, B. Sun, X. Zhang, L. Wang, X. Gao, H. Li, Z. Chen, J. Tang, W. Zhang, J. Dong, R. Bai, P.E. Lobie, Q. Wu, S. Liu, H. Zhang, F. Zhao, M.S. Wicha, T. Zhu, Y. Zhao, Gd-metallofullerenol nanomaterial as non-toxic breast cancer stem cell-specific inhibitor, Nat Commun 6 (2015) 5988.

[27] X. Deng, Z. Yin, Z. Zhou, Y. Wang, F. Zhang, Q. Hu, Y. Yang, J. Lu, Y. Wu, W. Sheng, Y. Zeng, Carboxymethyl Dextran-Stabilized Polyethylenimine-Poly(epsilon-caprolactone) Nanoparticles-Mediated Modulation of MicroRNA-34a Expression via Small-Molecule Modulator for Hepatocellular Carcinoma Therapy, ACS Appl Mater Interfaces 8(27) (2016) 17068-79.

[28] D. Wen, Y. Peng, F. Lin, R.K. Singh, R.I. Mahato, Micellar Delivery of miR-34a Modulator Rubone and Paclitaxel in Resistant Prostate Cancer, Cancer Res 77(12) (2017) 3244-3254.

[29] Y. Lu, A.A. Aimetti, R. Langer, Z. Gu, Bioresponsive materials, Nature Reviews Materials 2(1) (2017) 16075.

[30] S. Wang, P. Huang, X. Chen, Stimuli-Responsive Programmed Specific Targeting in Nanomedicine, ACS Nano 10(3) (2016) 2991-4.

[31] R.A. Gatenby, R.J. Gillies, A microenvironmental model of carcinogenesis, Nat Rev Cancer 8(1) (2008) 56-61.

[32] K. Pu, A.J. Shuhendler, J.V. Jokerst, J. Mei, S.S. Gambhir, Z. Bao, J. Rao, Semiconducting polymer nanoparticles as photoacoustic molecular imaging probes in living mice, Nat Nanotechnol 9(3) (2014) 233-9.

[33] Z.B. Zheng, G. Zhu, H. Tak, E. Joseph, J.L. Eiseman, D.J. Creighton, N-(2-hydroxypropyl)methacrylamide copolymers of a glutathione (GSH)-activated glyoxalase i inhibitor and DNA alkylating agent: synthesis, reaction kinetics with GSH, and in vitro antitumor activities, Bioconjug Chem 16(3) (2005) 598-607.

[34] F.Y. Lee, A. Vessey, E. Rofstad, D.W. Siemann, R.M. Sutherland, Heterogeneity of glutathione content in human ovarian cancer, Cancer Res 49(19) (1989) 5244-8.

[35] M. Wu, Q. Meng, Y. Chen, L. Zhang, M. Li, X. Cai, Y. Li, P. Yu, L. Zhang, J. Shi, Large Pore-Sized Hollow Mesoporous Organosilica for Redox-Responsive Gene Delivery and Synergistic Cancer Chemotherapy, Adv Mater 28(10) (2016) 1963-9.

[36] J. Wang, X. Sun, W. Mao, W. Sun, J. Tang, M. Sui, Y. Shen, Z. Gu, Tumor redox heterogeneity-responsive prodrug nanocapsules for cancer chemotherapy, Adv Mater 25(27) (2013) 3670-6.

[37] Q. Zhang, C. Shen, N. Zhao, F.J. Xu, Redox-Responsive and Drug-Embedded Silica Nanoparticles with Unique Self-Destruction Features for Efficient Gene/Drug Codelivery, Advanced Functional Materials 27(10) (2017).

[38] B. He, T. Tan, H. Wang, H. Hu, Z. Wang, J. Wang, J. Li, K. Sun, Z. Zhang, Y. Li, Rational Design of Tumor Microenvironment-Activated Micelles for Programed Targeting of Breast Cancer Metastasis, Advanced Functional Materials (2018).

[39] H. Yu, Z. Cui, P. Yu, C. Guo, B. Feng, T. Jiang, S. Wang, Q. Yin, D. Zhong, X. Yang, pH- and NIR light-responsive micelles with hyperthermia-triggered tumor penetration and cytoplasm drug release to reverse doxorubicin resistance in breast cancer, Advanced Functional Materials 25(17) (2015) 2489-2500.

[40] X. Xu, J. Wu, Y. Liu, M. Yu, L. Zhao, X. Zhu, S. Bhasin, Q. Li, E. Ha, J. Shi, O.C. Farokhzad, Ultra-pH-Responsive and Tumor-Penetrating Nanoplatform for Targeted siRNA Delivery with Robust Anti-Cancer Efficacy, Angew Chem Int Ed Engl 55(25) (2016) 7091-7094.

[41] Q. Jiang, Y. Nie, X. Chen, Y. He, D. Yue, Z. Gu, pH-Triggered Pinpointed Cascading Charge-Conversion and Redox-Controlled Gene Release Design: Modularized Fabrication for Nonviral Gene Transfection, Advanced Functional Materials 27(26) (2017).

[42] J. Dai, S. Lin, D. Cheng, S. Zou, X. Shuai, Interlayer-crosslinked micelle with partially hydrated core showing reduction and pH dual sensitivity for pinpointed intracellular drug release, Angew Chem Int Ed Engl 50(40) (2011) 9404-8.

[43] A.N. Lukyanov, V.P. Torchilin, Micelles from lipid derivatives of water-soluble polymers as delivery systems for poorly soluble drugs, Adv Drug Deliv Rev 56(9) (2004) 1273-89.

[44] A. Tagiuri, M. Mohamedali, A. Henni, Dissociation Constant (p K a) and Thermodynamic Properties of Some Tertiary and Cyclic Amines from (298 to 333) K, Journal of Chemical & Engineering Data 61(1) (2015) 247-254.

[45] K. Zhou, Y. Wang, X. Huang, K. Luby-Phelps, B.D. Sumer, J. Gao, Tunable, ultrasensitive pH-responsive nanoparticles targeting specific endocytic organelles in living cells, Angew Chem Int Ed Engl 50(27) (2011) 6109-14.

[46] D. Wang, T. Wang, J. Liu, H. Yu, S. Jiao, B. Feng, F. Zhou, Y. Fu, Q. Yin, P. Zhang, Z. Zhang, Z. Zhou, Y. Li, Acid-Activatable Versatile Micelleplexes for PD-L1 Blockade-Enhanced Cancer Photodynamic Immunotherapy, Nano Lett 16(9) (2016) 5503-13.

[47] J. Mao, Y. Li, T. Wu, C. Yuan, B. Zeng, Y. Xu, L. Dai, A Simple Dual-pH Responsive Prodrug-Based Polymeric Micelles for Drug Delivery, ACS Appl Mater Interfaces 8(27) (2016) 17109-17.

[48] S. Wang, S. Zhang, J. Liu, Z. Liu, L. Su, H. Wang, J. Chang, pH- and reduction-responsive polymeric lipid vesicles for enhanced tumor cellular internalization and triggered drug release, ACS Appl Mater Interfaces 6(13) (2014) 10706-13.

[49] T. Suma, J. Cui, M. Mullner, S. Fu, J. Tran, K.F. Noi, Y. Ju, F. Caruso, Modulated Fragmentation of Proapoptotic Peptide Nanoparticles Regulates Cytotoxicity, J Am Chem Soc 139(11) (2017) 4009-4018.

[50] Y. Guo, D. Wang, Q. Song, T. Wu, X. Zhuang, Y. Bao, M. Kong, Y. Qi, S. Tan, Z. Zhang, Erythrocyte Membrane-Enveloped Polymeric Nanoparticles as Nanovaccine for Induction of Antitumor Immunity against Melanoma, ACS Nano 9(7) (2015) 6918-33.

[51] I. Pastan, M. Gottesman, Multiple-drug resistance in human cancer, N Engl J Med 316(22) (1987) 1388-93.

[52] S. Raz, M. Stark, Y.G. Assaraf, Folylpoly-gamma-glutamate synthetase: A key determinant of folate homeostasis and antifolate resistance in cancer, Drug Resist Updat 28 (2016) 43-64.

[53] Y. Adar, M. Stark, E.E. Bram, P. Nowak-Sliwinska, H. van den Bergh, G. Szewczyk, T. Sarna, A. Skladanowski, A.W. Griffioen, Y.G. Assaraf, Imidazoacridinone-dependent lysosomal photodestruction: a pharmacological Trojan horse approach to eradicate multidrug-resistant cancers, Cell Death Dis 3 (2012) e293.

[54] A.C. MacIntyre, D.J. Cutler, The potential role of lysosomes in tissue distribution of weak bases, Biopharm Drug Dispos 9(6) (1988) 513-26.

[55] B. Zhitomirsky, Y.G. Assaraf, Lysosomes as mediators of drug resistance in cancer, Drug Resistance Updates 24 (2016) 23-33.

[56] A.R. Jazirehi, M.I. Vega, B. Bonavida, Development of rituximab-resistant lymphoma clones with altered cell signaling and cross-resistance to chemotherapy, Cancer Res 67(3) (2007) 1270-81.

[57] D.L. Wheeler, E.F. Dunn, P.M. Harari, Understanding resistance to EGFR inhibitors-impact on future treatment strategies, Nat Rev Clin Oncol 7(9) (2010) 493-507.

[58] C.R. Chong, P.A. Janne, The quest to overcome resistance to EGFR-targeted therapies in cancer, Nat Med 19(11) (2013) 1389-400.

[59] W. Li, H. Zhang, Y.G. Assaraf, K. Zhao, X. Xu, J. Xie, D.H. Yang, Z.S. Chen, Overcoming ABC transporter-mediated multidrug resistance: Molecular mechanisms and novel therapeutic drug strategies, Drug Resist Updat 27 (2016) 14-29.

[60] C.Y. Fong, O. Gilan, E.Y. Lam, A.F. Rubin, S. Ftouni, D. Tyler, K. Stanley, D. Sinha, P. Yeh, J. Morison, G. Giotopoulos, D. Lugo, P. Jeffrey, S.C. Lee, C. Carpenter, R. Gregory, R.G. Ramsay, S.W. Lane, O. Abdel-Wahab, T. Kouzarides, R.W. Johnstone, S.J. Dawson, B.J. Huntly, R.K. Prinjha, A.T. Papenfuss, M.A. Dawson, BET inhibitor resistance emerges from leukaemia stem cells, Nature 525(7570) (2015) 538-42.

[61] M. Dean, T. Fojo, S. Bates, Tumour stem cells and drug resistance, Nat Rev Cancer 5(4) (2005) 275-84.

[62] L. Li, T. Osdal, Y. Ho, S. Chun, T. McDonald, P. Agarwal, A. Lin, S. Chu, J. Qi, L. Li, Y.T. Hsieh, C. Dos Santos, H. Yuan, T.Q. Ha, M. Popa, R. Hovland, O. Bruserud, B.T. Gjertsen, Y.H. Kuo, W. Chen, S. Lain, E. McCormack, R. Bhatia, SIRT1 activation by a c-MYC oncogenic network promotes the maintenance and drug resistance of human FLT3-ITD acute myeloid leukemia stem cells, Cell Stem Cell 15(4) (2014) 431-446.

[63] J. Liang, Y. Li, G. Daniels, K. Sfanos, A. De Marzo, J. Wei, X. Li, W. Chen, J. Wang, X. Zhong, J. Melamed, J. Zhao, P. Lee, LEF1 Targeting EMT in Prostate Cancer Invasion Is Regulated by miR-34a, Mol Cancer Res 13(4) (2015) 681-8.

[64] Y. Wang, L. He, Y. Du, P. Zhu, G. Huang, J. Luo, X. Yan, B. Ye, C. Li, P. Xia, G. Zhang, Y. Tian, R. Chen, Z. Fan, The long noncoding RNA lncTCF7 promotes self-renewal of human liver cancer stem cells through activation of Wnt signaling, Cell Stem Cell 16(4) (2015) 413-25.

[65] V.N. Barton, J.L. Christenson, M.A. Gordon, L.I. Greene, T.J. Rogers, K. Butterfield, B. Babbs, N.S. Spoelstra, N.C. D'Amato, A. Elias, J.K. Richer, Androgen Receptor Supports an Anchorage-Independent, Cancer Stem Cell-like Population in Triple-Negative Breast Cancer, Cancer Res 77(13) (2017) 3455-3466.

[66] A. Pannuti, K. Foreman, P. Rizzo, C. Osipo, T. Golde, B. Osborne, L. Miele, Targeting Notch to target cancer stem cells, Clin Cancer Res 16(12) (2010) 3141-52.

[67] M.S. Shim, Y. Xia, A reactive oxygen species (ROS)-responsive polymer for safe, efficient, and targeted gene delivery in cancer cells, Angew Chem Int Ed Engl 52(27) (2013) 6926-9.

[68] C. Wang, J. Wang, X. Zhang, S. Yu, D. Wen, Q. Hu, Y. Ye, H. Bomba, X. Hu, Z. Liu, G. Dotti, Z. Gu, In situ formed reactive oxygen species-responsive scaffold with gemcitabine and checkpoint inhibitor for combination therapy, Sci Transl Med 10(429) (2018).

[69] I. Brigger, C. Dubernet, P. Couvreur, Nanoparticles in cancer therapy and diagnosis, Advanced drug delivery reviews 64 (2012) 24-36.

[70] A.V. Kabanov, E.V. Batrakova, V.Y. Alakhov, Pluronic block copolymers for overcoming drug resistance in cancer, Adv Drug Deliv Rev 54(5) (2002) 759-79.

Chapter IV

Conclusions and Perspective

4.1 Conclusions

With more and more NDDS being approved by FDA for clinical use and clinical trials, NDDS show great potentials of in treatment or diagnosis of various diseases [1, 2]. The interest in the development and application of NDDS in cancer treatment largely lie in its appealing features. NDDS solve some long existing problems in pharmaceutics: 1) potent drugs but fail to meet the Lipski' rule of five small molecule can be further evaluated for efficacy; 2) Blood circulation time of drugs can be elongated; 3) undesirable toxicity and potential off-target effect can be avoided. Nevertheless, there is a need for the development of smart NDDS for delivery of chemotherapeutic agents including genes and hydrophobic drugs and these smart NDDS can release the cargos in a temporal and spatial manner for target therapy.

Benefiting from recent advances in material science, we constructed a cationic NDDS with pendent arylboronic acids for codelivery of gene and drug. The NDDS exhibited high drug loading capability for volasertib with an alkyl amino group due to donor-receptor interaction and low N/P value (16:1) for complexation of miR-34a. Upon oxidization by H_2O_2, drug and gene were simultaneously released and exhibited synergistic effect in inhibition of tumor growth *in vitro* and *in vivo*.

Based on the discovery for the treatment of taxane resistant prostate cancer in our laboratory and other laboratory, we determined to conjugate the highly hydrophobic and rigid drug named rubone to the biocompatible polycarbonates to solve the low drug loading. With this strategy, up to 40% of drug loading can be achieved. Due to the ionizable tertiary amine group under acidic environment, the polymers expanded to facilitate the release of both drugs, DTX and conjugated rubone, from the micelles. Compared to non-responsive drug conjugate, the DTX/P-RUB significantly inhibit the growth of taxane resistant prostate cancer on nude mice.

Taken all together, the resultant NDDS mediated combination therapy of drug/gene or drug/drug among which one can induce the expression of tumor suppressor genes exhibited a

synergistic effect on the inhibition of tumor growth for efficacious treatment of pancreatic cancer or chemo-resistant prostate cancer. In addition, the strategies used in the projects provides a versatile approach for loading highly hydrophobic drugs, through donor-receptor interaction between alkyl amine group and arylboronic acid or conjugation with a disulfide containing linker. We believe the results from the projects will positively affect advances in smart NDDS development for the treatment of tumors.

4.2 Challenges and perspective

Despite the great process in the treatment of cancers using NDDS, we need to realize there are still some challenges ahead: 1) the complexity and heterogeneity of tumor make it hard for NDDS to reach to core area that locate it far from the abnormal vasculature; 2) burst and undesirable drug release of encapsulated small molecule drugs may lower the specificity and increase the adverse effect of NDDS, given that controlled drug release of some smart NDDS depends on stimuli-triggered degradation of polymers while the drug loading still relies on the weak hydrophobic interaction; 3) traditional methods to prepare NDDS can result in high polydispersity, making it hard for quality control.

One solution to the first concern is to use targeting ligands. Recent studies reported the conjugation of tumor-homing peptide, (CRGDK/RGPD/EC) (iRGD) onto the surface of NDDS can bind to tumor vessels and spread into the extravascular tumor parenchyma, in sharp contrast to the conventional RGD peptides that only deliver the cargo to the blood vessels [3-5].

The second challenge can be solved by conjugating the drug to the backbone of polymer as we did in the second work if the drugs have available functional groups, including -NH_2, -OH and -CHO [6-8]. For those drugs without functional groups for conjugation, the strong ionic interaction is also a good option for drug encapsulation, in light of gene delivery and the donor-receptor

interaction for drug encapsulation [9, 10]. Meanwhile, more strong bonds await being found and applied to physically load the drugs.

The emergence of microfluidic technologies can achieve high speed and good reproducibility in preparing NDDS with narrow size distribution and tunable physical and chemical characteristics [11-13]. Another nano-technique named particle replication in non-wetting template (PRINT) also allow the preparation of monodispersed NDDS with control size, shape and surface property [14, 15].

Taken together, smart NDDS with monodispersity and good quality control could be synthesized in the near future and can potentially achieve deep penetration and even more precise onsite drug release in order to kill the cancer cell locating in the interior of tumors and reduce the undesirable toxicity.

4.3 References

[1] A.C. Anselmo, S. Mitragotri, Nanoparticles in the clinic: An update, Bioeng Transl Med, 4 (2019) e10143.

[2] V. Bhardwaj, A. Kaushik, Z.M. Khatib, M. Nair, A.J. McGoron, Recalcitrant Issues and New Frontiers in Nano-Pharmacology, Front Pharmacol, 10 (2019) 1369.

[3] K.N. Sugahara, T. Teesalu, P.P. Karmali, V.R. Kotamraju, L. Agemy, O.M. Girard, D. Hanahan, R.F. Mattrey, E. Ruoslahti, Tissue-penetrating delivery of compounds and nanoparticles into tumors, Cancer cell, 16 (2009) 510-520.

[4] Z.-H. Peng, J.i. Kopeček, Enhancing accumulation and penetration of HPMA copolymer–doxorubicin conjugates in 2D and 3D prostate cancer cells via iRGD conjugation with an MMP-2 cleavable spacer, Journal of the American Chemical Society, 137 (2015) 6726-6729.

[5] K.N. Sugahara, T. Teesalu, P.P. Karmali, V.R. Kotamraju, L. Agemy, D.R. Greenwald, E. Ruoslahti, Coadministration of a tumor-penetrating peptide enhances the efficacy of cancer drugs, Science, 328 (2010) 1031-1035.

[6] F. Lin, D. Wen, X. Wang, R.I. Mahato, Dual responsive micelles capable of modulating miRNA-34a to combat taxane resistance in prostate cancer, Biomaterials, 192 (2019) 95-108.

[7] J. Khandare, T. Minko, Polymer–drug conjugates: progress in polymeric prodrugs, Progress in polymer science, 31 (2006) 359-397.

[8] J. Kopecek, Polymer-drug conjugates: origins, progress to date and future directions, Adv Drug Deliv Rev, 65 (2013) 49-59.

[9] S. Lv, Y. Wu, K. Cai, H. He, Y. Li, M. Lan, X. Chen, J. Cheng, L. Yin, High drug loading and sub-quantitative loading efficiency of polymeric micelles driven by donor–receptor coordination interactions, Journal of the American Chemical Society, 140 (2018) 1235-1238.

[10] D.W. Pack, A.S. Hoffman, S. Pun, P.S. Stayton, Design and development of polymers for gene delivery, Nat Rev Drug Discov, 4 (2005) 581-593.

[11] R. Karnik, F. Gu, P. Basto, C. Cannizzaro, L. Dean, W. Kyei-Manu, R. Langer, O.C. Farokhzad, Microfluidic platform for controlled synthesis of polymeric nanoparticles, Nano Lett, 8 (2008) 2906-2912.

[12] P.M. Valencia, P.A. Basto, L. Zhang, M. Rhee, R. Langer, O.C. Farokhzad, R. Karnik, Single-step assembly of homogenous lipid-polymeric and lipid-quantum dot nanoparticles enabled by microfluidic rapid mixing, ACS Nano, 4 (2010) 1671-1679.

[13] M. Rhee, P.M. Valencia, M.I. Rodriguez, R. Langer, O.C. Farokhzad, R. Karnik, Synthesis of size-tunable polymeric nanoparticles enabled by 3D hydrodynamic flow focusing in single-layer microchannels, Advanced Materials, 23 (2011) H79-H83.

[14] J.P. Rolland, B.W. Maynor, L.E. Euliss, A.E. Exner, G.M. Denison, J.M. DeSimone, Direct fabrication and harvesting of monodisperse, shape-specific nanobiomaterials, J Am Chem Soc, 127 (2005) 10096-10100.

[15] J. Xu, D.H. Wong, J.D. Byrne, K. Chen, C. Bowerman, J.M. DeSimone, Future of the particle replication in nonwetting templates (PRINT) technology, Angew Chem Int Ed Engl, 52 (2013) 6580-6589.